HEINRICH HEINE
UNIVERSITÄT DÜSSELDORF

Investigations on particle-induced apoptosis in macrophages

Inaugural-Dissertation

Zur Erlangung des Doktorgrades
der Mathematisch-Naturwissenschaftlichen Fakultät
der Heinrich-Heine-Universität Düsseldorf

vorgelegt von

Verena Judith Wilhelmi

aus Wuppertal

Düsseldorf, November 2012

aus dem Leibniz-Institut für umweltmedizinische Forschung (IUF)
an der Heinrich-Heine-Universität Düsseldorf

Gedruckt mit der Genehmigung der
Mathematisch-Naturwissenschaftlichen Fakultät der
Heinrich-Heine-Universität Düsseldorf

Referentin: Prof. Dr. Charlotte Esser
Korreferentin: Prof. Dr. Christine R. Rose

Tag der mündlichen Prüfung: 23.01.2013

Wenn es die letzte Minute nicht gäbe,
würde vieles überhaupt nicht erledigt.
(Lucius Annaeus Seneca)

Für meine Eltern

Chapter I

General Introduction

1 Nanoparticles

Nanoparticles have been produced by natural processes for eons. Consequently, every organism on earth is continuously exposed to tiny particles derived from volcanic eruptions, dust storms or forest fires as well as from biological sources like pollen or viruses. Therefore, our body evolved highly effective clearance mechanisms targeting these potentially harmful nano-intruders, in particular the reticuloendothelial system. Nowadays, we are additionally exposed to an increasing pool of man-made particles due to industrial air pollution or automobile exhaust fumes on the one hand and the emerging marketing of novel consumer products containing nanoparticles on the other hand. Among a number of definitions regarding nanomaterials over time, the common used classification is in line with the British Standards Institution (BSI): A nano-object exhibits at least one and nanoparticles all three dimensions at the nanoscale. The nanoscale size ranges from approximately 1 to 100 nm [BSI 2007] (Figure 1-1). A nanorod is classified as nano-object with two dimensions in the nanoscale and the third one significantly larger. Nanotubes are a special case of hollow nanorods, even existing in multi-walled structures. Nanotechnological modifications of bulky matter at the scale of atoms may exploit quantum and surface effects to create materials with outstanding characteristics. In spite of the increasing application in consumer products, the evaluation of possible adverse health effects lags behind. There is need for a comprehensive risk assessment regarding toxicological questions. In this context, the very new field of nanotoxicology strives for a structured standardisation and regulation of nanoparticles.

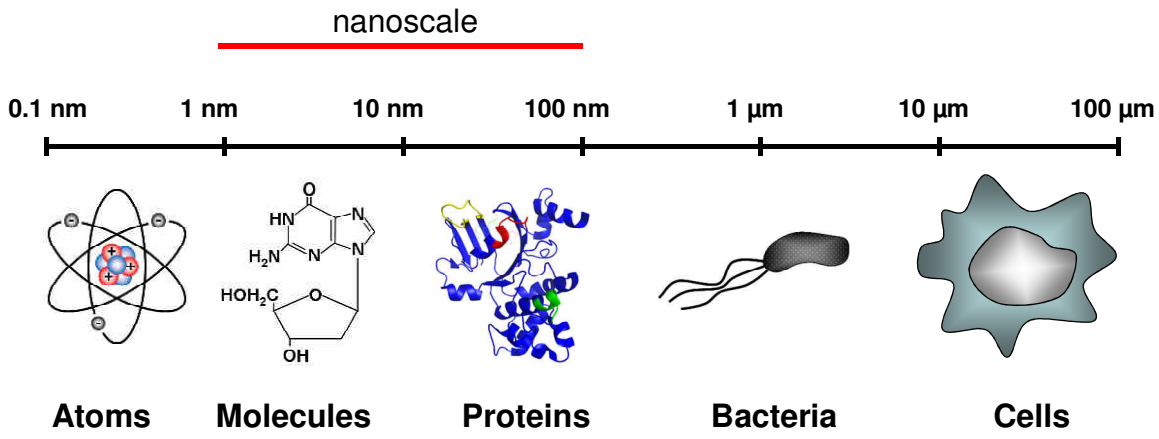

Figure 1-1: Grading of objects around the nanoscale, ranging from 1 to 100 nm and defining the dimension of nanoparticles.

1.1 Nanotechnology – an increasing part of our life

The nanotechnology sector is seen to be the key technology of the next decades worldwide. In this highly interdisciplinary field, research is cross-linked between commercial concerns, specialised centres of excellence and universities. Nanomaterials find application in a wide range of fields in nearly every industrial scope and medical innovations. Currently, we primarily benefit from nano-supplements in common consumer products such as cosmetics, antimicrobial textiles or food additives [Frohlich *et al.,* 2012]. The very special properties of nanoparticles compared to the bulk material are mainly based on surface effects (cf. paragraph 1.2 Nanotoxicology). Entering the nanoscale offers an enormous increase of the materials surface area per unit of mass and therefore increases chemical reactivity. Characteristics of new nanomaterials are not always predictable because of quantum effects occurring at nanoscale dimensions. Operating with measures smaller than 100 nm allows for manipulating the physical and chemical properties. The resulting magnetical, optical and electrical phenomena offer enormous chances in nanomedicine and information technology [Jun *et al.,* 2008; Banerjee *et al.,* 2010]. Especially metal or metal oxide containing nanomaterials may provide these unique optical properties. Nanopowders of zinc oxide, magnesium oxide, titanium dioxide and silicon dioxide make up a major part of the total industrial production of nanomaterials with countless applications. These particulates are used e.g. in the attenuation of UV light, in specialised additives for manufacturing high-grade ceramics, in batteries, in cosmetics or in food packing materials. Further application fields are high-temperature lubricants in engines, fire retardants in plastic trades, various carriers used in the radio industry, insulating material fillers or food additives, to name only a few examples. [US_Research_Nanomaterials_Inc.]. A very innovative scope is the development of metal nanoparticles for biosensing applications [Doria *et al.,* 2012]. Also, single walled carbon nanotubes (SW-CNT) find efficient use in *in vivo* sensor technology due to their intrinsic near-infrared fluorescence emission spectrum detectable throughout tissues without photo bleaching [Barone *et al.,* 2005]. Other photo absorbing properties were exploited by the invention of nanoshells, miniscule spheres composed of a dielectric silica score wrapped by a metallic shell [West *et al.,* 2003]. Transferred into tumours, the following photo-thermal tissue ablation promises a non-invasive cancer therapy [O'Neal *et al.,* 2004]. The very unique fluorescent properties of quantum dots are based on quantum effects within these semiconductor nanocrystals and are convenient to a size-dependent light emission during excitation. Throughout biomedicine and electronics, a multitude of cutting-edge applications especially in bionanotechnology are under development [Drummen 2010]. The

implementation of carbon nanotubes (CNTs) provide outstanding mechanical properties for instance for the improvement of composite materials in terms of low mass density coupled with an enormous tensile strength and elasticity modulus, especially in multi-walled construction known as multi walled carbon nanotubes (MW-CNT) [Donaldson *et al.,* 2006; Saito *et al.,* 2008]. Compared to conventional materials used in electronic industry, CNTs excel in ampacity, thermal conductivity and can be deployed as electronic semiconductor to fabricate transistors [Gruner 2006]. Moreover, both SW-CNT and MW-CNT are being developed for a host of biomedical and biotechnological applications as well as spherical nanoparticles [Martin *et al.,* 2003]. Since nanotechnology will be increasingly used in our everyday life, we need to consider the potential adverse effects regarding the environmental and human exposure.

1.2 Nanotoxicology

From the ongoing development and large scale commercialisation of many different engineered nanomaterials a new branch of toxicology evolved, i.e. nanotoxicology. This new field addresses possible adverse health effects of nanoparticles as well as the proper characterisation of nanomaterials used in toxicology studies [Donaldson *et al.,* 2004; Oberdorster *et al.,* 2005b]. Naturally occurring nanoparticles like atmospheric matter or biological nanostructures such as pollen and viruses may cause distinct health effects compared to engineered nanomaterials. However, there are significant common aspects of intrusion and translocation with conferrable fundamentals derived from epidemiologic studies of air pollution, virology and bacteriology [Buzea *et al.,* 2007].

Historically, particle toxicology emerged during the early industrial activities, observing severe lung diseases to coal miners and citizens exposed to combustion derived smog [Borm 2002; Seaton 2010]. Ambient air particulate matter (PM) represents a heterogeneous mixture of particulate components of varying chemical composition; they can be subdivided into different size fractions, based on the way they can be collected with specific particle matter samplers, into a coarse (2.5-10 µm), fine (0.1-2.5 µm) and ultrafine (< 0.1 µm) mode [van Berlo *et al.,* 2012]. Since the early 1990s, epidemiological studies investigating lung cancer and cardiovascular diseases found associations between mortality rates and air pollution due to long-term exposure to fine particles [Dockery *et al.,* 1993]. In more recent years it has become clear from both epidemiological and toxicological studies that adverse pulmonary and cardiovascular effects of PM are mainly due to ultrafine particles [van Berlo *et al.* 2012]. These observations have led to an increased concern about the potential toxicity of engineered

nanoparticles. Interestingly, some recent studies also indicate that ambient ultrafine particles play also a role in the development or progression of neurodegenerative diseases [Block *et al.,* 2009].

Due to their dimensions, nanoparticles may easily enter organisms, translocate through physiological barriers and interfere with biological systems. The proposed exposure route for reaching the brain may take place upon nasal deposition of inhaled nanoparticles, crossing the epithelia to the olfactory bulb [Kreuter *et al.,* 2002; Oberdorster *et al.,* 2004]. Even the passage through the blood-brain-barrier, which is the tightest endothelial barrier of the body containing a well-regulated system of transport proteins, is possible by specific nanoparticles [Peters *et al.,* 2006]. The access may be facilitated by circulatory pathologies and inflammatory processes [Borm *et al.,* 2006]. A growing number of studies also indicate that there are correlations between particle exposure by uptake via the gastrointestinal tract and the exacerbation of diseases, which are previously attributed only to genetic factors and lifestyle. Among these are inflammatory bowel diseases of the gastrointestinal tract with unknown aetiology [Hoet *et al.,* 2004] and type II diabetes [Lafuente *et al.,* 2012].

Regarding the physico-chemical characteristics associated with particle-toxicity, the common concept of dose-dependency may not be valid. Comparing TiO_2 particles of the same chemistry but different sizes, the impact on pulmonary inflammation was shown to increase in a direct correlation to the particles surface area as illustrated in Figure 1-2 [Oberdorster *et al.,* 2005b]. The so called “ultrafine particle hypothesis” depicts the biological reactivity of particles potentially interacting with subcellular components, since the number of surface molecules per unit mass is increasing exponentially with decreasing particle diameters [Utell *et al.,* 2000]. Therefore, TiO_2, commonly assumed as non-toxic bulk material, reveals a considerable reactivity on a mass basis at the nanoscale.

Nanoparticles currently available may be chemically simple but also can consist of very complex compositions. Featuring diverse physical structures like porosity, crystal structure or shape, the biological interactions are not easily predictable. Especially for therapeutic purposes, specific properties may interact selectively with the immune system, distinct tissues, or proteins [Donaldson *et al.,* 2004]. The capacity of protein binding is a strong point of interest in particle toxicology, since it affects the cellular protein metabolism, enzyme function, and may alter the particle properties like solubility and hydrophobicity itself [Sethi *et al.,* 2010].

In vitro assays may be a sufficient and low cost alternative to animal testing [Richmond 2002]. They are useful to assess potential effects in various target organs and tissues, and

there is a comprehensive market of tools and ready-to-use-kits available for the evaluation of a multitude of endpoints. However, (nano-)particle research takes in an exceptional position with regard to *in vitro* toxicology research. To prevent misinterpretation of data, particular attention has to be paid on the fact that the materials studied tend to interfere with commonly used test systems because of their complex physico-chemical properties [Stone *et al.,* 2009]. Particles with highly light absorbing, scattering or auto-fluorescent characteristics may be critical confounders in a variety of assays based on optical detection [Monteiro-Riviere *et al.,* 2009]. Moreover, due to their large adsorptive surface, the physiological behaviour of nanoparticles is influenced by their affinity to become coated with proteins of the medium, assay components or cells [Kane *et al.,* 2007]. Nanomaterial absorption may also directly affect the function of assay substrates or dyes, even presenting catalytic activity [Kroll *et al.,* 2009].

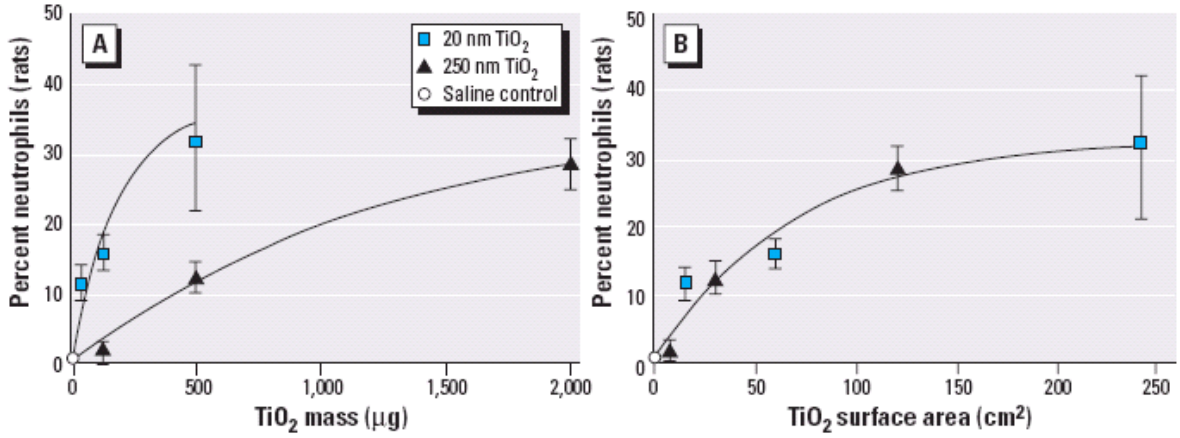

Figure 1-2: Comparison of two sizes of TiO_2 particles regarding the inflammatory potential in rat lungs determined by the influx of neutrophils. (A) Nanosized particles display much stronger effects in mass-correlating dose-dependency than microparticles. (B) The dose expressed as particle surface area reveals the same neutrophil response to both particle samples. [Oberdorster *et al.* 2005b]

To address the toxicity of new nanomaterials, there is an urgent need of standardised screening-technics for nanoparticle hazard characterisation. Therefore, the quality of studies has to be improved to enhance stringency and reliability [Stone *et al.,* 2009]. As a subject of current research, experimental reproducibility should be based on the often lacking adequate characterisation of the materials studied as well as an appropriate study design with the inclusion of appropriate negative and positive controls [Krug *et al.,* 2011]. A long-term objective of these investigations is seen in Quantitative Structure-Activity Relationship (QSAR) strategies to understand relationships between the physico-chemical properties and the behaviour of nanomaterials in biological systems [Burello *et al.,* 2011].

1.2.1 Nanoparticles in the respiratory tract

There are three main sites of exposure, whereby environmental (nano-)particles may enter the human body: The skin, the gastro-intestinal tract and the lung. The skin is an effective barrier to foreign substances, whereas the two other ones are specialised for assimilation with high surface areas and therefore more vulnerable. In recent years, the role of the gastro-intestinal tract in particle toxicology is increasingly in the focus of investigations. Besides of food containing particles, there is a link to airborne particles reaching the gastro-intestinal tract, since clearance mechanisms of the respiratory tract via the mucocilliary escalator partially result in swallowing [Oberdorster *et al.,* 2005a]. However, pulmonary exposure of (nano-)particles is generally accepted to be the most relevant.

Our lungs present an enormous interface to the environment consisting of a wide network of airways to ventilate about 300 millions of alveoli with a total surface area of about 140 m² in adults [Hoet *et al.,* 2004]. In the gas exchange area, the air-blood-barrier of just 0.5 micron in scale is very thin and therefore highly susceptible. The adverse effects of particulate material in the lungs depend on the lung burden, a result of insufficient clearance mechanisms during particle exposure as depicted in Figure 1-3A.

In dependence of the diameter of inhaled particulate matter, the deposition targets different regions of the respiratory tract due to the five mechanisms, i.e. inertial impaction, gravitational sedimentation, Brownian diffusion, inception, and electrostatic precipitation [Lippmann et al., 1980]. In most cases, the first three mentioned will be important. As shown in Figure 1-3B, a predictive mathematical model provided by [ICRP 1994] evaluated particles smaller than 10 microns as capable to reach the alveoli, especially nanoparticles of 10-20 nm. Half of the amount of this fraction gets deposited in the alveolar region, whilst the entire rest is captured by the two other regions to nearly the same shares. The nasopharyngeal region mainly captures the larger particles as well as nanoparticles smaller than 10 nm.

During evolution, highly effective clearance mechanisms emerged in higher developed organisms to remove inhaled particles out of the respiratory tract [Ferin 1994]. The entire lower respiratory tract is lined with respiratory epithelium, generating the mucocilliary escalator. Secretion of mucus serves as wetting fluid for airborne particles, and promotes their neutralising opsonisation by specific phospholipids, proteins and antioxidants [Lai *et al.*, 2009]. A continuous cilial motion provokes an upstream transport of mucus, until reaching the oropharynx to get either swallowed or expelled by coughing. In humans, this process of alveolar cleaning from solid particles has been estimated to take up to 700 days [Oberdorster *et al.,* 2005b].

Although epithelial cells also have some phagocyting ability to engulf particles; the most prevalent step in particle cleaning of distal regions in the lung is formed by alveolar macrophages. These professional cleaners are capable of a very efficient receptor-mediated phagocytosis of deposited particles. They leave the alveolar region, either via the mucocilliary escalator or the lymphatic system.

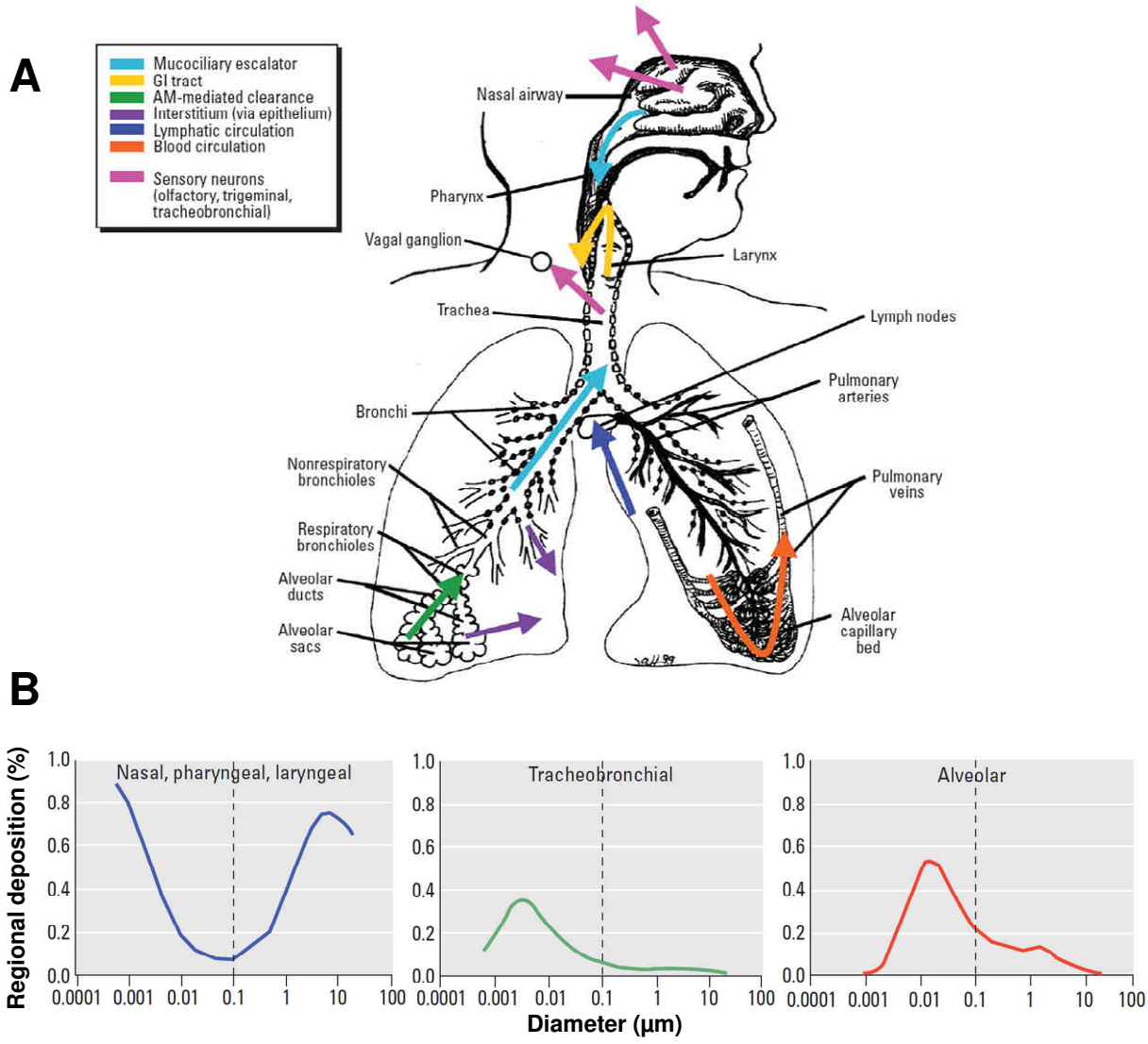

Figure 1-3: (A) Possible disposition pathways of (nano-)particles in the respiratory tract are mainly driven by clearance mechanisms (B) Regional particle deposition in the human respiratory tract according to the particle diameter. Modified from [Oberdorster *et al.*, 2005b]

However, there is some kind of respirable matter which potentially makes these clearance mechanisms fail: high aspect ratio particles (fibres) or very small particles, which may therefore interact directly with the lung epithelium. The most prominent example in fibre toxicology is the naturally occurring material asbestos. Since many decades, asbestos

exposure has been implicated in the development of various severe pathologies, including fibrosis (known as asbestosis), lung cancers and the development of malignant mesotheliomas [Rom *et al.,* 1974]. The classical concept of fibre pathogenicity, i.e. the structure-activity paradigm, describes the specific hazard of fibres for the lungs on the basis of three morphological characteristics [Donaldson *et al*., 2010]. First, a small aerodynamic diameter enables a deposition beyond the ciliated airways. Secondly, due to a great length of particles, macrophages may fail during the attempt of enclosure into "frustrated phagocytosis" resulting in chronic inflammation. The third particle specificity of biopersistence retains these adverse conditions without breaking off in smaller fragments. These shapes and chemical characteristics may also apply to some types of carbon nanotubes as shown in Figure 1-4. Therefore, CNTs are currently of specific concern due to studies detecting inflammatory effects after aspiration [Shvedova *et al.,* 2005; Sanchez *et al.,* 2009]. Even the formation of asbestos-like pathogenicity was already shown in mice [Poland *et al.*, 2008; Takagi *et al.*, 2008].

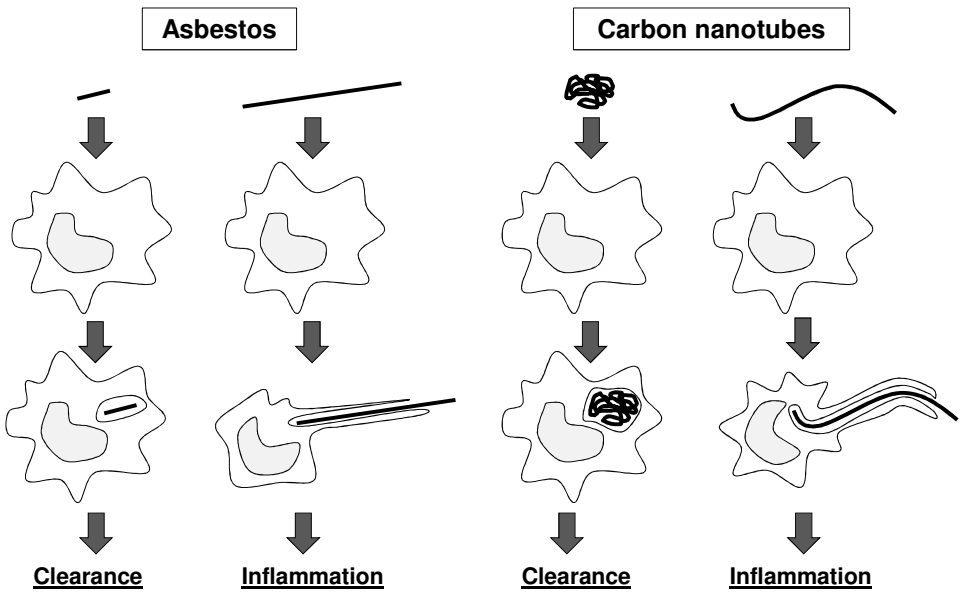

Figure 1-4: The "frustrated phagocytosis" paradigm. An appropriate macrophage clearance can only proceed if the fibres are short enough or compact tangled to get completely engulfed. Incomplete, "frustrated phagocytosis" due to fibres that are too long for enclosure results into inflammation. Modified from [Donaldson *et al.*, 2010]

The most extensively studied occupational disease of the lung with ongoing relevance around the world is the progressive and irreversible disease silicosis which is a specific type of pneumoconiosis [Castranova *et al*., 2000]. It is caused by prolonged deposition of fine and ultrafine airborne particulates of crystalline silica in the lung, affecting alveolar macrophages,

epithelial cells, and fibroblasts. Several *in vitro* and *in vivo* studies revealed a rapid progression of cell death due to silica exposure, with a significant amount of apoptosis [Hamilton *et al.*, 2008]. Due to a chronic situation of ROS formation, abnormal cell proliferation and persistent inflammation in the alveoli and bronchioles, silicosis takes place with the development of fibrotic scar tissue impairing the respiratory function as well as the mucocilliary escalator [van Berlo *et al.*, 2010]. Furthermore, exposures are strongly associated with lung cancers leading to the classification of crystalline silica as a Class I carcinogen in 1997 by the International Agency for Research on Cancer [IARC 1997]. Therefore, silica particles are used as benchmark particle to investigate the adverse effects of other particulate matter. A hazard identification of other particles regarding their potential to induce pulmonary fibrosis may be linked to the detection of the particulate ability to induce apoptosis in macrophages [Iyer *et al.*, 1996].

1.3 Macrophages – scavengers and more

Macrophages are typical scavenger cells functionalised for the removal of cellular debris, foreign material and infectious intruders. Throughout the mammalian organism, macrophages serve versatile functions as a significant part of both the innate and adaptive immune system [Kende 1982]. They are highly heterogeneous cells with distinct functions that are strongly influenced by local microenvironmental signals. Depending on the organ in which they are based, these phagocytic cells have specific names, such as Kupffer cells (in the liver), microglia (in neural tissue) or alveolar macrophages in the distal region of the lung [Murray *et al.,* 2011].

Like all cells of the immune system, macrophages are originally derived from multipotent haematopoietic stem cells in the bone marrow, as shown in Figure 1-5. During haematopoiesis, multipotent stem cells develop in either the progenitor cells of lymphocytes, or the myeloid progenitors [Nelson 1990]. This lineage splits into the development of erythroid cells and the myelocytes, which comprise the granulocytes. Monocytes are the direct precursor cells of macrophages, circulating in the blood until they get recruited by inflammatory signals to enter damaged or infected tissues. The subsequent differentiation into the specific mature macrophages is mediated by distinct growth factors [Smith 1990]. Macrophage differentiation is associated with the expression of very special surface-markers which relate to cell migration, adhesion or receptor-molecules. The application of monoclonal antibodies against these specific antigens is a useful tool in macrophage characterization [Martinez-Pomares *et al.,* 1996].

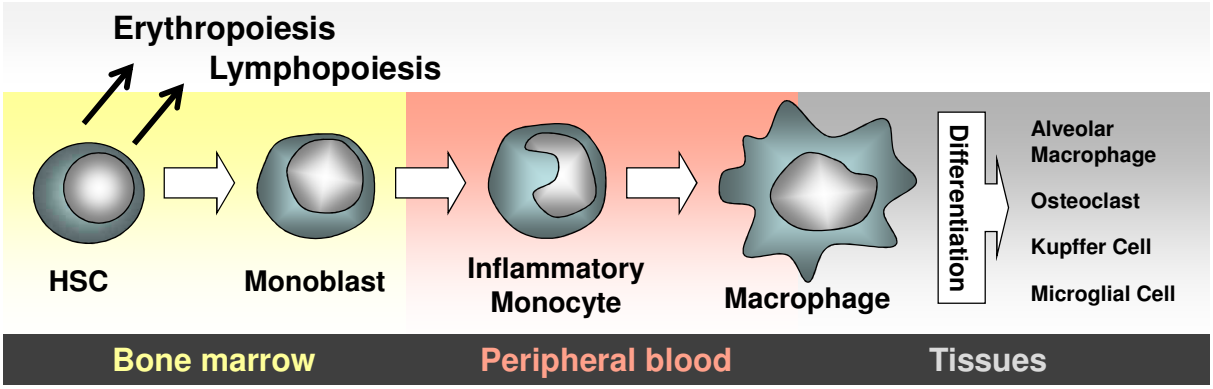

Figure 1-5: Maturation of macrophages during myelopoiesis derived from haematopoietic stem cells (HSC).

As a typical member of the mononuclear phagocyte system [van Furth 1982], the primary assignment of a macrophage is phagocytosis. The ingestion of pathogens forms the first line of the innate immune system proceeding in several steps initiated by receptor recognition and the subsequent cytoskeleton rearrangements [Park 2003]. Trapped in phagosomes, the intruders become digested by fusion with lysosomes forming phagolysosomes [Aderem *et al.,* 1999]. Since macrophages belong to professional antigen-presenting cells, digested protein fragments get processed and exposed via the major histocompatibility complex class II. This extracellular antigen presentation is part of the defence mechanism of the adaptive immune system. Naive T helper cells may recognize the specific epitope as a non-self antigen and stimulate the respective B-cells to produce antibodies against the pathogen. Phagocytosis by macrophages is facilitated after opsonisation of pathogens [Aderem *et al.,* 1999].

Depending on exogenous immune stimuli, macrophages display a remarkable plasticity in changing their phenotype and physiology that allows them to efficiently respond to environmental signals [Mosser *et al.,* 2008]. According to their specific function, macrophages are classified in two major subgroups: M1 macrophages are known as the classical pro-inflammatory activated immune effector cells, whereas M2 macrophages are anti-inflammatory immune regulators involved in wound healing. Correspondingly, these cell types are modulated to release a distinct repertoire of cytokines, as discussed in the following section.

1.3.1 Cytokines – the immunomodulating signalling

Cytokines are intercellular signalling molecules classified as soluble peptides or glycoproteins with extensive functions in homeostasis. Cell growth, differentiation, and even haematopoiesis are regulated by cytokines [Geissmann *et al.,* 2010]. During immune responses, a complex network of cytokine interactions harmonises cells to react against pathological events. All nucleated cells, but mainly endo-/epithelial cells, lymphocytes and especially activated macrophages are producers of cytokines. There are distinct cell-surface receptors with cytokine-affinity mediating the respective response of target cells [Debets *et al.,* 1996]. One prevalent nature of cytokines is pleiotropism, inducing varied effects depending on the target cells receptor configuration, as well as redundancy, what means that several cytokines can take over each other's effects [Ozaki *et al.,* 2002]. The binding of a cytokine to a corresponding receptor may initiate intracellular mitogen activated protein (MAP) kinase cascades through phosphorylation. The resulting activation of transcription factors like nuclear factor κB (NFκB) may lead to the expression of further surface receptors, the production of other cytokines or the respective inhibitors [Curfs *et al.,* 1997].

Cytokines have been classified according to various characteristics, but none of the systems is entirely satisfying. Even a strong structural similarity of different cytokines may not correlate to their function. Here, a characterisation only based on the major functions for respective groups of cytokines is used.

The effects mediated by *interferons* are geared to trigger protective defences for host cells affected by microbial and viral pathogens or tumour cells. There are systemic effects like the development of fever symptoms and the activation of immune cells as well as upregulations in antigen presentation and interrelations in p53 signalling pathways with functions in tumour suppression [Takaoka *et al.,* 2003]. *Interleukins* are the main cytokines coordinating the interactions between leucocytes, but are also involved in systemic effects like fever, blood flow or increasing tissue-permeabilization synergistic with *tumour necrosis factors* (TNFs) [Kaufmann 1987]. It is obvious, that each cytokine acts in a predominantly pro- or rather anti-inflammatory manner. Interleukin-10 for instance inhibits a number of cytokines like IL-1β or TNF-α, which are members of the acute phase proteins in response to inflammation. The migration of immune cells is controlled by chemotactic cytokines, i.e. *chemokines*, on the basis of attractant concentration levels [Ben-Baruch *et al.,* 1995]. The recruitment of phagocytes to a site of infection is mediated by Macrophage Inflammatory Proteins (MIP) and Monocyte Chemotactic Proteins (MCP). In case of an exceeding requirement of further

immune cells, haematopoietic stem cells differentiate into the respective type of cell by the action of *colony-stimulating factors* (CSFs) [Curfs *et al.,* 1997].

The fact, that each cytokine release entails the release of further cytokines resulting in cascades of immune cell activation, implies a source of increased oxidant stress, which in turn induces the release of inflammatory cytokines. Therefore, these relationships are on focus in pathologies of chronic inflammation [Imrich *et al.,* 2007].

1.4 Reactive oxygen species and oxidative stress

A number of essential processes in cell biology are based on redox (reduction-oxidation) reactions, operating with series of complex electron transfers. Endogenous cellular reactions and a wide range of environmental factors are sources of oxidants. Since these molecules are highly reactive, they exhibit an inherent risk for cellular integrity. Adverse cellular effects of free radicals may be the consequences of lipid peroxidation, resulting in membrane damage, protein oxidation leading to denaturation, or oxidative DNA damage [Cheeseman *et al.,* 1993]. The main oxidants in eukaryotic cells are reactive oxygen and reactive nitrogen species (ROS/RNS). Both are commonly denominated as ROS since RNS are also oxygen-derived. Disturbances in the normal cellular redox homeostasis may lead to "oxidative stress", a systemic imbalance in favour to ROS formation contrary to detoxification and repair mechanisms [Sies *et al.,* 1985]. Free radicals are defined as atoms or molecules that contain one or more unpaired electrons [Stohs 1995]. The most important reactant in the biosphere is oxygen with its bi-radical nature [Cheeseman *et al.,* 1993]. Hydroxyl ($HO^{\bullet}$), superoxide ($O_2^{-\bullet}$), nitric oxide ($NO^{\bullet}$), and peroxyl ($RO_2^{\bullet}$) are prevalent free radicals in living organisms, whereas peroxynitrite ($ONOO^-$), hypochlorous acid (HOCl), hydrogen peroxide (H_2O_2), singlet oxygen ($^1O_2$), and ozone (O_3) are non-free radicals, but easily converted into such and therefore commonly called ROS [Poljsak *et al.,* 2012]. In this connection, the Fenton reaction (Equation 1 and 2) is presumably the main endogenous source of free radicals, since hydrogen peroxide constitutively arises as by-product of aerobic metabolism [Wardman *et al.,* 1996].

$$(1)\ Fe^{2+} + H_2O_2 \rightarrow Fe^{3+} + HO^- + HO^{\bullet}$$

$$(2)\ Fe^{3+} + H_2O_2 \rightarrow Fe^{2+} + HOO^{\bullet} + H^+$$

Iron is an essential element of biological processes ubiquitary present in proteins, enzymes and cofactors [Wang *et al.,* 2011]. Therefore, the content of intracellular free iron is tightly regulated by sequestration in ferritin, the major intracellular iron storage protein [Pantopoulos *et al.,* 1995]. Disturbances of this balance are also relevant for particle toxicology: One mechanism of ROS formation due to particulate matter is described as Fenton-like reaction, since particle surfaces may contain transition metal ions [Knaapen *et al.,* 2004; Schins *et al.,* 2007]. Not only iron, but also nickel, copper and vanadium can act as catalysts like the dismutation redox reaction mentioned, forming out one peroxide radical under consumption of two hydrogen peroxides.

The DNA molecule is highly susceptible to ROS-induced reactions resulting in oxidation, nitration, depurination, methylation and deamination [Knaapen *et al.,* 2006]. Whilst some radicals like superoxide are less reactive, the hydroxyl radical is the most potent generator of multitude DNA transformations affecting all four bases [Pryor 1988]. 8-hydroxydeoxyguanosine (8-OHdG) is one of the major DNA derivates serving as proficient marker for oxidative stress and the efficiency of the well-studied corresponding repair system [Kasai 1997] (Figure 1-6). Because of its extremely high reactivity (i.e. short half-life) of hydroxyl radicals they can only induce 8-OHdG lesions when they are generated in close proximity to the DNA [Pryor 1988].

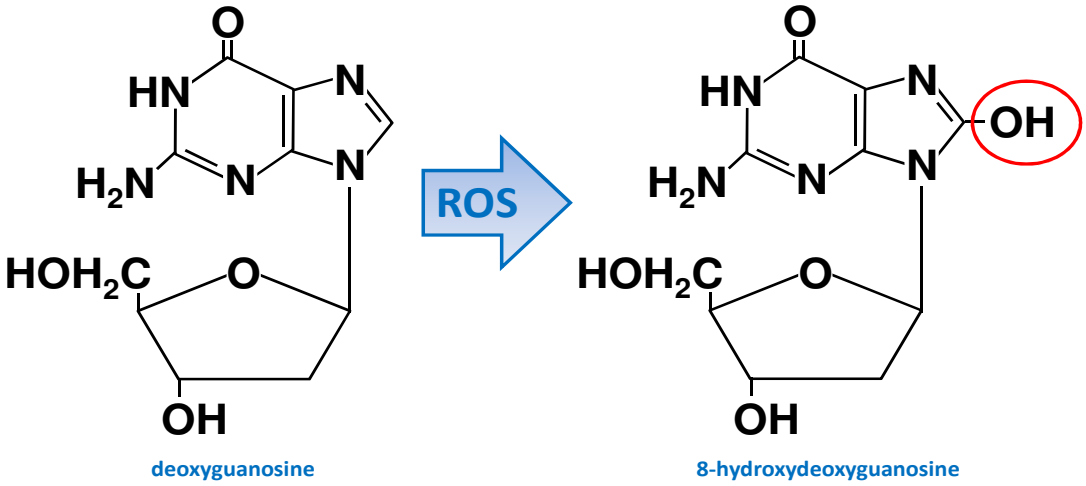

Figure 1-6: Formation of 8-hydroxydeoxyguanosine by oxygen radicals.

Due to a reaction to various chemical, physical or inflammatory stimuli cells are capable to release ROS, generated by membrane bound enzyme complexes of the NOX (nicotinamide adenine dinucleotide phosphate (NADPH) oxidase) family [Jiang *et al.,* 2011]. Also particles like silica are known to activate this enzyme complex [van Berlo *et al.,* 2010], and it is also

discussed as an important factor in the toxicity of nanoparticles [Unfried *et al.,* 2007]. It contains seven members: NOX1, NOX2, NOX3, NOX4, NOX5, DUOX1 and DUOX2, with NOX2 especially found in professional phagocytes contributing in host defence. During phagocytosis, the highly NOX2-containing outer membrane becomes the inner membrane of phagosomes, producing the so called "respiratory burst" due to a systemic activation of the enzyme [de Oliveira-Junior *et al.,* 2011]. Under consumption of NADPH, NOX2 catalyses the reduction of oxygen to superoxide, resulting in a cascade of ROS formation with microbicidal, tumouricidal and inflammatory activity. Upon cell activation, the inactive NADPH oxidase enzyme complex perform an assembly of its subunits as depicted in Figure 1-7. The catalytic component NOX2 is also termed as gp91^{phox} (91-kDa glycoprotein of phagocyte oxidase), forming out the heterodimer flavocytochrome b_{558} in association with p22^{phox} in the membrane of resting cells. Cytochrome b_{558} is the terminal electron donor to oxygen in the active enzyme [Nauseef 2008]. Phosphorylation of the cytosolic p47^{phox} initiates the assembly of the other cytoplasmic compounds including p67^{phox}, p40^{phosx}, and GTPases (Rac 1/2). The interaction with cytochrome b_{558} results in the active NADPH oxidase [Babior 2004].

Superoxide which is generated due to NADPH oxidase activation following phagocytotic processes is described to cause apoptosis [Park 2003].

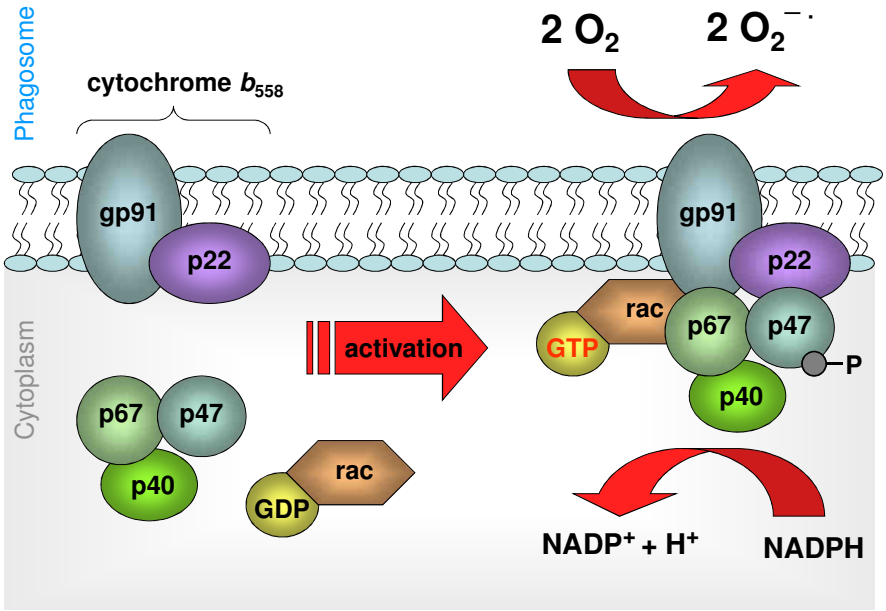

Figure 1-7: Assembly of the phagocyte NADPH oxidase during activation.

1.4.1 Cellular antioxidant defence mechanisms

Beside endogenous inducers of ROS, mainly derived from aerobic metabolism or activated phagocytes, cells are additionally confronted with multiple exogenous stressors that can cause ROS like inhaled particulate matter, UV-irradiation, ozone, a number of drugs or nutritional compounds [Jaeschke *et al.,* 2002; Lodovici *et al.,* 2011; Poljsak *et al.,* 2012]. The constitutive presence of reactive oxygen species is not mandatory harmful to cells. Many biological processes are under control of these reactants, acting as secondary messengers in highly specific signalling pathways with distinct enzyme configuration [Finkel 1999]. The field of "redox signalling" describes for instance the involvement of apoptotic processes, activated by stress-responsive regulators [Wang *et al.,* 2009], as well as the role of redox-sensitive transcription factors via MAP kinase pathways activating nuclear factor κB (NFκB). Resulting cell responses may encompass an altered expression of endogenous antioxidants, the stimulation of mitochondrial biogenesis [Jacobs *et al.,* 2009], or the formation of pro-respective anti-inflammatory mediators apparent in signs of chromatin remodelling [Rahman *et al.,* 2004].

Moderate oxidative stress can induce the transcription of stress defence genes, part of the "antioxidant system" protecting cellular compounds from oxidative damage. A non-enzymatic pool of radical neutralising agents include the small thiol molecule thioredoxin, located in the inner mitochondrial membrane for the reduction of hydrogen and lipid peroxides as well as proteins with oxidatively modified sulfhydryl residues [Thannickal *et al.,* 2000]. Furthermore, reduced glutathione (GSH) is the major antioxidant in mammalian cells. Amongst these, several antioxidant enzymes directly neutralise radicals. The superoxide dismutase (SOD) converts the superoxide anion into hydrogen peroxide, which in turn can be detoxificated into H_2O and O_2 by catalase, peroxiredoxin or glutathione peroxidase. In the latter process, GSH serves as substrate which is oxidised into glutathione disulfide (GSSG). To maintain a sufficient GSH level for ROS removal in the cytoplasm, cells are capable to recover GSSG by GSH reductase. In addition, GSH biosynthesis is catalysed by gamma-glutamylcysteine synthetase (γ-GCS) and controlled by feedback inhibition of glutathione itself. In laboratory applications, the ratio between GSH to GSSG serves as a useful marker to determine the cellular redox status [Pastore *et al.,* 2001].

Phase II detoxifying enzymes, primary assigned as xenobiotic metabolising enzymes, are now recognised as antioxidant enzymes in maintaining redox-homeostasis [Thimmulappa *et al.,* 2002]. Along with the classical conjugating enzymes (glutathione S-transferases and UDP-

glucuronosyl transferases), there are some which contribute to biosynthesis or recycling of thiols (γ-GCS or GSH/thioredoxin reductases). Others are involved in the reduction of reactive intermediates like NAD(P)H, and stress response proteins [Talalay 2000]. Besides the ferritin mentioned above, one further stress response protein is heme oxygenase-1 (HO-1). It catalyses the conversion of heme, a potent pro-oxidant, into carbon monoxide and biliverdin, which is a precursor of bilirubin with antioxidant properties [Tenhunen *et al.*, 1968]. Regarding these cellular responses to oxidative stress on transcription level, the transcription factor nuclear factor erythroid-derived 2 related factor 2 (Nrf2) takes a key position in the expression of cytoprotective genes [Nguyen *et al.*, 2009]. Nrf2 is found ubiquitary in all tissues, but is highly active in those tissues related to detoxification (liver and kidney) and those exposed to the environment (skin, intestinal tract and lung). The activity of Nrf2 is regulated by the cytoplasmic zinc-metalloprotein Keap1 (Kelch-like ECH-associated protein 1), as depicted in Figure 1-8.

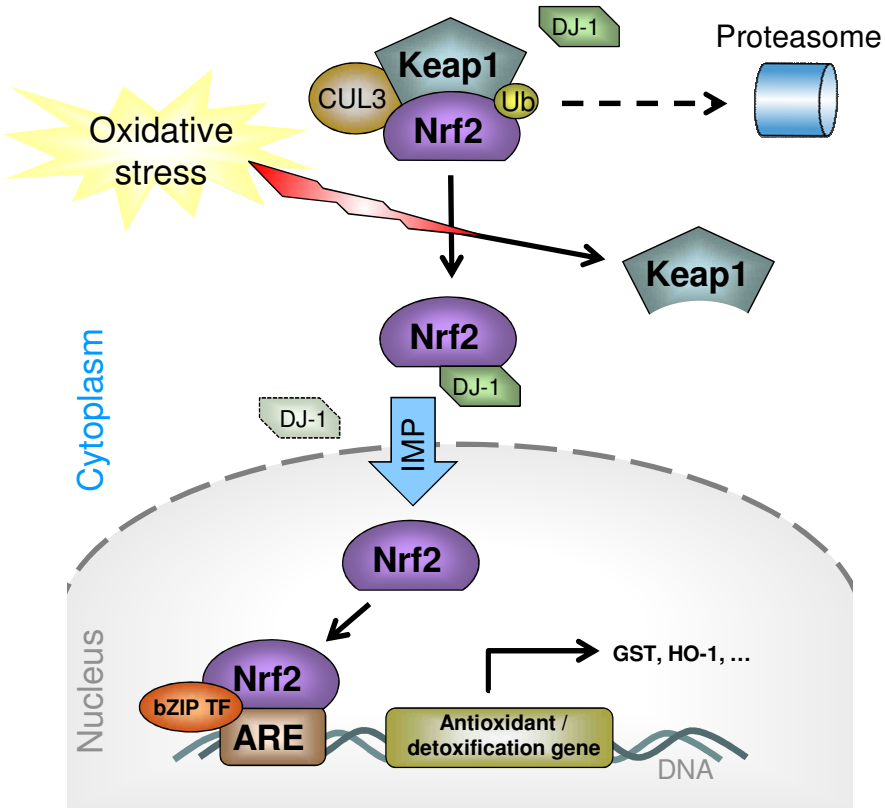

Figure 1-8: Under basal conditions, ubiquitination (Ub) of Nrf2 and subsequent proteasomal degradation takes place by CUL3 E3 ubiquitin ligase in a complex with its adaptor protein Keap1. In response to oxidative stress, dissociation of the Nrf2-Keap1 complex and Nrf2-stabilization by DJ-1 facilitates the translocation into the nucleus via the importin complex (IMP). Nrf2 heterodimerizes with other basic leucine zipper transcription factors (bZIP TF). Binding to ARE stimulates the transcription of antioxidant and detoxification genes.

Under normal conditions, Nrf2 is expressed constitutively in the cell with a rapid turnover due to proteasome degradation with a half-life less than 20 min [Kobayashi *et al.*, 2004]. Ubiquitylation takes place within a complex of Keap1 molecules during cullin-based E3 ligase activity [Kobayashi *et al.,* 2004; McMahon *et al.,* 2006]. Keap1 serves as a sensor for electrophilic substances and mediates the release of Nrf2 out of the complex. After translocation to the nucleus, the transcription factor can bind to the antioxidant response element (ARE) and stimulate gene expression. Since many phase II genes are driven by this *cis*-acting element, ARE is on central relevance regulating the antioxidant gene expression, and Nrf2 is in turn an essential element for regulation of the ARE [Itoh *et al.*, 1997; Zhang *et al.*, 2004].

1.5 Apoptosis – the cellular self-destruction

The concept of "programmed cell death" in terms of a well-defined process of cell death was established in 1964 by Lockshin and coworkers [Lockshin *et al.,* 1964]. In 1972, the conventional term "apoptosis" was coined by Kerr and colleagues according to the association of falling leaves reflected in the Greek origin ("apo": away from; "ptosis": to fall) [Kerr *et al.,* 1972].

Considered as a central feature of multicellular organisms in embryonic development, the maturation of the adaptive immune system, adult tissue homeostasis and normal cell turnover, apoptosis is known to be a well-regulated system conserved and refined during evolution [Vaux 1993; Tadakuma 1994; Tittel *et al.,* 2000]. Dysregulations of this process are associated with prevalent disorders, including autoimmune and degenerative diseases as well as cancer, and therefore form a central subject of biomedical research [Thompson 1995; Favaloro *et al.,* 2012]. These pathological processes are also described in relation to particle exposure [Stone *et al.,* 2007; Chang 2010; Win-Shwe *et al.,* 2011]. Therefore, investigations on apoptotic mechanisms triggered by particles will increase our understanding in nanotoxicology.

1.5.1 Morphology of apoptotic cells

The progression of apoptosis was defined as a type of programmed cell death. Morphologically, biochemically, and molecularly it is very different from necrosis, the traumatic form of cell death [Kerr *et al.,* 1972]. Typical morphological and biochemical hallmarks are illustrated in Figure 1-9. Cells undergoing apoptosis are performing controlled steps of auto digestion. First signs are shrinking by contraction of the cytoplasm concomitant with a loss of adherence from the cell's assembly [Van Cruchten *et al.,* 2002]. Chromatin as well as the cytoplasm becomes condensated. The genomic DNA gets fragmented by cleavage between nucleosomes resulting in fragments of 185 bp [Kerr *et al.,* 1991]. Hence, the plasma membrane as well as the nucleus form buds (zeiosis) and break down into vesicles containing functional organelles.

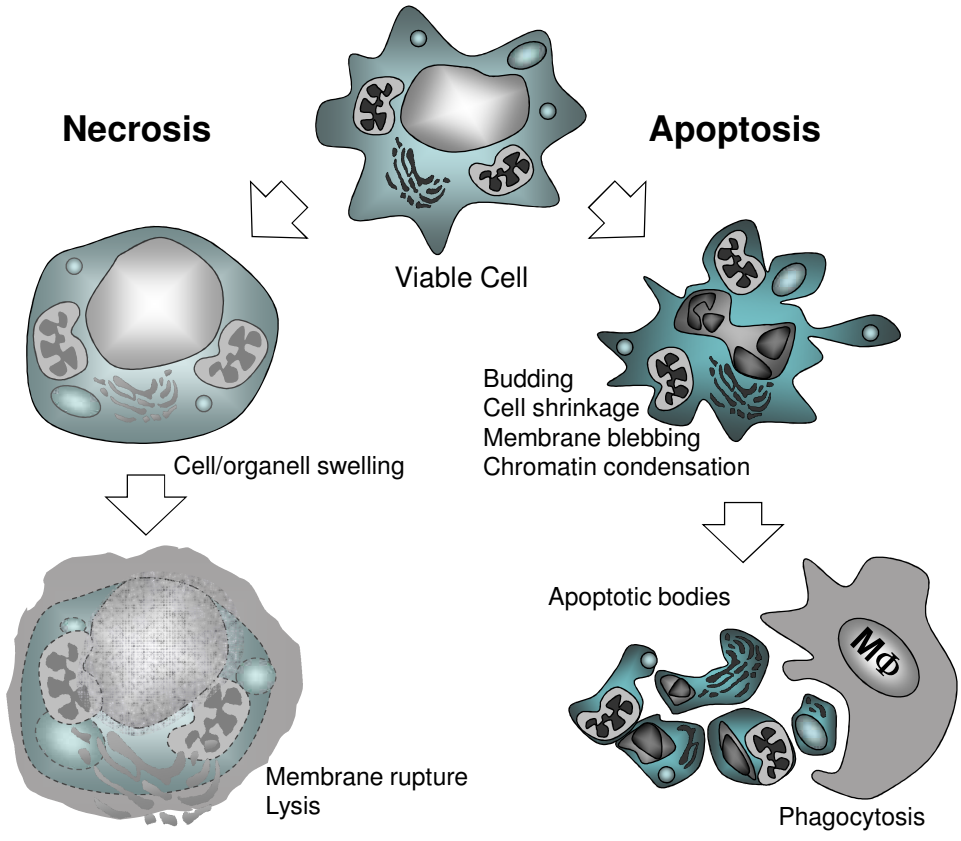

Figure 1-9: Morphological hallmarks of the apoptotic and necrotic cell death process. During apoptosis, cellular shrinking, chromatin condensation, membrane blebbing and the subsequent formation of apoptotic bodies containing intact organelles does not trigger inflammatory processes in the cells environment. Apoptotic bodies exhibit "eat me" signals to get phagocyted by macrophages (MΦ). In contrast, the necrotic cell death is characterised by swelling, uncontrolled membrane ruptures, and the release of lysed contents into the surrounding tissue.

Changes in the composition of the plasma membrane, especially phosphatidylserine-externalisation, act as the so called “eat-me“-signal for phagocyting cells engulfing the apoptotic bodies [Fadok *et al.,* 1992]. Therefore, no cell content is released into the surrounding tissue which would lead to inflammatory processes [Fink *et al.,* 2005]. In contrast, this is the case during necrosis, the accidental cell death. In merely a passive result of a major insult the necrotic cell including their organelles swells up resulting in membrane ruptures and the uncontrolled release of cellular contents into the cell’s environment [Majno *et al.,* 1995]. Surrounding cells may suffer substantial damage due to a strong inflammatory response.

1.5.2 Caspases – the executioners of apoptosis

The typical hallmarks of apoptosis are mediated by a family of cysteine proteases, designated as “caspases” (***c****ysteinyl* ***a****spartate–****sp****ecific prote****ases***). The denotation is composed according to the obligatory cysteine-residue within the conserved active-site of the large subunit of the enzyme (QACXG, see Figure 1-10A) and its distinct cleavage pattern of substrates after asparagine-residues. Since caspases are synthesised as zymogens, these catalytically inactive cytoplasmic procaspases need to be activated during the apoptotic signalling cascade [Nicholson *et al.,* 1997]. Cleavage at the specific Asp-X bonds removes the prodomain and leads to formation of the mature caspase, composed of a heterotetramer of two small (p10) and two large (p20) subunits.

Historically, investigations of the nematode *Caenorhabditis elegans* mapped out a distinct number of somatic cells which become eliminated by apoptosis [Ellis *et al.*, 1991]. The identification of four genes required for the progression of programmed cell death and its regulation revealed highly conserved motifs through evolution and led to the elucidation of components forming out the death machinery [Yuan *et al.*, 1993; Hengartner *et al.*, 1994]. Hence, the worms cysteine protease ced-3 was found to be homologue to the first mammalian caspase described at that time, caspase-1. Currently, twelve different caspases have been described in humans, with additionally two members only identified in mice [Lavrik *et al.*, 2005]. The numbers within their nomenclature follow the order of publication. A distinction is drawn between caspases functionally involved in the proteolytic maturation of proinflammatory cytokines versus the caspases functionalised in apoptosis (Figure 1-10B). Initiator procaspases contain specific protein-protein interaction domains (CARD, DED) that are essential for their activation (cf. the following paragraph 1.5.3 Signalling pathways of apoptosis).

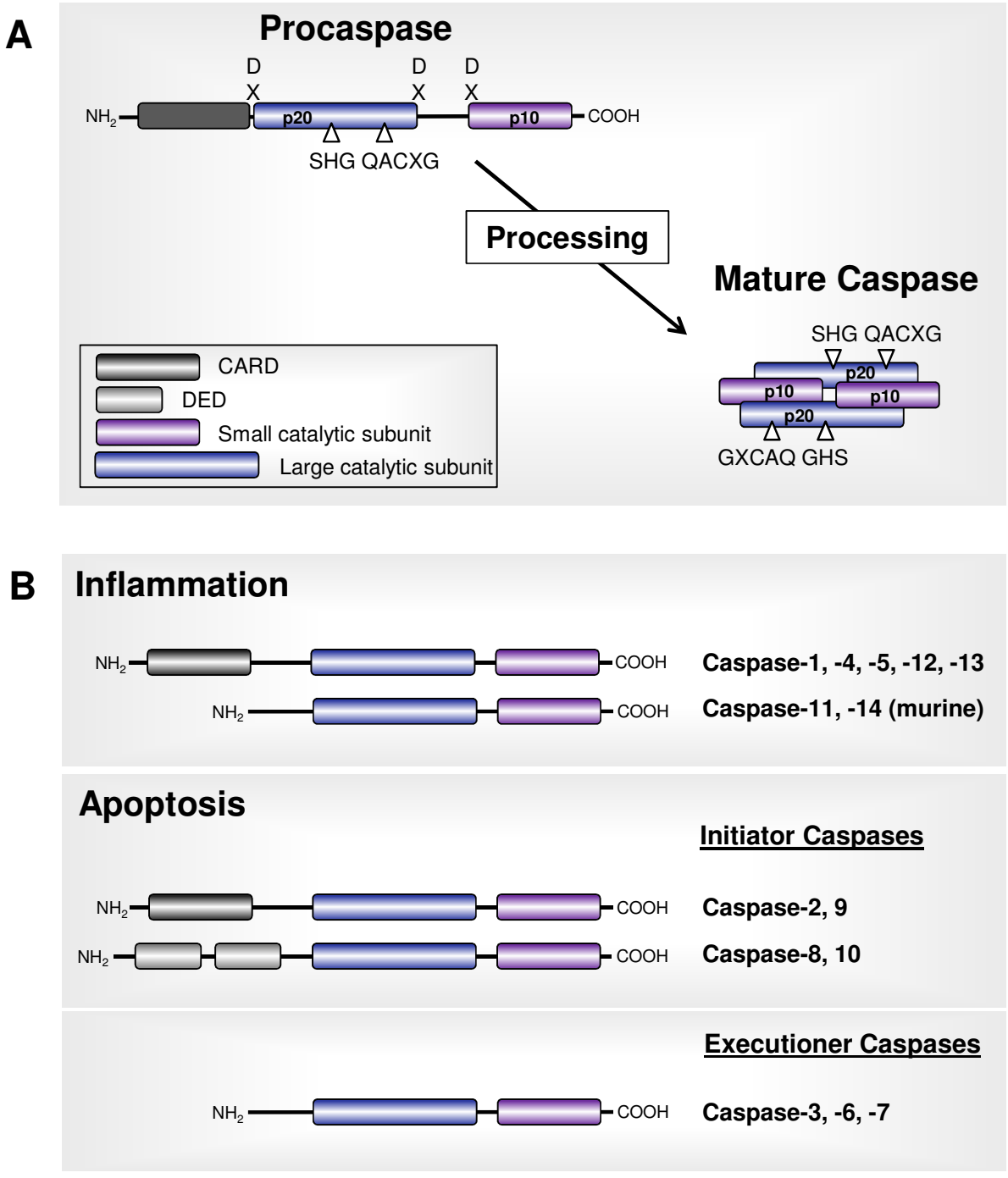

Figure 1-10: Caspase structure. (A) Procaspases are activated by cleavage at their specific Asp-X bonds. The mature caspase is composed of two heterodimers, forming out the active centre of residues located at the large subunits. (B) The caspase family comprises 14 members so far, which can be classified according to their role in apoptosis or inflammation.

1.5.3 Signalling pathways of apoptosis

The apoptotic cell death program is a highly conserved process and tightly regulated by a multitude of factors. In most mammalian cells, the required machinery of proteins is constitutively expressed and therefore prepared for a rapid response to death-inducing stimuli [Raff *et al.,* 1994]. These stimuli may occur from various sources within the cell or from outside. A certain trigger of apoptosis is DNA damage caused by failings in DNA repair mechanisms, exposure to cytotoxic drugs or irradiation. DNA damage and initiation of apoptosis are linked by the tumour suppressor p53, a transcription factor named the "guardian of the genome" [Lane 1992].

There are two main signalling cascades as schematically depicted in Figure 1-11 and described in the following. Both the extrinsic and the intrinsic pathway of apoptosis can trigger the activation of executioner caspases [Zimmermann *et al.,* 2001]. The more direct extrinsic one is mediated by activation of death receptors, a specific subgroup of the TNF-receptor superfamily [Schulze-Osthoff *et al.,* 1998]. These transmembrane receptors form a trimeric complex upon extracellular ligand binding followed by the recruitment of adapter proteins at their specific death domains. Additionally, the adaptors contain death effector domains matching those present at procaspase-8 in a homophilic interaction. In this formation, called the death-inducing signalling complex (DISC), the zymogen gets cleaved autoproteolytically and is released as the activated heterotetrameric caspase-8.

In apoptosis research, cells are classified in two types [Scaffidi *et al.,* 1999]. In such referred to type I cells, activation of the initiator caspase-8 directly processes downstream effector caspases resulting in cell death. In contrast, the so-called type II cells are not suffering a lethal caspase cascade upon receptor signalling on its own; the signal needs to be amplified by the mitochondria. Subsequent signalling cascades are linked by members of the Bcl-2 family. These are the mammalian homologues of the cell death involved proteins of *C. elegans*; i.e. egl-1, representative for the pro-apoptotic BH3-only proteins, and ced-9 belonging to the anti-apoptotic Bcl-2 family [Hengartner *et al.,* 1994]. The balance and location of these two subgroups is of central relevance in regulatory mechanisms of apoptosis signalling, and determines the fate of the cell [Borner 2003]. In type II cells, activated caspase-8 cleaves the BH3-only protein Bid into its truncated form tBid, which translocates to the mitochondria and provokes the pro-apoptotic Bcl-2 family members Bak and Bax in mitochondrial pore formation [Korsmeyer *et al.,* 2000]. Pro-survival antagonists of this process are the Bcl-2 family members Bcl-2 and Bcl-XL [Strasser 2005].

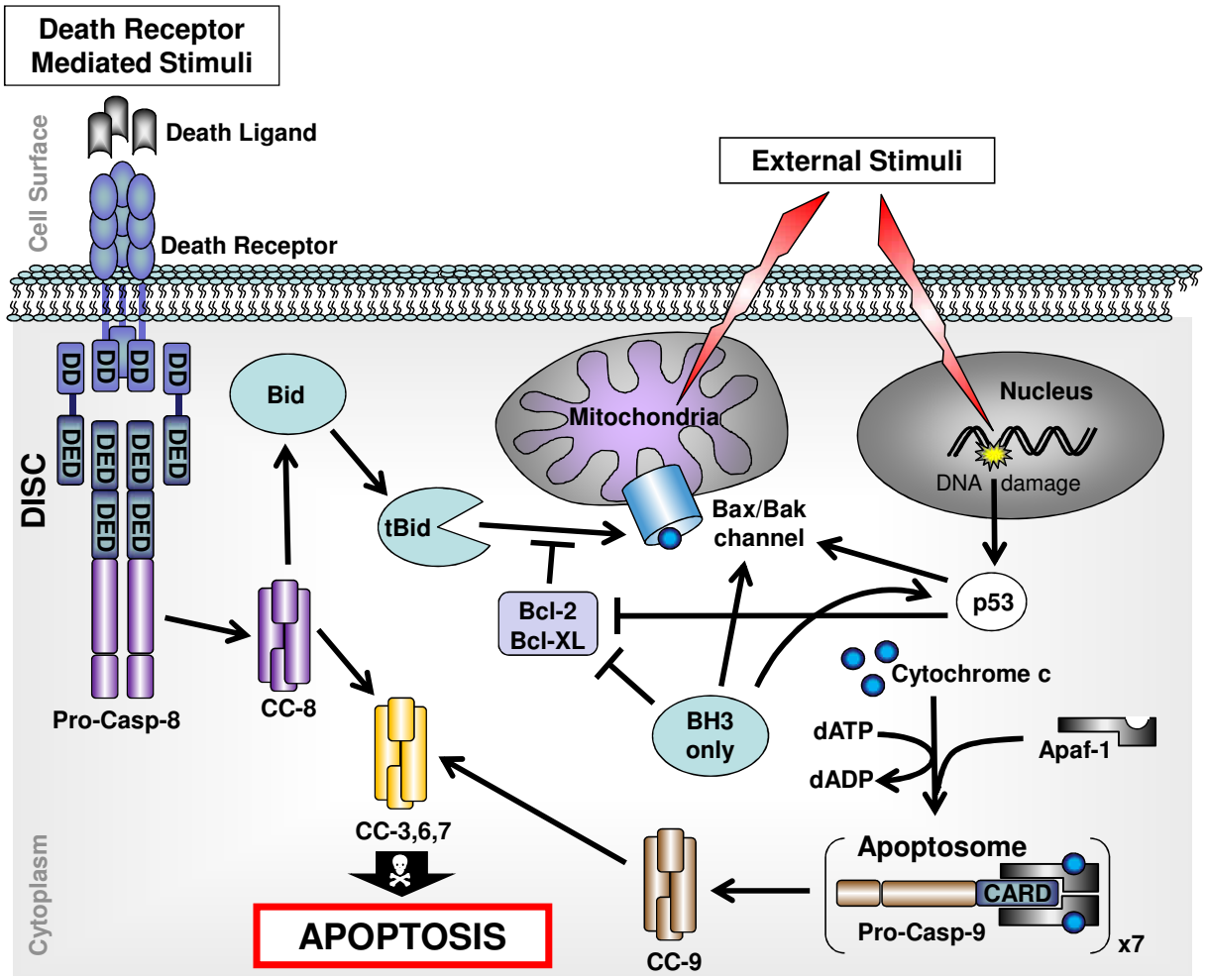

Figure 1-11: Schematic illustration of the major apoptosis signalling pathways. The "extrinsic signal" can be mediated by ligation of a subgroup of the tumour necrosis factor receptor (TNF-R) family, called "death receptor" (e.g. CD95/Fas/APO-1 or TNFR1). Activated pro-caspase-8 ("cleaved caspase-8", CC-8) may trigger the caspase-cascade of executioner caspases-3, -6 and -7 resulting in apoptosis (Type I cells), or excite the "intrinsic pathway" of apoptosis (Type II cells). This mitochondria-driven pathway may also be triggered by further stress stimuli and is tightly regulated by members of the Bcl-2 protein family. Bcl-2 and Bcl-XL are examples of pro-survival stimulators, whereas members of the BH3-only subgroup like Bid, Bax or Bak act in a pro-apoptotic manner. Cytoplasmic accumulation of the transcription factor p53 due to DNA damage may also trigger the intrinsic pathway of apoptosis. Mitochondrial release of cytochrome c may lead to apoptosome-formation resulting in a caspase-9 initiated effector caspase cascade.

However, mitochondrial membrane permeabilization accompanied by disruption of the mitochondrial inner transmembrane potential can be a consequence of death receptor signalling as well as an intrinsic stimulation of cell death. Damage of the outer mitochondrial membrane provokes the release of pro- and anti-apoptotic proteins into the cytoplasm [Hirsch *et al.,* 1997]. Hence, cytochrome c, a member of the mitochondrial respiratory chain in vital cells, assumes the role of a second messenger when released into the cytosol. Under

consumption of dATP, cytochrome c provokes a conformational change of the adapter protein Apaf-1 (***a****poptotic* ***p****rotease* ***a****ctivating* ***f****actor*), the mammalian homologous of ced-4 from *C. elegans*. Activated Apaf-1 in turn starts the formation of the apoptosome [Zou *et al.,* 1999]. This high molecular heptameric holoenzyme complex then includes procaspase-9, which thereby gets activated to mature caspase-9 [Cain *et al.,* 2002]. Once the initiator caspase-9 is activated, the caspase cascade runs by cleavage of the executioner caspases-3, -6 and -7, which in turn proceed in the cleavage of substrates leading to apoptotic features of cell death.

1.6 Aim of the thesis

As discussed in the previous paragraphs, inflammation and oxidative stress are implicated in various severe lung diseases, e.g. fibrosis, induced by classical particles such as silica and asbestos. Herein, apoptosis of macrophages has emerged as a key event that determines the extent and severity of these pathological responses. However, for novel engineered nanoparticles the significance of apoptotic processes in this cell type, and possibly associated health effects are still poorly understood.

The aim of the thesis was to investigate the strengths and mechanisms of pro-apoptotic responses in macrophages by a set of particulate materials in relation to their physico-chemical properties. Therefore, the following specific research questions have been addressed:

1.) Are currently applied methods for the investigation of *in vitro* cell death, including commercially available tests, appropriate for the testing of particles, including those in nano-size dimensions?

2.) Are the formation of reactive oxygen species and the associated induction of oxidative stress implicated in pro-apoptotic responses in nanoparticle exposed macrophages?

3.) Can the measurement of nanoparticle-induced apoptosis in macrophages *in vitro* be applied to predict nanoparticle-induced pathogenicity, specifically the induction of inflammatory and pro-fibrotic responses, in the mouse lung?

Accordingly, three specific studies were designed in the framework of this thesis.
In the first study (**Chapter II**) a selection of six types of particles was used to establish a valid test battery to address the apoptotic potential of particulate samples in RAW 264.7 macrophages. With inclusion of appropriate negative and positive controls, specific attention was paid to detect distinct particle-interferences with the particular principle of the assay. Where possible, assays were modified to eliminate the identified artefacts. The selection of the particle types that was made for this study allowed for the investigation of the impact of physico-chemical properties on assay conditions as well as on toxic effects. The crystalline SiO_2 sample DQ12, well known as apoptosis inducer, served as a particulate positive control

and was used to compare with a sample of amorphous ultrafine SiO_2. In order to further investigate the effect of particle size, one fine and one ultrafine TiO_2 sample was used. Finally, two more metallic nanoparticles, i.e. ZnO and MgO, were investigated as monoxides of a comparable primary particle size.

In order to investigate the mechanisms of ZnO-induced apoptosis in macrophages, which was identified in the first study as the most potent particle sample, a follow-up study was performed (**Chapter III**). To address the question, whether oxidative stress is responsible for the toxicity of ZnO particles, primary bone-marrow derived macrophages from two different knockout mouse models were used. The mouse models were chosen to provide insights in the role in ZnO-induced apoptotic processes of the phagocytic $p47^{phox-/-}$ NADPH oxidase on the one hand and the redox-sensitive transcription factor Nrf2 on the other hand. Jurkat T lymphocytes deficient in caspase-9, and therefore resistant to apoptosis, were included to reveal the involvement of the intrinsic mitochondrial apoptotic pathway.

In a third study (**Chapter IV**) two particulate samples of carbon nanotubes mainly differing in their length and agglomeration behaviour were investigated regarding their cytotoxic and in particular their apoptotic effects in the *in vitro* RAW 264.7 model in combination with evaluation of pathological endpoints *in vivo*. Therefore, it was decided to investigate the induction of apoptosis, inflammation and pulmonary fibrosis after pharyngeal aspiration of the carbon nanotubes in C57Bl/6J mice.

All together, the key goal of this thesis was to provide novel findings on the pro-apoptotic potential of particulate samples in macrophages as well as to obtain new insights in responsible underlying mechanisms, by using validated laboratory test systems and models.

1.7 References

Aderem, A and Underhill, DM (1999). Mechanisms of phagocytosis in macrophages. Annu Rev Immunol 17: 593-623.

Babior, BM (2004). NADPH oxidase. Curr Opin Immunol 16(1): 42-47.

Banerjee, R, Katsenovich, Y, Lagos, L, McIintosh, M, Zhang, X and Li, CZ (2010). Nanomedicine: magnetic nanoparticles and their biomedical applications. Curr Med Chem 17(27): 3120-3141.

Barone, PW, Baik, S, Heller, DA and Strano, MS (2005). Near-infrared optical sensors based on single-walled carbon nanotubes. Nat Mater 4(1): 86-92.

Ben-Baruch, A, Michiel, DF and Oppenheim, JJ (1995). Signals and receptors involved in recruitment of inflammatory cells. J Biol Chem 270(20): 11703-11706.

Block, ML and Calderon-Garciduenas, L (2009). Air pollution: mechanisms of neuroinflammation and CNS disease. Trends Neurosci 32(9): 506-516.

Borm, PJ (2002). Particle toxicology: from coal mining to nanotechnology. Inhal Toxicol 14(3): 311-324.

Borm, PJ, Robbins, D, Haubold, S, Kuhlbusch, T, Fissan, H, Donaldson, K, Schins, R, Stone, V, Kreyling, W, Lademann, J, Krutmann, J, Warheit, D and Oberdorster, E (2006). The potential risks of nanomaterials: a review carried out for ECETOC. Part Fibre Toxicol 3: 11.

Borner, C (2003). The Bcl-2 protein family: sensors and checkpoints for life-or-death decisions. Mol Immunol 39(11): 615-647.

BSI (2007). Terminology for nanomaterials. British Standards Institution, London PAS 136.

Burello, E and Worth, AP (2011). QSAR modeling of nanomaterials. Wiley Interdiscip Rev Nanomed Nanobiotechnol 3(3): 298-306.

Buzea, C, Pacheco, II and Robbie, K (2007). Nanomaterials and nanoparticles: sources and toxicity. Biointerphases 2(4): MR17-71.

Cain, K, Bratton, SB and Cohen, GM (2002). The Apaf-1 apoptosome: a large caspase-activating complex. Biochimie 84(2-3): 203-214.

Castranova, V and Vallyathan, V (2000). Silicosis and coal workers' pneumoconiosis. Environ Health Perspect 108 Suppl 4: 675-684.

Chang, C (2010). The immune effects of naturally occurring and synthetic nanoparticles. J Autoimmun 34(3): J234-246.

Cheeseman, KH and Slater, TF (1993). An introduction to free radical biochemistry. Br Med Bull 49(3): 481-493.

Curfs, JH, Meis, JF and Hoogkamp-Korstanje, JA (1997). A primer on cytokines: sources, receptors, effects, and inducers. Clin Microbiol Rev 10(4): 742-780.

de Oliveira-Junior, EB, Bustamante, J, Newburger, PE and Condino-Neto, A (2011). The human NADPH oxidase: primary and secondary defects impairing the respiratory burst function and the microbicidal ability of phagocytes. Scand J Immunol 73(5): 420-427.

Debets, R and Savelkoul, HF (1996). Cytokines as cellular communicators. Mediators Inflamm 5(6): 417-423.

Dockery, DW, Pope, CA, 3rd, Xu, X, Spengler, JD, Ware, JH, Fay, ME, Ferris, BG, Jr. and Speizer, FE (1993). An association between air pollution and mortality in six U.S. cities. N Engl J Med 329(24): 1753-1759.

Donaldson, K, Aitken, R, Tran, L, Stone, V, Duffin, R, Forrest, G and Alexander, A (2006). Carbon nanotubes: a review of their properties in relation to pulmonary toxicology and workplace safety. Toxicol Sci 92(1): 5-22.

Donaldson, K, Murphy, FA, Duffin, R and Poland, CA (2010). Asbestos, carbon nanotubes and the pleural mesothelium: a review of the hypothesis regarding the role of long fibre retention in the parietal pleura, inflammation and mesothelioma. Part Fibre Toxicol 7: 5.

Donaldson, K, Stone, V, Tran, CL, Kreyling, W and Borm, PJ (2004). Nanotoxicology. Occup Environ Med 61(9): 727-728.

Doria, G, Conde, J, Veigas, B, Giestas, L, Almeida, C, Assuncao, M, Rosa, J and Baptista, PV (2012). Noble metal nanoparticles for biosensing applications. Sensors (Basel) 12(2): 1657-1687.

Drummen, GP (2010). Quantum dots-from synthesis to applications in biomedicine and life sciences. Int J Mol Sci 11(1): 154-163.

Ellis, RE, Yuan, JY and Horvitz, HR (1991). Mechanisms and functions of cell death. Annu Rev Cell Biol 7: 663-698.

Fadok, VA, Voelker, DR, Campbell, PA, Cohen, JJ, Bratton, DL and Henson, PM (1992). Exposure of phosphatidylserine on the surface of apoptotic lymphocytes triggers specific recognition and removal by macrophages. J Immunol 148(7): 2207-2216.

Favaloro, B, Allocati, N, Graziano, V, Di Ilio, C and De Laurenzi, V (2012). Role of Apoptosis in disease. Aging (Albany NY) 4(5): 330-349.

Ferin, J (1994). Pulmonary retention and clearance of particles. Toxicol Lett 72(1-3): 121-125.

Fink, SL and Cookson, BT (2005). Apoptosis, pyroptosis, and necrosis: mechanistic description of dead and dying eukaryotic cells. Infect Immun 73(4): 1907-1916.

Finkel, T (1999). Signal transduction by reactive oxygen species in non-phagocytic cells. J Leukoc Biol 65(3): 337-340.

Frohlich, E and Roblegg, E (2012). Models for oral uptake of nanoparticles in consumer products. Toxicology 291(1-3): 10-17.

Geissmann, F, Manz, MG, Jung, S, Sieweke, MH, Merad, M and Ley, K (2010). Development of monocytes, macrophages, and dendritic cells. Science 327(5966): 656-661.

Gruner, G (2006). Carbon nanotube transistors for biosensing applications. Anal Bioanal Chem 384(2): 322-335.

Hamilton, RF, Jr., Thakur, SA and Holian, A (2008). Silica binding and toxicity in alveolar macrophages. Free Radic Biol Med 44(7): 1246-1258.

Hengartner, MO and Horvitz, HR (1994). C. elegans cell survival gene ced-9 encodes a functional homolog of the mammalian proto-oncogene bcl-2. Cell 76(4): 665-676.

Hirsch, T, Marzo, I and Kroemer, G (1997). Role of the mitochondrial permeability transition pore in apoptosis. Biosci Rep 17(1): 67-76.

Hoet, PH, Bruske-Hohlfeld, I and Salata, OV (2004). Nanoparticles - known and unknown health risks. J Nanobiotechnology 2(1): 12.

IARC (1997). IARC Working Group on the Evaluation of Carcinogenic Risks to Humans: Silica, Some Silicates, Coal Dust and Para-Aramid Fibrils. Lyon, 15-22 October 1996. IARC Monogr Eval Carcinog Risks Hum 68: 1-475.

ICRP (1994). Human respiratory tract model for radiological protection. A report of a Task Group of the International Commission on Radiological Protection. Ann ICRP 24(1-3): 1-482.

Imrich, A, Ning, Y, Lawrence, J, Coull, B, Gitin, E, Knutson, M and Kobzik, L (2007). Alveolar macrophage cytokine response to air pollution particles: oxidant mechanisms. Toxicol Appl Pharmacol 218(3): 256-264.

Itoh, K, Chiba, T, Takahashi, S, Ishii, T, Igarashi, K, Katoh, Y, Oyake, T, Hayashi, N, Satoh, K, Hatayama, I, Yamamoto, M and Nabeshima, Y (1997). An Nrf2/small Maf heterodimer mediates the induction of phase II detoxifying enzyme genes through antioxidant response elements. Biochem Biophys Res Commun 236(2): 313-322.

Iyer, R, Hamilton, RF, Li, L and Holian, A (1996). Silica-induced apoptosis mediated via scavenger receptor in human alveolar macrophages. Toxicol Appl Pharmacol 141(1): 84-92.

Jacobs, RA, Donovan, EL and Robinson, MM (2009). Parallels of snipe hunting and ROS research: the challenges of studying ROS and redox signalling in response to exercise. J Physiol 587(Pt 5): 927-928.

Jaeschke, H, Gores, GJ, Cederbaum, AI, Hinson, JA, Pessayre, D and Lemasters, JJ (2002). Mechanisms of hepatotoxicity. Toxicol Sci 65(2): 166-176.

Jiang, F, Zhang, Y and Dusting, GJ (2011). NADPH oxidase-mediated redox signaling: roles in cellular stress response, stress tolerance, and tissue repair. Pharmacol Rev 63(1): 218-242.

Jun, YW, Seo, JW and Cheon, J (2008). Nanoscaling laws of magnetic nanoparticles and their applicabilities in biomedical sciences. Acc Chem Res 41(2): 179-189.

Kane, RS and Stroock, AD (2007). Nanobiotechnology: protein-nanomaterial interactions. Biotechnol Prog 23(2): 316-319.

Kasai, H (1997). Analysis of a form of oxidative DNA damage, 8-hydroxy-2'-deoxyguanosine, as a marker of cellular oxidative stress during carcinogenesis. Mutat Res 387(3): 147-163.

Kaufmann, SH (1987). [Lymphokines, interleukins, cytokines: function and action]. Immun Infekt 15(4): 127-134.

Kende, M (1982). Role of macrophages in the expression of immune responses. J Am Vet Med Assoc 181(10): 1037-1042.

Kerr, J and Harmon, B (1991). Definition and incidence of apoptosis: an historical perspective. Apoptosis: The Molecular Basis of Cell Death. Edited by LD Tomei, FO Cope. Cold Spring Harbor Laboratory Press: p 5.

Kerr, JF, Wyllie, AH and Currie, AR (1972). Apoptosis: a basic biological phenomenon with wide-ranging implications in tissue kinetics. Br J Cancer 26(4): 239-257.

Knaapen, AM, Borm, PJ, Albrecht, C and Schins, RP (2004). Inhaled particles and lung cancer. Part A: Mechanisms. Int J Cancer 109(6): 799-809.

Knaapen, AM, Gungor, N, Schins, RP, Borm, PJ and Van Schooten, FJ (2006). Neutrophils and respiratory tract DNA damage and mutagenesis: a review. Mutagenesis 21(4): 225-236.

Kobayashi, A, Kang, MI, Okawa, H, Ohtsuji, M, Zenke, Y, Chiba, T, Igarashi, K and Yamamoto, M (2004). Oxidative stress sensor Keap1 functions as an adaptor for Cul3-based E3 ligase to regulate proteasomal degradation of Nrf2. Mol Cell Biol 24(16): 7130-7139.

Korsmeyer, SJ, Wei, MC, Saito, M, Weiler, S, Oh, KJ and Schlesinger, PH (2000). Pro-apoptotic cascade activates BID, which oligomerizes BAK or BAX into pores that result in the release of cytochrome c. Cell Death Differ 7(12): 1166-1173.

Kreuter, J, Shamenkov, D, Petrov, V, Ramge, P, Cychutek, K, Koch-Brandt, C and Alyautdin, R (2002). Apolipoprotein-mediated transport of nanoparticle-bound drugs across the blood-brain barrier. J Drug Target 10(4): 317-325.

Kroll, A, Pillukat, MH, Hahn, D and Schnekenburger, J (2009). Current in vitro methods in nanoparticle risk assessment: limitations and challenges. Eur J Pharm Biopharm 72(2): 370-377.

Krug, HF and Wick, P (2011). Nanotoxicology: an interdisciplinary challenge. Angew Chem Int Ed Engl 50(6): 1260-1278.

Lafuente, JV, Sharma, A, Patnaik, R, Muresanu, DF and Sharma, HS (2012). Diabetes exacerbates nanoparticles induced brain pathology. CNS Neurol Disord Drug Targets 11(1): 26-39.

Lai, SK, Wang, YY, Wirtz, D and Hanes, J (2009). Micro- and macrorheology of mucus. Adv Drug Deliv Rev 61(2): 86-100.

Lane, DP (1992). Cancer. p53, guardian of the genome. Nature 358(6381): 15-16.

Lavrik, IN, Golks, A and Krammer, PH (2005). Caspases: pharmacological manipulation of cell death. J Clin Invest 115(10): 2665-2672.

Lippmann, M, Yeates, DB and Albert, RE (1980). Deposition, retention, and clearance of inhaled particles. Br J Ind Med 37(4): 337-362.

Lockshin, RA and Williams, CM (1964). Programmed cell death—II. Endocrine potentiation of the breakdown of the intersegmental muscles of silkmoths. J Insect Physiol 10: 643–649.

Lodovici, M and Bigagli, E (2011). Oxidative stress and air pollution exposure. J Toxicol 2011: 487074.

Majno, G and Joris, I (1995). Apoptosis, oncosis, and necrosis. An overview of cell death. Am J Pathol 146(1): 3-15.

Martin, CR and Kohli, P (2003). The emerging field of nanotube biotechnology. Nat Rev Drug Discov 2(1): 29-37.

Martinez-Pomares, L, Platt, N, McKnight, AJ, da Silva, RP and Gordon, S (1996). Macrophage membrane molecules: markers of tissue differentiation and heterogeneity. Immunobiology 195(4-5): 407-416.

McMahon, M, Thomas, N, Itoh, K, Yamamoto, M and Hayes, JD (2006). Dimerization of substrate adaptors can facilitate cullin-mediated ubiquitylation of proteins by a "tethering" mechanism: a two-site interaction model for the Nrf2-Keap1 complex. J Biol Chem 281(34): 24756-24768.

Monteiro-Riviere, NA, Inman, AO and Zhang, LW (2009). Limitations and relative utility of screening assays to assess engineered nanoparticle toxicity in a human cell line. Toxicol Appl Pharmacol 234(2): 222-235.

Mosser, DM and Edwards, JP (2008). Exploring the full spectrum of macrophage activation. Nat Rev Immunol 8(12): 958-969.

Murray, PJ and Wynn, TA (2011). Protective and pathogenic functions of macrophage subsets. Nat Rev Immunol 11(11): 723-737.

Nauseef, WM (2008). Biological roles for the NOX family NADPH oxidases. J Biol Chem 283(25): 16961-16965.

Nelson, DA (1990). The biology of myelopoiesis. Clin Lab Med 10(4): 649-659.

Nguyen, T, Nioi, P and Pickett, CB (2009). The Nrf2-antioxidant response element signaling pathway and its activation by oxidative stress. J Biol Chem 284(20): 13291-13295.

Nicholson, DW and Thornberry, NA (1997). Caspases: killer proteases. Trends Biochem Sci 22(8): 299-306.

O'Neal, DP, Hirsch, LR, Halas, NJ, Payne, JD and West, JL (2004). Photo-thermal tumor ablation in mice using near infrared-absorbing nanoparticles. Cancer Lett 209(2): 171-176.

Oberdorster, G, Maynard, A, Donaldson, K, Castranova, V, Fitzpatrick, J, Ausman, K, Carter, J, Karn, B, Kreyling, W, Lai, D, Olin, S, Monteiro-Riviere, N, Warheit, D and Yang, H (2005a). Principles for characterizing the potential human health effects from exposure to nanomaterials: elements of a screening strategy. Part Fibre Toxicol 2: 8.

Oberdorster, G, Oberdorster, E and Oberdorster, J (2005b). Nanotoxicology: an emerging discipline evolving from studies of ultrafine particles. Environ Health Perspect 113(7): 823-839.

Oberdorster, G, Sharp, Z, Atudorei, V, Elder, A, Gelein, R, Kreyling, W and Cox, C (2004). Translocation of inhaled ultrafine particles to the brain. Inhal Toxicol 16(6-7): 437-445.

Ozaki, K and Leonard, WJ (2002). Cytokine and cytokine receptor pleiotropy and redundancy. J Biol Chem 277(33): 29355-29358.

Pantopoulos, K and Hentze, MW (1995). Rapid responses to oxidative stress mediated by iron regulatory protein. EMBO J 14(12): 2917-2924.

Park, JB (2003). Phagocytosis induces superoxide formation and apoptosis in macrophages. Exp Mol Med 35(5): 325-335.

Pastore, A, Piemonte, F, Locatelli, M, Lo Russo, A, Gaeta, LM, Tozzi, G and Federici, G (2001). Determination of blood total, reduced, and oxidized glutathione in pediatric subjects. Clin Chem 47(8): 1467-1469.

Peters, A, Veronesi, B, Calderon-Garciduenas, L, Gehr, P, Chen, LC, Geiser, M, Reed, W, Rothen-Rutishauser, B, Schurch, S and Schulz, H (2006). Translocation and potential neurological effects of fine and ultrafine particles a critical update. Part Fibre Toxicol 3: 13.

Poland, CA, Duffin, R, Kinloch, I, Maynard, A, Wallace, WA, Seaton, A, Stone, V, Brown, S, Macnee, W and Donaldson, K (2008). Carbon nanotubes introduced into the abdominal cavity of mice show asbestos-like pathogenicity in a pilot study. Nat Nanotechnol 3(7): 423-428.

Poljsak, B and Dahmane, R (2012). Free radicals and extrinsic skin aging. Dermatol Res Pract 2012: 135206.

Pryor, WA (1988). Why is the hydroxyl radical the only radical that commonly adds to DNA? Hypothesis: it has a rare combination of high electrophilicity, high thermochemical reactivity, and a mode of production that can occur near DNA. Free Radic Biol Med 4(4): 219-223.

Raff, MC, Barres, BA, Burne, JF, Coles, HS, Ishizaki, Y and Jacobson, MD (1994). Programmed cell death and the control of cell survival. Philos Trans R Soc Lond B Biol Sci 345(1313): 265-268.

Rahman, I, Marwick, J and Kirkham, P (2004). Redox modulation of chromatin remodeling: impact on histone acetylation and deacetylation, NF-kappaB and pro-inflammatory gene expression. Biochem Pharmacol 68(6): 1255-1267.

Richmond, J (2002). Refinement, reduction, and replacement of animal use for regulatory testing: future improvements and implementation within the regulatory framework. ILAR J 43 Suppl: S63-68.

Rom, WN and Palmer, PE (1974). The spectrum of asbestos-related diseases. West J Med 121(1): 10-21.

Saito, N, Usui, Y, Aoki, K, Narita, N, Shimizu, M, Ogiwara, N, Nakamura, K, Ishigaki, N, Kato, H, Taruta, S and Endo, M (2008). Carbon nanotubes for biomaterials in contact with bone. Curr Med Chem 15(5): 523-527.

Sanchez, VC, Pietruska, JR, Miselis, NR, Hurt, RH and Kane, AB (2009). Biopersistence and potential adverse health impacts of fibrous nanomaterials: what have we learned from asbestos? Wiley Interdiscip Rev Nanomed Nanobiotechnol 1(5): 511-529.

Scaffidi, C, Schmitz, I, Zha, J, Korsmeyer, SJ, Krammer, PH and Peter, ME (1999). Differential modulation of apoptosis sensitivity in CD95 type I and type II cells. J Biol Chem 274(32): 22532-22538.

Schins, RP and Knaapen, AM (2007). Genotoxicity of poorly soluble particles. Inhal Toxicol 19 Suppl 1: 189-198.

Schulze-Osthoff, K, Ferrari, D, Los, M, Wesselborg, S and Peter, ME (1998). Apoptosis signaling by death receptors. Eur J Biochem 254(3): 439-459.

Seaton, A (2010). From dust and ashes: the 1950s. Occup Med (Lond) 60(1): 2-4.

Sethi, M, Pacardo, DB and Knecht, MR (2010). Biological surface effects of metallic nanomaterials for applications in assembly and catalysis. Langmuir 26(19): 15121-15134.

Shvedova, AA, Kisin, ER, Mercer, R, Murray, AR, Johnson, VJ, Potapovich, AI, Tyurina, YY, Gorelik, O, Arepalli, S, Schwegler-Berry, D, Hubbs, AF, Antonini, J, Evans, DE, Ku, BK, Ramsey, D, Maynard, A, Kagan, VE, Castranova, V and Baron, P (2005). Unusual inflammatory and fibrogenic pulmonary responses to single-walled carbon nanotubes in mice. Am J Physiol Lung Cell Mol Physiol 289(5): L698-708.

Sies, H and Cadenas, E (1985). Oxidative stress: damage to intact cells and organs. Philos Trans R Soc Lond B Biol Sci 311(1152): 617-631.

Smith, BR (1990). Regulation of hematopoiesis. Yale J Biol Med 63(5): 371-380.

Stohs, SJ (1995). The role of free radicals in toxicity and disease. J Basic Clin Physiol Pharmacol 6(3-4): 205-228.

Stone, V, Johnston, H and Clift, MJ (2007). Air pollution, ultrafine and nanoparticle toxicology: cellular and molecular interactions. IEEE Trans Nanobioscience 6(4): 331-340.

Stone, V, Johnston, H and Schins, RP (2009). Development of in vitro systems for nanotoxicology: methodological considerations. Crit Rev Toxicol 39(7): 613-626.

Strasser, A (2005). The role of BH3-only proteins in the immune system. Nat Rev Immunol 5(3): 189-200.

Tadakuma, T (1994). [The role of apoptosis in the development of T cells]. Hum Cell 7(1): 20-26.

Takagi, A, Hirose, A, Nishimura, T, Fukumori, N, Ogata, A, Ohashi, N, Kitajima, S and Kanno, J (2008). Induction of mesothelioma in p53+/- mouse by intraperitoneal application of multi-wall carbon nanotube. J Toxicol Sci 33(1): 105-116.

Takaoka, A, Hayakawa, S, Yanai, H, Stoiber, D, Negishi, H, Kikuchi, H, Sasaki, S, Imai, K, Shibue, T, Honda, K and Taniguchi, T (2003). Integration of interferon-alpha/beta signalling to p53 responses in tumour suppression and antiviral defence. Nature 424(6948): 516-523.

Talalay, P (2000). Chemoprotection against cancer by induction of phase 2 enzymes. Biofactors 12(1-4): 5-11.

Tenhunen, R, Marver, HS and Schmid, R (1968). The enzymatic conversion of heme to bilirubin by microsomal heme oxygenase. Proc Natl Acad Sci U S A 61(2): 748-755.

Thannickal, VJ and Fanburg, BL (2000). Reactive oxygen species in cell signaling. Am J Physiol Lung Cell Mol Physiol 279(6): L1005-1028.

Thimmulappa, RK, Mai, KH, Srisuma, S, Kensler, TW, Yamamoto, M and Biswal, S (2002). Identification of Nrf2-regulated genes induced by the chemopreventive agent sulforaphane by oligonucleotide microarray. Cancer Res 62(18): 5196-5203.

Thompson, CB (1995). Apoptosis in the pathogenesis and treatment of disease. Science 267(5203): 1456-1462.

Tittel, JN and Steller, H (2000). A comparison of programmed cell death between species. Genome Biol 1(3): REVIEWS0003.

Unfried, K, Albrecht, C, Klotz, L, von Mikecz, A, Grether-Beck, S and Schins, R (2007). Cellular responses to nanoparticles: target structures and mechanisms. . Nanotoxicology 1: 52-71.

US_Research_Nanomaterials_Inc. http://www.us-nano.com/.

Utell, MJ and Frampton, MW (2000). Acute health effects of ambient air pollution: the ultrafine particle hypothesis. J Aerosol Med 13(4): 355-359.

van Berlo, D, Hullmann, M and Schins, RP (2012). Toxicology of ambient particulate matter. EXS 101: 165-217.

van Berlo, D, Wessels, A, Boots, AW, Wilhelmi, V, Scherbart, AM, Gerloff, K, van Schooten, FJ, Albrecht, C and Schins, RP (2010). Neutrophil-derived ROS contribute to oxidative DNA damage induction by quartz particles. Free Radic Biol Med 49(11): 1685-1693.

Van Cruchten, S and Van Den Broeck, W (2002). Morphological and biochemical aspects of apoptosis, oncosis and necrosis. Anat Histol Embryol 31(4): 214-223.

van Furth, R (1982). Current view on the mononuclear phagocyte system. Immunobiology 161(3-4): 178-185.

Vaux, DL (1993). Toward an understanding of the molecular mechanisms of physiological cell death. Proc Natl Acad Sci U S A 90(3): 786-789.

Wang, J and Pantopoulos, K (2011). Regulation of cellular iron metabolism. Biochem J 434(3): 365-381.

Wang, K, Fang, H, Xiao, D, Zhu, X, He, M, Pan, X, Shi, J, Zhang, H, Jia, X, Du, Y and Zhang, J (2009). Converting redox signaling to apoptotic activities by stress-responsive regulators HSF1 and NRF2 in fenretinide treated cancer cells. PLoS One 4(10): e7538.

Wardman, P and Candeias, LP (1996). Fenton chemistry: an introduction. Radiat Res 145(5): 523-531.

West, JL and Halas, NJ (2003). Engineered nanomaterials for biophotonics applications: improving sensing, imaging, and therapeutics. Annu Rev Biomed Eng 5: 285-292.

Win-Shwe, TT and Fujimaki, H (2011). Nanoparticles and neurotoxicity. Int J Mol Sci 12(9): 6267-6280.

Yuan, J, Shaham, S, Ledoux, S, Ellis, HM and Horvitz, HR (1993). The C. elegans cell death gene ced-3 encodes a protein similar to mammalian interleukin-1 beta-converting enzyme. Cell 75(4): 641-652.

Zhang, DD, Lo, SC, Cross, JV, Templeton, DJ and Hannink, M (2004). Keap1 is a redox-regulated substrate adaptor protein for a Cul3-dependent ubiquitin ligase complex. Mol Cell Biol 24(24): 10941-10953.

Zimmermann, KC, Bonzon, C and Green, DR (2001). The machinery of programmed cell death. Pharmacol Ther 92(1): 57-70.

Zou, H, Li, Y, Liu, X and Wang, X (1999). An APAF-1.cytochrome c multimeric complex is a functional apoptosome that activates procaspase-9. J Biol Chem 274(17): 11549-11556.

Chapter II

Evaluation of apoptosis induced by nanoparticles and fine particles in RAW 264.7 macrophages: Facts and artefacts

Verena Wilhelmi, Ute Fischer, Damiën van Berlo, Klaus Schulze-Osthoff,
Roel P.F. Schins, Catrin Albrecht

Toxicology In Vitro 26 (2012): 323-334

Study 1: Evaluation of apoptosis induced by nanoparticles and fine particles in RAW 264.7 macrophages: Facts and artefacts

Declaration

The manuscript is published at Toxicology In Vitro.
All experimental work was performed by Verena Wilhelmi.
The impact on authoring this paper can be estimated in total with 90%.

Toxicology in Vitro 26 (2012) 323–334

Contents lists available at SciVerse ScienceDirect

Toxicology in Vitro

journal homepage: www.elsevier.com/locate/toxinvit

Evaluation of apoptosis induced by nanoparticles and fine particles in RAW 264.7 macrophages: Facts and artefacts

Verena Wilhelmi [a], Ute Fischer [b], Damiën van Berlo [a], Klaus Schulze-Osthoff [c], Roel P.F. Schins [a], Catrin Albrecht [a,*]

[a] Leibniz Research Institute for Environmental Medicine, Düsseldorf, Germany
[b] Clinic of Pediatric Oncology, Haematology and Clinical Immunology, Center of Child and Adolescent Health, Medical Faculty, Heinrich-Heine-University of Düsseldorf, Germany
[c] Interfaculty Institute for Biochemistry, University of Tübingen, Germany

ARTICLE INFO

Article history:
Received 1 July 2011
Accepted 6 December 2011
Available online 14 December 2011

Keywords:
Nanoparticles
Necrosis
Apoptosis
In vitro testing
Assay validation

ABSTRACT

Current hazard characterisation of nanoparticles (NP) is predominantly based on *in vitro* test systems, being established for small molecules of drugs and chemicals. However, specific physicochemical properties of NP may result in interference with assay components, biomarkers, or detection systems. In the present study, six types of (nano)particles were screened in RAW 264.7 macrophages by common cytotoxicity methods (WST-1, LDH). Our specific focus was on the investigation of apoptosis (analysis of hypodiploid DNA, phosphatidylserine exposure, caspase 3/7 activation, and Cell Death Detection ELISA). Assays were validated by the well-known apoptosis inducer staurosporine.

Our results show that ZnO, DQ12 quartz and amorphous silica are cytotoxic with strong indications for apoptotic effects in RAW 264.7 macrophages, whereas toxicity was absent for MgO. For fine as well as ultrafine TiO_2, no apoptotic effects could be detected except for induction of DNA fragmentation. The results of our study demonstrate the necessity to control on a case-by-case basis for assay interference to avoid misinterpretation of specific *in vitro* test findings. To obtain valid statements on the potential induction of apoptosis by specific NP the measurement of multiple endpoints is a prerequisite.

1. Introduction

Human exposure to engineered nanomaterials, which can be defined as objects with at least one dimension less than 100 nm (BSi_report, 2007), is gaining importance in recent years. There is an increasing market for industrial nanoproducts applied in almost all branches (e.g. cosmetics, electronics, textiles, medicine, food). Especially the application of metal oxide nanoparticles (NP) provides a huge potential in nanotechnology because of their outstanding characteristics. Four different types of metal oxide particles produced in high tonnage are ZnO, MgO, SiO_2 and TiO_2. These materials have a long-standing use in various applications, e.g. in paints, coatings, cosmetics, toothpaste, sunscreens and/or as (quantum satis) food additives and novel food packaging materials (Chaudhry et al., 2008).

The metallic component of specific NP is known to impact the human body (Valko et al., 2005; Auffan et al., 2009). Zinc and magnesium are essential trace elements for the organism and titanium is a harmless, non-toxic metal. Particle modification in nanotechnology may increase the biological reactivity and facilitate the uptake into the body compared to the bulk material. Toxicity of specific NP has been related to numerous physicochemical parameters like size, shape, chemical composition, and surface area (Unfried et al., 2007). New test strategies for hazard identification are urgently needed and are the subject of current research (Donaldson et al., 2004). The smaller a particle, the more concern exists regarding human exposure. Particles reaching distal areas of the lung after inhalation may translocate across epithelial and endothelial cells into the blood and lymph circulation and are discussed to target multiple organs (Oberdorster et al., 2005b). Decreased particle size is also associated with increased uptake and potential toxicity in the intestine after oral uptake (Powell et al., 2010). For inhaled (nano)particles, macrophages in the alveolar region play a central role in their clearance. NP uptake may lead to a persistent activation of these cells, associated with the release of various cytokines and reactive oxygen and nitrogen species (ROS/RNS). Chronic inflammation is discussed to be related to formation of fibrosis and cancer (Fubini and Hubbard, 2003; Albrecht et al., 2005). In particle-induced pulmonary fibrosis, studies have shown a contribution of apoptosis in macrophages (Ortiz et al., 1998; Borges et al., 2001). Furthermore, there are indications that only fibrogenic particles cause apoptosis induction in macrophages *in vitro* (Iyer et al., 1996). Concerning

* Corresponding author. Address: Particle Research, IUF – Leibniz Research Institute for Environmental Medicine, Auf'm Hennekamp 50, 40225 Düsseldorf, Germany. Tel.: +49 211 3389 351; fax: +49 211 3389 331.
E-mail address: catrin.albrecht@uni-duesseldorf.de (C. Albrecht).

0887-2333/$ - see front matter © 2011 Elsevier Ltd. All rights reserved.
doi:10.1016/j.tiv.2011.12.006

hazard identification of a specific type of (nano)particle, the detection of its ability to induce apoptosis in macrophages therefore seems a highly promising readout.

The apoptosis research community has provided a huge battery of commercial assays and standardised methods especially for current *in vitro* research. However, investigation of particles bears the fundamental problem of their interference with assay reagents, released cellular markers or detection systems which may cause false positive or negative results (Kroll et al., 2009; Stone et al., 2009). The implementation of REACH (Registration, Evaluation, Authorisation and Restriction of Chemicals) and the lack of standards for nanomaterial testing require a basic adjustment of common assays for every nanomaterial studied and are the subject of international projects (Balbus et al., 2007; Monteiro-Riviere et al., 2009; Riviere, 2009). In the long term, the aim is to develop quantitative structure–activity relationships which will allow for the identification of the potential toxicity of particles on the basis of physico-chemical and structural characteristics (Duffin et al., 2007). In the present study we have investigated the toxic properties of a set of widely available (nano)particles in RAW 264.7 mouse macrophages, by means of commonly used *in vitro* assays to detect cytotoxicity, and specifically, the induction of apoptosis. With our study we aimed to contribute to improved hazard assessment of NP by an in-depth evaluation of the potential introduction of artefacts in specific toxicity assays.

2. Materials and methods

2.1. Cell culture

The macrophage-like murine cell line RAW 264.7 (ATCC Number TIB-71; American Type Culture Collection, Manassas, VA) was cultured at 37 °C and 5% CO_2 in Dulbecco's modified Eagle's medium (Sigma–Aldrich, Germany) supplemented with 4 mM L-glutamine adjusted to contain 1.5 g/l sodium bicarbonate and 4.5 g/l glucose, 1% penicillin/streptomycin and 10% fetal calf serum (Sigma–Aldrich, Germany). Experiments were performed 24 h after seeding (2×10^5 cells/cm^2) in appropriate cell culture dishes as mentioned for the specific assays at approximately 30% confluence.

2.2. Particle characteristics and treatment

Particulates used in this study are specified in Table 1. Possible endotoxins were destroyed by baking of the particles (220 °C, 16 h). For treatment, the particles were freshly suspended in complete cell culture medium by sonication (60 W, 35 Hz, water bath sonicator Sonorex TK 52; Schaltech, Germany) in a stock solution of 1 g/l. Cells were treated with final concentrations of 1, 5, 10, 40 or 80 μg/cm^2 for 4, 6 or 24 h. As positive control, the well-known apoptosis inducer staurosporine (Sigma–Aldrich, Germany) was used in concentrations of 0.1 or 1 μM for 24 or 4 h, respectively. After 24 h phase contrast pictures of untreated cells as well as of cells treated with 40 μg/cm^2 particle samples or 0.1 μM staurosporine were obtained without rinsing of cells using an Olympus IX70-S8F2 microscope (Japan).

2.3. Quenching of photometric signal by particles

In order to investigate quenching effects, the particles were suspended in complete cell culture medium and were applied at a concentration of 80 μg/cm^2 (i.e. the highest dose used in the cell-based assays) in 96-well-plates. Measurement was done using a Multiscan ELISA reader (Thermo Fisher Scientific, Germany). Wavelength-dependent absorption units derived from medium sample were subtracted from values of particle samples.

2.4. Cytotoxicity

To detect effects on cell viability after particle treatment two independent 96-well-assays were performed. The WST-1 conversion assay (Roche, Germany) is based on the mitochondrial function of intact cells, which enables them to metabolise the stable tetrazolium salt WST-1 (4-[3-(4-iodophenyl)-2-(4-nitrophenyl)-2H-5-tetrazolio]-1,3-benzene disulfonate) to a soluble violet formazan product. Cells were treated in octoplicate in a total volume of 100 μl. After 24 h, for each treatment 10 μl of WST-1 solution was added to five wells for 10 min at 37 °C; the other three wells without substrate serve as particle and accordingly background control. Colour development was measured at 450 nm using a Multiscan ELISA reader (Thermo Fisher Scientific, Germany). Viability was calculated by subtraction of the mean values without WST-1 from those with WST-1 substrate and was expressed as percentage of control. To investigate the interaction of particles with formazan, this assay specific metabolic product was obtained by WST-1 incubation in vital cells. The cell free supernatant (obtained by centrifugation) was mixed 1:1 with particle suspensions at final concentrations of 1, 5, 10, 40, 80 μg/cm^2. Absorption of centrifuged supernatant (10 min, 200*g*) was measured at 450 nm in duplicates and related to non-particle-treated control supernatants.

The LDH assay (Roche, Germany) detects the amount of lactate dehydrogenase (LDH) enzyme released by cells with damaged membranes as indicator of necrosis. Cells were treated as described for the WST-1 assay, however in triplicate incubations per experiment. Additional cell-free triplicates with particles were prepared for subtraction of absorption effects. Maximal release was determined after complete cell lysis using the kit-included lysis buffer. In order to investigate particle interferences with the measurement, cell supernatants were transferred after centrifugation (10 min, 200*g*) in a new 96-well plate, and LDH assay was performed as described. The amount of LDH released in the supernatant was expressed as fold increase of untreated cells. In order to investigate potential particle-induced quenching artefacts, particle containing medium (80 μg/cm^2) as well as particle-free medium (controls) were subjected to the LDH assay either with or without spiking with LDH enzyme (1 h, 37 °C). The amount of LDH used for the spiking experiment was obtained by full lysis of RAW 264.7 cells using the lysis buffer included in the LDH kit.

2.5. Flow cytometry

The processes of apoptosis compared to necrosis lead to characteristic cell morphologies which can be determined by flow cytom-

Table 1
Characteristics of the (nano)particles used in present study.

Code	Material specification	BET (m^2/g)	Primary particle size (nm)	Source
DQ12	Crystalline silica	9.6	960	IUF Düsseldorf, Batch 6
a-SiO_2	Amorphous silica, fumed	200	14	Sigma
uf TiO_2	TiO_2 ultrafine (80% anatase, 20% rutile)	50	20–80	Degussa
f TiO_2	TiO_2 fine (pure anatase)	10	40–300	Aldrich
ZnO	ZnO	48	10	Nanoscale Materials Inc., USA
MgO	MgO	600	8	Nanoscale Materials Inc., USA

etry. The forward scatter (FSC) correlates with the event-size which varies between healthy versus apoptotic and necrotic cells, apoptotic blebs and even free particles or cell debris. The sideward scatter (SSC) depends on the event's granularity. Fluorescence channels provide additional opportunities to detect apoptotic and/or necrotic cell markers. However, specifically in particle research there is a major challenge concerning data analysis and interpretation. Each particle has its unique properties in auto-fluorescence as well as fluorochrome-binding and light-scattering behaviour. Event-separation of free particles and cells is a delicate process of gating as described in detail in the result section. Flow cytometric measurements were performed with the FACS *Calibur* (fluorescent-activated cell sorter, Becton Dickinson, Germany) by counting 10,000 gated events per sample. Data were analysed using the software FlowJo (Version 7.6.0, TreeStar Inc., USA).

2.5.1. Analysis of DNA fragmentation

Chromosomal DNA fragmentation with formation of nucleosome-sized DNA fragments is one of the most distinguishing parameters between apoptosis and necrosis. The red fluorescent dyes 7-Aminoactinomycin D (7-AAD, Sigma–Aldrich, Germany) and propidium iodide (PI, Sigma–Aldrich, Germany) intercalate with double-stranded DNA of cells with permeabilised membranes. Cells treated in 24-well dishes were harvested by scraping on ice, washed with $HBSS^{-/-}$ (GIBCO, Germany) and suspended in 250 µl of staining buffer (0.1% sodium citrate, 0.1% Triton X-100, 50 mg/l 7-AAD or PI). After 15 min of incubation FACS analysis was performed using standard settings with the red-collecting fluorescent channels FL-2 and FL-3 for PI and 7-AAD emission, respectively. Following exclusion of particle events, resulting DNA histograms were used to determine the percentage of cells with hypodiploid DNA content.

In order to evaluate possible binding of the fluorochromes to particles, untreated cells were supplemented with the highest concentration (80 µg/cm^2) of the used particle samples, immediately before assay performance either with 7-AAD or with PI.

2.5.2. Analysis of phosphatidylserine exposure and cell permeability

During apoptotic cell death phosphatidylserine (PS), a phospholipid component of the inner-leaflet of cell membranes, becomes available at the cell surface. This early marker of apoptotic cell death can be detected by staining with the green fluorescent dye Annexin V-FITC (BD Pharmingen, Germany), a fluorochrome-conjugated Ca^{2+}-dependent PS-binding protein. In combination with the 7-AAD-DNA-staining, dye exclusion of vital cells permits a discrimination between apoptotic and necrotic cells (van Engeland et al., 1998). Cells treated in 24-well dishes were centrifuged (200*g*, 5 min, 4 °C), washed with $HBSS^{-/-}$ (GIBCO, Germany) and stained with 150 µl of buffer (10 mM HEPES/NaOH pH 7.4, 150 mM NaCl, 5 mM KCl, 2 mM CaCl) containing 5 µl Annexin V-FITC (1 mg/ml) and 1.5 µM 7-AAD at 37 °C. After 10 min, additional 500 µl of ice-cold buffer were added and cells were harvested by scraping on ice. After centrifugation (200*g*, 5 min, 4 °C) cells were suspended in 250 µl buffer and analysed immediately by flow cytometry using the green-collecting fluorescent channels FL-1 for Annexin V-FITC and FL-3 for 7-AAD, as described above. Quadrant separation in the fluorescent channels FL-1 (Annexin V-FITC) versus FL-3 (7-AAD) represents events of necrotic respectively late apoptotic cells, which are 7-AAD positive (Q1 + Q2); apoptotic cells (Q3, Annexin V-FITC positive and 7-AAD negative) and viable cells (Q4, fluorescent negative) expressed as percentage of total cells.

2.6. Detection of apoptotic nucleosomes and necrotic DNA release

The Cell Death Detection ELISA^{PLUS} (CDDE) kit is a photometric enzyme-immunoassay for the qualitative and quantitative *in vitro* determination of DNA in the supernatant of treated cells indicating necrosis and cytoplasmic histone-associated DNA fragments (mono- and oligonucleosomes) indicating apoptosis (Roche, Germany). Application according to manufacturer's instruction provides concurrent detection of apoptosis and necrosis in the same well. Colour development of samples was determined as enrichment factor of the amount of DNA fragments in cytoplasm or cell supernatant indicating apoptosis or necrosis, respectively, and expressed relative to untreated cells. In order to investigate possible interferences with the assay, particles were added to the cells in a concentration twofold higher than the final concentration used in above experiment (160 µg/cm^2). Subsequently, the samples were centrifuged (10 min, 200g) conform the CDDE kit protocol. Supernatant was then mixed 1:1 with lysate of staurosporine-treated cells using lysis buffer included in the kit, and analysed according to manufacturer's instructions. Data were expressed relative to the particle-free sample (control).

2.7. Detection of activated executioner caspases-3 and -7

The Caspase-Glo® 3/7 Assay (Promega, Germany) was used according to manufacturer's instruction to detect caspase 3/7-activity. In this assay, cleavage of the caspase substrate leads to a luminescent signal produced by luciferase, which is proportional to the amount of caspase activity present. After 1 h incubation luminescence was measured (MicroLumat Plus Microplate Luminometer LB 96 V, EG&G Berthold, Germany) and expressed as percentage of untreated control.

Potential quenching effects of particles in the assay were tested under cell-free conditions. Therefore, 80 µg/cm^2 particles was incubated with recombinant caspase-3 (Fischer et al., 2006) for 4 h at 37 °C and then subjected to the activity assay. The concentration of caspase-3 used was in the same order of magnitude as the activity measured in staurosporine-treated RAW 264.7 cells.

2.8. Statistical analysis

Data are presented as mean ± SD of *n* independent experiments, as indicated in the figure legend for each specific assay. Statistical analysis of particle effects was performed employing SPSS (version 19) for Windows using analysis of variance (ANOVA) with LSD post hoc comparison. Effects of staurosporine were analysed by *t*-test for independent groups. Statistically significant effects are indicated in the figures by up to three asterisks (*, **, ***) representing significance at cutoff levels of $p < 0.05$, $p < 0.01$, and $p < 0.001$, respectively.

3. Results

3.1. Viability

In Fig. 1, phase contrast pictures of cells after 24 h (nano)particle treatment as well as untreated controls are shown. Control and MgO-treated cells display similar healthy conditions regarding their morphology and number, indicating absence of toxicity for the MgO. Staurosporine treatment resulted in a reduced macrophage number and changed shape, similar to ZnO-treated cells. Cell viability of DQ12- and a-SiO_2-treated cells appeared to be less affected, but distinct damage could be observed. However, there was a clear difference in the appearance of the particles. The amorphous SiO_2 formed bulky liquid agglomerates, in contrast to the DQ12. After treatment with TiO_2 cell number was not diminished; the particle-free areas that surround the cells after treatment may be explained by a massive uptake of these types of particles.

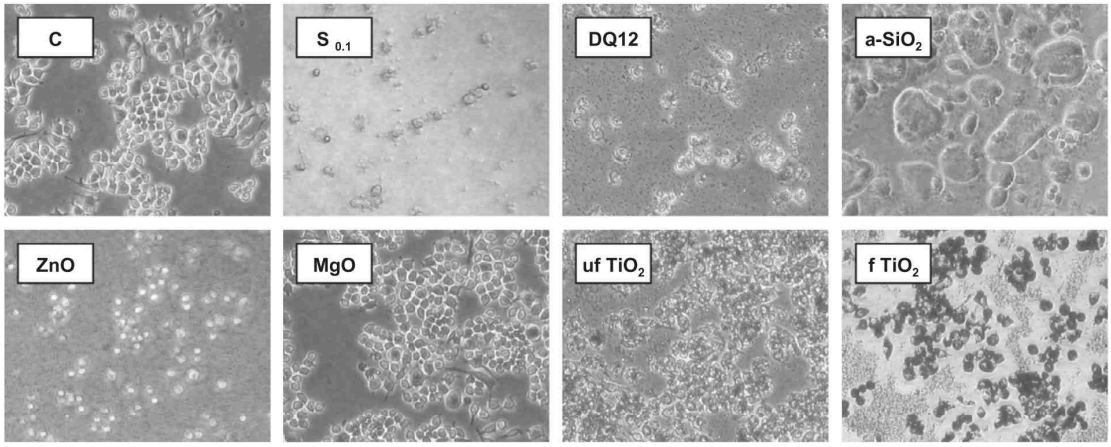

Fig. 1. Morphology of RAW 264.7 macrophages 24 h after treatment with 40 μg/cm² particles or 0.1 μM staurosporine ($S_{0.1}$), in comparison to controls (C) using phase contrast microscopy (original magnification 100×).

3.2. Evaluation of cytotoxicity by WST-1 and LDH assays

Since cytotoxicity assays, including the WST-1 assay and the LDH-assay are usually based on detection by an ELISA-reader, we investigated potential quenching effects of the used set of particles at various wavelengths. Results are shown in Fig. 2. The highest quenching of the light signal was seen by uf TiO_2 particles at low wavelengths. The signal is inversely related to the wavelength. At 450 nm, which represents the filter used for the WST-1 assay, both TiO_2 fractions showed an equal level of quenching. The quenching characteristic of f TiO_2 was obvious, but much less prominent than that of uf TiO_2 and slightly increasing with increasing wavelengths. ZnO and DQ12 showed only minor light quenching with a marginal dependence on wavelength. For a-SiO_2 and MgO, the quenching effect was found to be negligible under the applied experimental conditions.

Cytotoxic effects of the particles are determined by the WST-1 assay and the LDH assay shown in the Figs. 3 and 4, respectively. Investigation of possible interferences of particles under cell-free conditions revealed no artefacts in the WST-1 assay (Fig. 3A), while in the LDH assay for the ZnO particles a slightly increased activity was observed (Fig. 4B). The toxicity of DQ12, a-SiO_2 and ZnO could be clearly identified. In the WST-1 assay, these three particle types

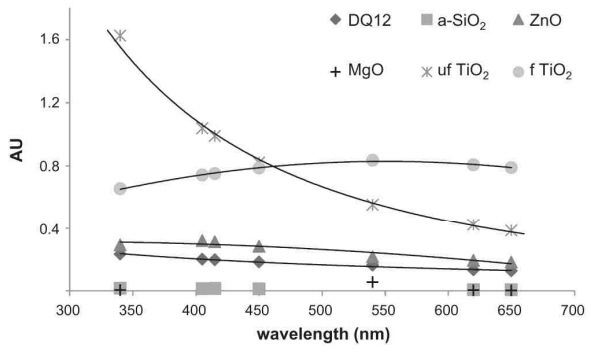

Fig. 2. Light absorbance of the six investigated types of particles applied at 80 μg/cm² was analysed by ELISA reader at seven wavelength filters (350, 405, 415, 450, 540 620 and 650 nm). Absorption units (AU) derived from medium used for particle suspensions were subtracted.

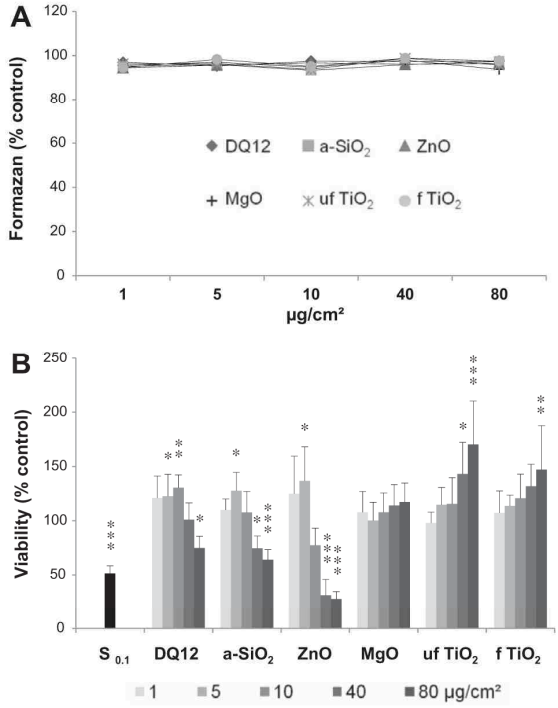

Fig. 3. Cytotoxicity of six particles and staurosporine (0.1 μM) was investigated using the WST-1 assay in RAW 264.7 macrophages. Potential interferences of the particles with the formazan dye were determined in the absence of cells. Results are shown in panel A. Effects of the particles and staurosporine (0.1 μM, S_{01}) in cell cultures after 24 h exposure ($n = 4$) are shown in panel B.

showed a significantly diminished cell viability in a dose-dependent manner (Fig. 3B). At lower concentrations, however, these particles showed an increased signal compared to untreated cells. A similar effect was observed in the WST-1 assay for ultrafine and fine TiO_2, at concentrations above 40 and 80 μg/cm², respectively. MgO did not induce changes in cell viability. The amount of LDH release from the cells was significantly increased after treatment for 24 h with DQ12 or a-SiO_2 at the two highest concen-

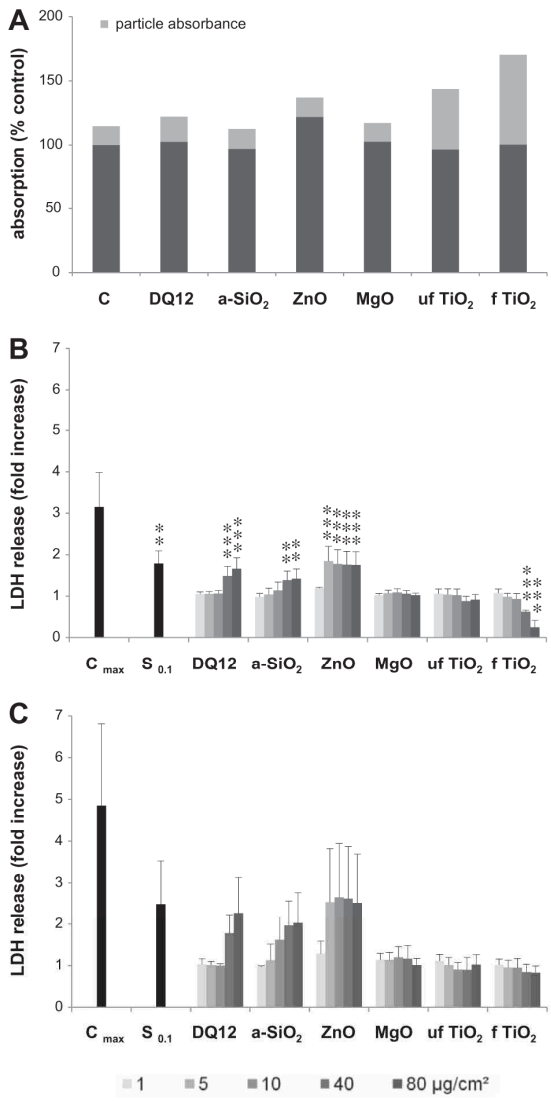

Fig. 4. Cytotoxicity of six particles and staurosporine (0.1 μM) was investigated using the LDH assay in RAW 264.7 macrophages. Potential effects of the particles on LDH activity measurements in the absence of cells are shown in panel A. The heights of the bars (dark + light bars) represent the absorptions for the six particle suspensions or the particle free suspension (*C* = control) after spiking with LDH. The height of the light bars depicts the absorptions of the same suspensions in the absence of spiked LDH. Accordingly, the dark bars represent the calculated LDH values upon correction of particle and medium absorption. Panel B shows the LDH release expressed as fold increase of untreated control from RAW 264.7 macrophages after 24 h treatment with particles or staurosporine (0.1 μM, S_{01}), measured according to manufacturer's instructions (i.e. analysing the whole sample containing particles, $n = 4$). Panel C shows the LDH measurement following setup modification by analysing particle-free cell supernatants ($n = 2$). Maximal increase following complete cell lysis was determined (C_{max}).

trations (Fig. 4B). No increased LDH release was measured after treatment with MgO and both types of TiO_2. Remarkably, f TiO_2 treatment reduced the LDH level in the supernatant compared to untreated cells. In order to investigate possible artefacts resulting from the particles themselves, particle-free cell supernatants were also analysed for LDH (Fig. 4C). The results were comparable to the prior assay with exception of f TiO_2.

3.3. Analysis of necrosis and apoptosis by Cell Death Detection ELISA

The principle of the CDDE is based on the concurrent detection of necrosis and apoptosis. Necrosis was observed after specific treatments by detection of DNA fragments released into the cell supernatant (Fig. 5B and D), whereas apoptosis was revealed by nucleosome-enrichment in the cytoplasm (Fig. 5C and E). Investigation of possible assay interferences with the used particles showed a reduced signal only for fine TiO_2 sample (Fig. 5A). After 4 h treatment, the highest concentration of DQ12 led to a significant induction of necrosis (Fig. 5B) as well as apoptosis (Fig. 5C). Apoptosis, in the absence of necrosis, was measured after 4 h treatment with a-SiO_2. At this time point, a small but significant apoptosis effect was also identified with ZnO, but in the absence of any dose-dependency.

After 24 h treatment, necrosis and apoptosis were detected in the CDDE assay with DQ12, a-SiO_2 and ZnO (Fig. 5D and E). In the DQ12-treated macrophages a marked dose-dependent induction of necrosis was observed; at this time point necrosis was also observed by the two highest concentrations of a-SiO_2. The enrichment of DNA fragments was also clearly detectable for ZnO-treated cells, although this reached statistical significance only at the lowest treatment concentration. At the same time point, DQ12 and a-SiO_2 caused a clear dose-dependent apoptotic signal (Fig. 5E). ZnO- treated cells already revealed a significant induction of apoptosis at 10 μg/cm^2 but, similar to the observations after 4 h, there was no clear dose-dependency. At both time points, MgO and the two types of TiO_2 increased neither apoptosis nor necrosis. Staurosporine, the positive control for apoptosis, dose-dependently and markedly increased the apoptotic signal. This treatment also induced the necrotic signal after 4 h treatment, but only at the higher concentration. After 24 h treatment with 0.1 μM staurosporine, necrosis appeared to dominate.

3.4. Apoptosis analysis by flow cytometry-based DNA fragmentation analysis

As an independent assay to determine apoptosis, a commonly used flow cytometry analysis was performed. Hypodiploid DNA was analysed following staining with a DNA-intercalating fluorescent dye. Specific attention was paid to the fact that particles, also included in cell samples, tend to become stained too and as such might lead to serious artefacts in analysis. The plotting of FSC versus FL-3 channels became apparent as the most suitable combination to exclude particles from the measurement. In order to separate particles from cell events, an accurate gating procedure is required. A direct comparison of the conventional fluorescent DNA stain PI versus 7-AAD identified the latter as more suitable for FACS analysis (Table 2). Considering a tolerance of 5% increase due to particle supplementation, analysis of a-SiO_2 had to be excluded for both staining compounds. However, the use of 7-AAD instead of PI enabled a successful gating procedure to discriminate cells from particles for the ZnO sample as well as for both TiO_2 samples.

Results of the appropriate gating for 7-AAD-stained samples are shown in Fig. 6A. Again, the highest tolerated percentage of residual particle events inside the gate should not exceed 5%. This target was convincingly reached for DQ12 (0.50%), ZnO (0.48%), uf TiO_2 (0.30%), f TiO_2 (1.25%) and MgO (0.81%) with a loss of cells less than 1%. Comparing control cells versus apoptotic cells show the delicate position of this gate in the range of hypodiploid cells as well as fluorescent particles (arrow). An appearance of 92.9% of a-SiO_2 particles inside the gate demonstrated that this material is not applicable in the current assay.

Histogram plotting of gated events allowed for counting of the percentage of hypodiploid cells by marker placement adjacent to the clear G1-peak of cells with diploid DNA content (Fig. 6B). In

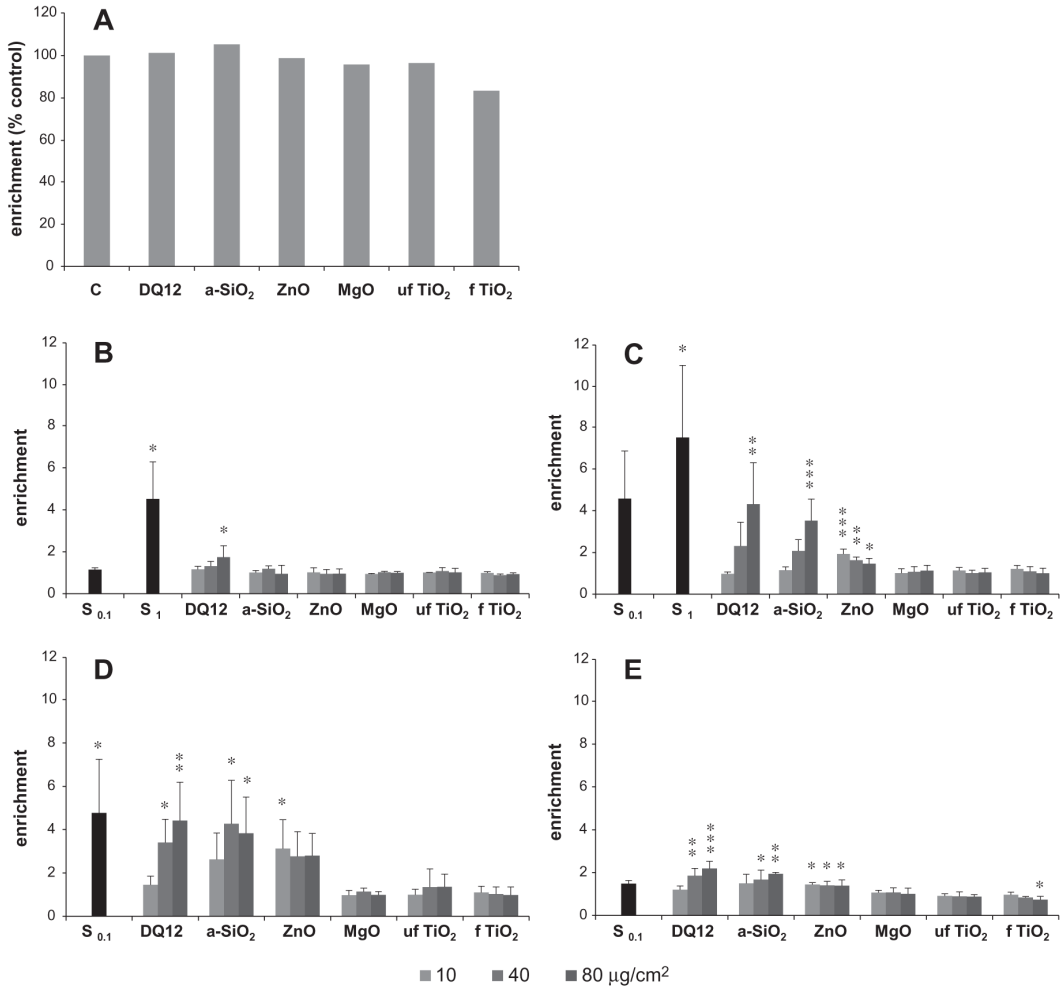

Fig. 5. Particle interference on the Cell Death Detection ELISA (CDDE) was determined in cell lysates of staurosporine-treated cells (A). CDDE was performed to detect necrosis (B and D) and apoptosis (C and E) of RAW 264.7 macrophages after 4 h (B and C) and 24 h (D and E) of particle treatment. Staurosporine was applied at 0.1 µM ($S_{0.1}$) for both time points and additionally at a concentration of 1 µM (S_1) for the 4 h time point. Enrichment of DNA refers to fold increase versus untreated cells ($n = 3$).

Table 2
Percentage of events detected as hypodiploid cells in dependence on the two fluorescent dyes 7-AAD and PI. Cells were supplemented with medium or the respective particle sample immediately before flow cytometric measurement.

Untreated cells supplemented with	Hypodiploid cells (%)	
	PI	7-AAD
Medium	3,37	2,95
DQ12	4,27	3,77
a-SiO_2	25,6	18,9
ZnO	8,55	4,44
MgO	3,32	5,29
uf TiO_2	40,4	6,88
f TiO_2	12,6	4,11

PI, propidium iodide.
7-AAD, 7-actinoaminomycin D.

contrast to control and MgO-treated cells, staurosporine-treated cells revealed apoptosis as indicated from the logarithmic bell-shaped hypodiploid DNA distribution. The a-SiO_2-treated cells would lead to similar outcome, but – as shown in 6A – in that case would be an artefact.

Using the aforementioned assay adaptations the ultimate analyses are shown in Fig. 6C. The flow cytometric analysis of the particle treated cells revealed a high content of hypodiploid DNA for DQ12 treatment at a concentration of 80 µg/cm^2. ZnO led to an almost complete DNA fragmentation after 24 h in a dose-dependent manner. MgO-treated cells appeared similar to untreated cells at all particle concentrations tested. For ultrafine TiO_2 a clear dose-dependent increase in DNA fragmentation could also be detected. Finally, for the fine TiO_2 particles a small increase of hypodiploid DNA was observed, reaching statistical significance at the highest treatment concentration.

3.5. Evaluation of apoptosis by flow cytometry-based phosphatidylserine detection

Analysis of PS exposure versus cell permeability was used to discriminate between apoptosis and necrosis using flow cytometry. Simultaneous staining with two fluorochromes, in our case with Annexin V-FITC and 7-AAD, presents an advancement of the gating procedure described in previous paragraph. For the present assay, the most appropriate channel combination for particle

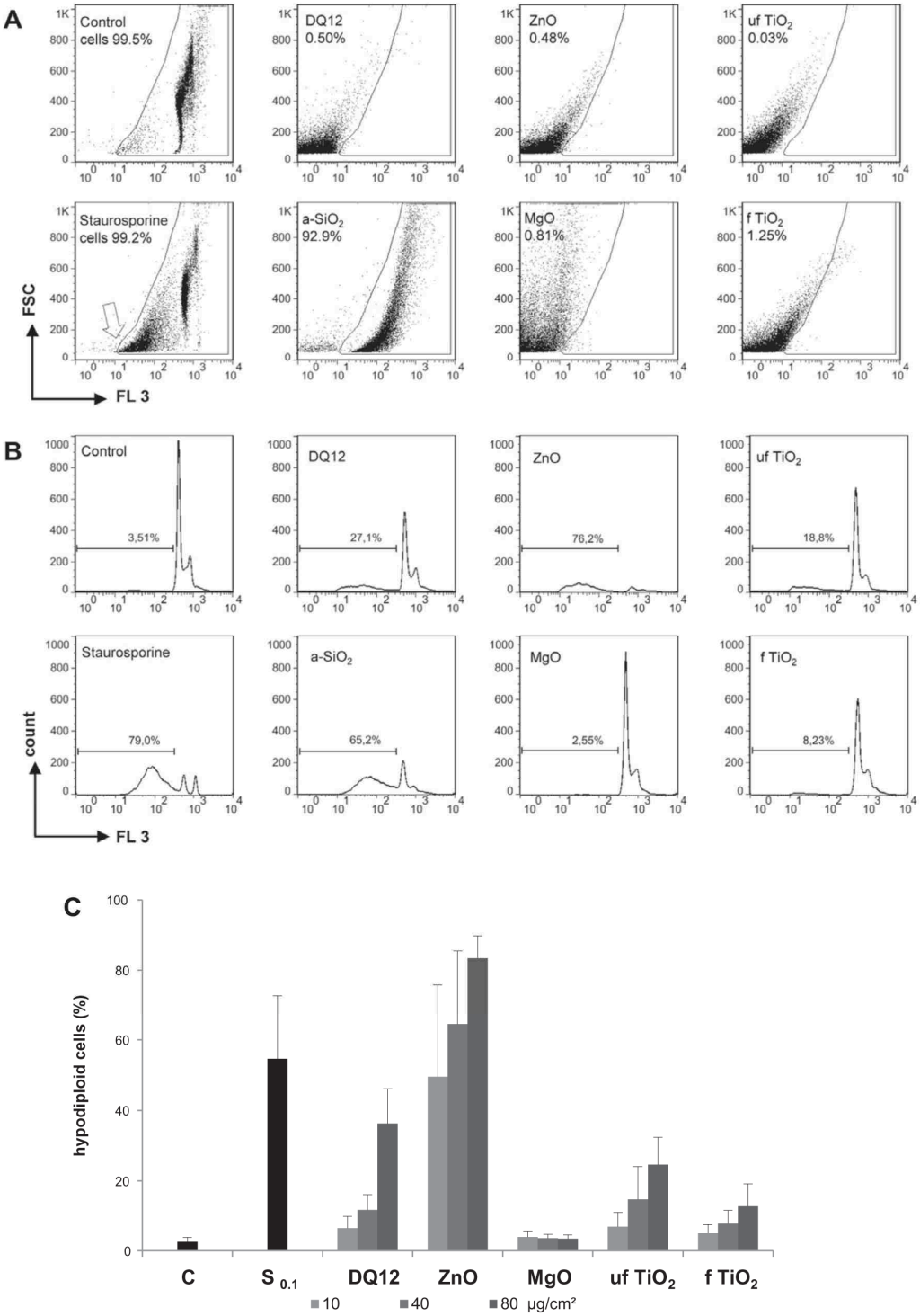

Fig. 6. DNA fragmentation in RAW 264.7 macrophages was determined using flow cytometry after staining with 7-AAD. (A) The arrow indicates the critical region of the gating procedure to separate cell- and particle-events. Percentages count for events residual inside the particle-exclusion gate. Adjustment is shown for control and 0.1 μM staurosporine-treated cells (24 h) as well as for the six cell-free particle suspensions. (B) Histogram plotting was used for evaluation of the hypodiploid fraction, exemplary shown for control and apoptotic cells (0.1 μM staurosporine-treated) as well as for all particles after treatment at 80 μg/cm^2 for 24 h, upon applying the exclusion gate. (C) The percentage of hypodiploid cells was analysed after 24 h particle or 0.1 μM staurosporine treatment (n = 3).

gating was shown to be FSC versus SSC using the following three crucial selection criteria:

First of all, we considered 5% as the maximum tolerated percentage of particle events residual out of the exclusion-gate. This approach is shown in the left column of Fig. 7A for all types of particles used in our study.

As a second consideration for the validity of assay, we decided that the application of the respective particle gates should not lead to a loss of more than 5% of staurosporine-treated cells. Therefore, the gate settings which were selected for each particle type were validated on the basis of the measurements in the staurosporine treated versus untreated cells following quadrant separation in the fluorescent channels FL-1 versus FL-3. The findings for the procedure are depicted in the two rightmost columns of Fig. 7A. Since apoptotic cells are smaller than normal cells and hence more sensitive to gate-overlapping, this approach can result in the detection of a reduced number of total events in the staurosporine-treated compared to untreated cells. Indeed, such an effect could be observed for DQ12 (loss of 15%) and a-SiO_2 (loss of 78%). Notably, both particle samples also demonstrated variations in quadrant analysis, that is, a reduction of apoptotic cells (Q3) caused by the a-SiO_2 gate contrasting with an increase of cells in Q3 by the DQ12 gate. We therefore conclude that our flow cytometry-based DNA fragmentation assay is not applicable for both types of silica particles.

The third important assay consideration was that the respective gating should not exclude treated cells that may display a change in granularity after particle uptake, and thereby affect the sideward scatter. This is shown in the second left column of Fig. 7A. The analysis of the cell populations after particle uptake versus free particles captured in the gate resulted in a clear separation for ZnO, MgO and both TiO_2 particles. Interestingly, the MgO demonstrated a specific behaviour after particle uptake, i.e. no increase of granularity was detectable. Therefore, the gating area for MgO is acceptable across the whole range of the forward scatter in the demonstrated form.

The results of the PS exposure measurements, performed with four out of the six particle types for which artefacts could be excluded after our assay modifications (i.e. MgO, ZnO, fine TiO_2, ultrafine TiO_2), are shown in Fig. 7B. The positive control staurosporine caused a significant increase of the apoptotic cell population and, to a lesser extent, also of necrotic cells. However, none of the four tested particles revealed a significant increase in phosphatidylserine exposure to indicate apoptosis. Moreover, all particles except ZnO, did not show significant signs of necrosis for the present assay. Remarkably, the ZnO treatment led to an almost entire 7-AAD positive cell population in this method, irrespective of the concentration tested.

3.6. Luminescence-based caspase assay

Caspase activation, as a specific marker of the induction of apoptosis, was determined by a luminescent activity assay for activated executioner caspases 3 and 7. All particles were also evaluated for possible quenching effects with this method. As shown in Fig. 8A, a decreased luminescent signal could be observed with ZnO and, to larger extent, with uf TiO_2. The crystalline silica sample DQ12 was found to induce a significant dose-dependent activation of caspase 3/7 in the cells after 6 h treatment (Fig. 8B). A marked activation of caspase 3/7 was also observed with staurosporine. At this time point also a-SiO_2 tended to cause a notable caspase activation, although the effects did not reach statistical significance as a result of the observed large inter-experimental variability. After 24 h treatment, no significant increase in caspase 3/7 activation was found (Fig. 8C). However, the effect was lower than that of staurosporine. Remarkably, the ZnO treatment was found to reduce the caspase signal clearly below that of untreated cells.

4. Discussion

In the current study, the toxicity of six particulate materials of different size and chemical composition was analysed in RAW 264.7 macrophages using a set of widely applied assays, including methods that specifically detect apoptosis. A general overview of our findings is summarised in Table 3. Staurosporine, a strong inducer of apoptosis (Tamaoki et al., 1986), was used as positive control and demonstrated that all assays used in our study were appropriate to determine apoptosis in the RAW 264.7 macrophages. The dose- and time-dependent effects observed with staurosporine in the cytotoxicity tests (WST-1, LDH) and the CDDE assay is in support of the feasibility of this latter assay to discriminate between necrosis, apoptosis and secondary necrosis (Silva, 2010). The variations in assay outcomes to detect pro-apoptotic effects of staurosporine observed in our study underscore the need to combine multiple approaches in apoptosis research to substantiate conclusions (Riss and Moravec, 2004).

All assays that we used in our present study are originally developed for the assessment of *in vitro* cytotoxicity of small molecular drugs and chemicals, and hence provide valid data for hazard assessment. Some of the assays are meanwhile used in high-throughput-studies. However, it is nowadays accepted that *in vitro* investigations on the biological effects of (nano)particles have to be performed with particular caution regarding the potential introduction of assay artefacts (Monteiro-Riviere et al., 2009; Stone et al., 2009). In the present study we could identify a number of pitfalls when measuring cytotoxicity and induction of apoptosis. Consequently, we have provided specific modifications to these commonly used assays, as will be discussed below.

Since a number of classical *in vitro* testing assays are based on colorimetric dyes, quantified by light absorption measurement, we evaluated potential wavelength-dependent absorbance artefacts. Among all particles evaluated, TiO_2 appeared to be the most critical material. To correct for an artificial overestimation of cell viability in the WST-1 assay, background subtraction of particle-cell-samples without WST-1 reagent was performed. This procedure provided accurate dose-dependent viability data for DQ12, a-SiO_2 and ZnO treatments. However, low concentrations of cytotoxic materials and high concentrations of TiO_2 lead to increased signals possibly linked to a proliferative stimulation for the used macrophage cell line, e.g. as shown previously for DQ12 in lung epithelial cells (Albrecht et al., 2002). However, such proliferation effect could not be confirmed for the TiO_2 by cell counting (data not shown). Interestingly, in the LDH assay, fine TiO_2 particles were found to show strong absorptive effects, despite the use of particle controls in the calculations (see Section 2 for details). However, this artefact for TiO_2 disappeared by performing the LDH measurements in cell free supernatants after centrifugation, a procedure which already was recommended from earlier nanoparticle toxicity studies (Stone et al., 2009). While this approach did not introduce novel artefacts for the other materials investigated in our study (Figs. 4B versus C), we conclude that similar comparisons need to be made on a case-by-case basis for each new particulate material investigated. Sensitising for possible interferences of NP with assays should systematically lead to an adequate study design (Stone et al., 2009).

Assay feasibility was also evaluated for the specific identification of apoptosis by (nano)particles for the assays used in our present study. Among those, the CDDE provides a technique to measure particle-induced apoptosis versus necrosis within an individual sample. Several washing steps required during the assay procedure allow for particle-free analysis and therefore imply minimal particle interferences as could be demonstrated for the majority of the used particles. However, small particles and possibly solubilised

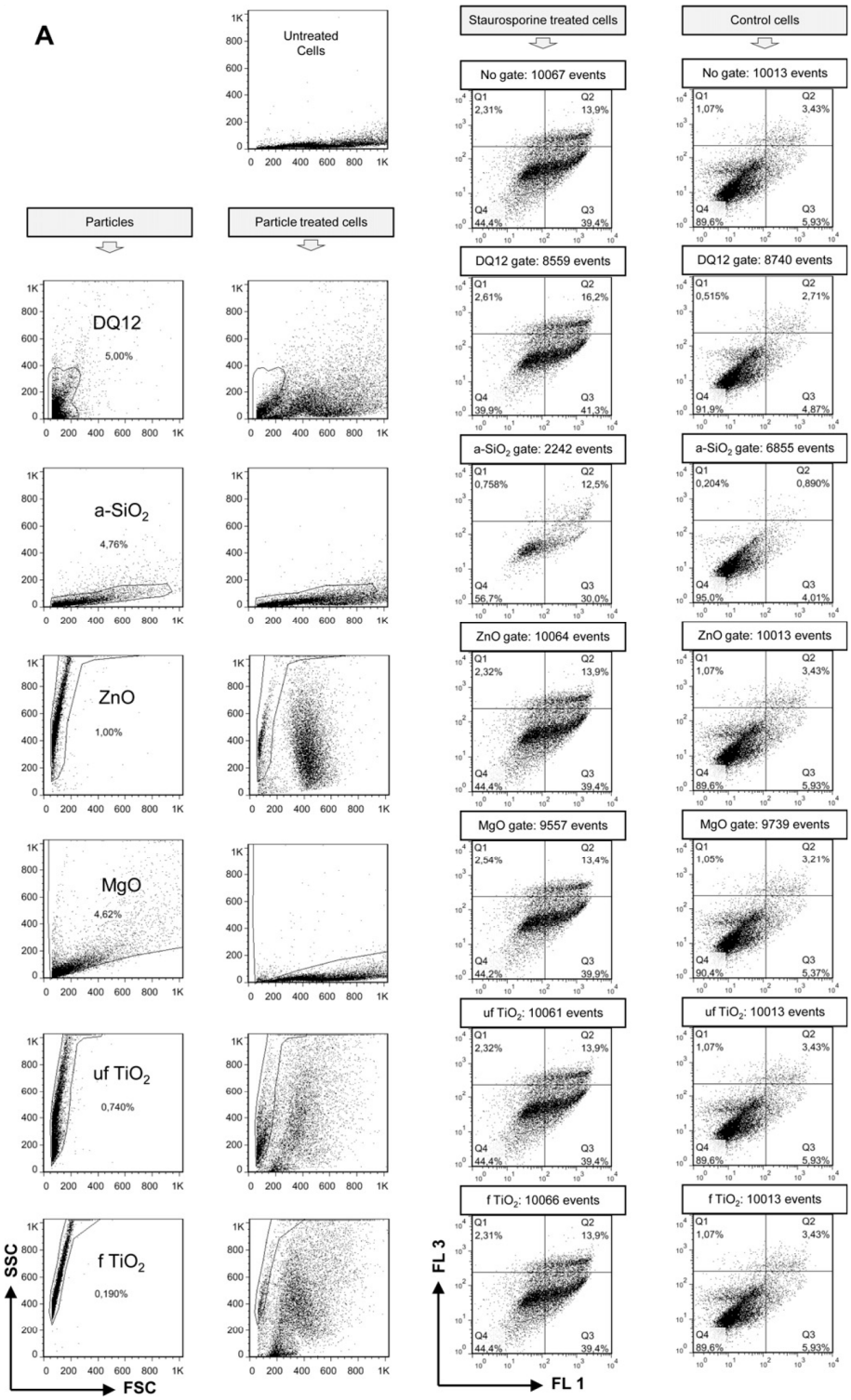

Fig. 7. Phosphatidylserine exposure and cell permeability were analysed by Annexin V-FITC and 7-AAD staining in order to discriminate between apoptosis and necrosis, respectively. (A) The procedure of creating and verifying gates for particle separation is shown in the left column: cell-free particle samples included in individual gates with at least 95% residual events. The third and fourth columns present a quadrant separation with the respective particle gates applied on staurosporine-treated (third column) and control (fourth column) cells. Residual cell events are shown in the field above each plot and should reach at least 95% of total cells. The second left column shows evaluation of the respective gates on particle-treated cells. (B) Following assay validation, the percentages of apoptotic and necrotic cells were determined after treatment for 24 h with the four particle samples appropriate for this assay ($n = 2$).

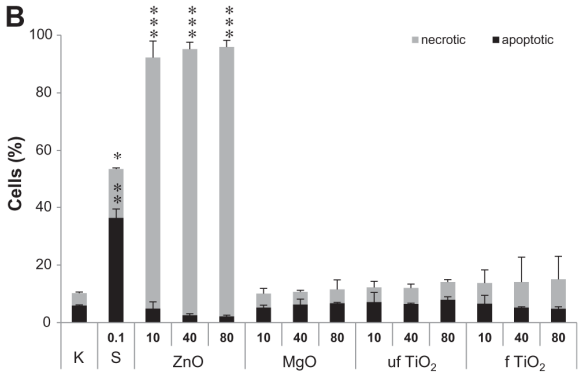

Fig. 7 (*continued*)

ions may remain in the supernatant despite centrifugation and thereby affect histone-binding on coated plates or bind and remove histone-associated DNA. Such artefacts could explain for the observed trends in retrograde dose–response effect with ZnO, and also for TiO_2. For the latter particle type this was supported by the findings in the cell-free CDDE assay (Fig. 5A). A reason that this could not be detected for ZnO may be its relatively stronger cytotoxicity, and hence a reduced absolute cell number. Herein, the recently discussed contributions of particulate ZnO versus soluble Zn ions (Xia et al., 2008; Cho et al., 2011) represent an interesting aspect for future investigation.

In contrast to the CDDE, both flow cytometry approaches use macrophage samples that contain membrane-bound and internalised particles. Strong interferences were seen for all particles used, demonstrating the need to exclude them from the measurement or to perform appropriate corrections in the data analysis. First, we could improve the gating procedure by replacing the most commonly used dye PI with 7-AAD. Secondly, we demonstrate in this study that for each material a case-by-case gating procedure is required to avoid false positive or false negative results. It has to be considered, that all efforts in our current study to minimise artefacts, including the gating procedure, exclusively focused on the avoidance of interference of the particles themselves. For (partly) soluble particulates such as the ZnO, ion effects need to be tested separately.

In our present study we used the RAW 264.7 mouse cell line but obviously, such corrections should also take into account cell-specificity of effects (Sohaebuddin et al., 2010). To our opinion, a thorough discrimination of particles from apoptotic cells or from cells with ingested particles is highly neglected in current flow cytometry based procedures and poses a challenge for future research. The analysis of hypodiploid DNA content, commonly seen as a specific marker for apoptosis (Krysko et al., 2008), could be determined in a validated manner for most of the particles used, except for the a-SiO_2 data. This sample clearly showed false positive apoptotic events due to an apparent particle inclusion in the cell gate. Because of typical physico-chemical properties of (nano)particles, interference problems during their testing are likely to increase when using multi-colour-applications in flow cytometry. Indeed, the phosphatidylserine based life/death-staining analyses in our hands revealed false positive as well as false negative results (DQ12 and a-SiO_2). Life/death-staining assay can also be performed by microscopy (Hanley et al., 2008), and may be considered as an alternative approach to determine particle-induced apoptosis, albeit in a less quantitative manner than flow cytometry.

Finally, our study also revealed potential artefacts in the commonly used caspase 3/7-assay for the detection of apoptosis. Possible false positive results due to particle–substrate-activation were

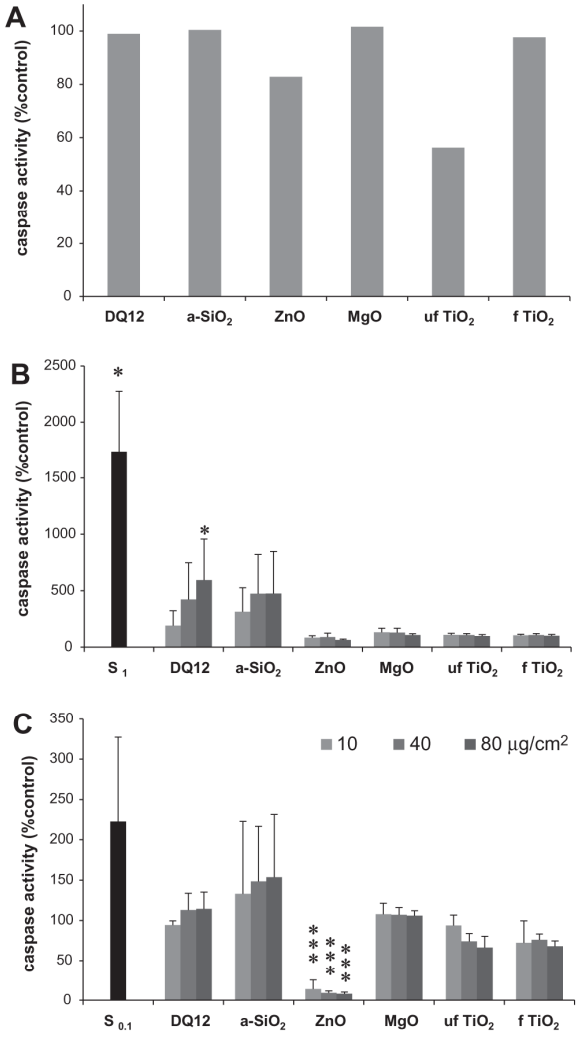

Fig. 8. Caspase 3/7 activity was determined using a chemiluminescence assay. (A) The capacity of particles to bind or modify the enzyme was determined by mixing in a concentration of 80 µg/cm^2 with recombinant caspase-3 in a cell-free system to detect possible quenching effects. (B and C) Activated executioner caspases were detected after particle treatment in RAW 264.7 macrophages after 6 h (B, $n = 2$) and 24 h (C, $n = 3$).

Table 3
Summary of particle effects in RAW 264.7 macrophages as detected by the specific assays.

	WST-1	LDH	CDDE		Flow cytometry			C 3/7
			Necrosis	Apoptosis	hDNA	PS	Necrosis	
S	+	+	+	+	+	+	+	+
DQ12	+	+	+	+	+	n.a.	n.a.	+
a-SiO_2	+	+	+	+	n.a.	n.a.	n.a.	–
ZnO	+	n.a.	+	+	+	–	+	n.a.
MgO	–	–	–	–	–	–	–	–
f TiO_2	–	–	n.a.	n.a.	+	–	–	–
uf TiO_2	–	–	–	–	+	–	–	n.a.

+, Positive effect in the specific assay; –, no effect in the specific assay, S, staurosporine; n.a., not applicable; hDNA, hypodiploid DNA content; PS, phosphatidylserine exposure; C 3/7, caspase 3/7 activity.

excluded by cell-free testing of all materials (data not shown). Conceivable interactions were the elimination of caspase or assay substrate due to particle binding. In fact, we could demonstrate a quenching effect using recombinant caspase-3, when mixed with ZnO or ultrafine TiO_2 particles. A straightforward quantitative extrapolation of this effect to cellular systems is not possible, and further research is needed to determine whether such potential interference has any biological implication in nanoparticle-exposed cells. The markedly diminished caspase signal seen for all ZnO treatment concentrations after 24 h might at least in part also be explained by the relatively strong reduction of cell numbers as indicated from the WST-1 assay. Nevertheless, our findings indicate that the detection of effector caspases in the used assay may be impaired in cells treated with specific types of particles and as such, possibly result in false negative data.

When considered altogether, the data from our present study have revealed that a correct identification of necrotic and apoptotic effects of specific types of (nano)particles highly depends both on the selection of assays and on a flawless correction of assay interferences (see Table 3). For the interpretation of our findings one should be aware of the fact that one single cell line was used and that the overview in Table 3 may not necessarily be extrapolated to other cell types. With the exception of MgO, which was found to be non-toxic and non-apoptotic in all our assays, for all particles used in our present study a potentially biased interpretation was identified. Exemplary, the crystalline silica sample DQ12, which we selected as a positive particle control for our current study (Oberdorster et al., 2005a), could not be appropriately analysed in the phosphatidylserine exposure assay. However, this particle showed up positive in all further necrosis and apoptosis assays in concordance with the established literature (Sarih et al., 1993; Fubini, 1998). Among the other particles, the amorphous silica NP turned out to be the most complicated to test. Because of the invalid measurements in the flow cytometric approaches, its ability to trigger apoptosis was only revealed from the CDDE and, to some extent (i.e. no statistical significance) for the caspase 3/7-assay. The resulting interpretation difficulties may very well reflect the contrasting literature findings for amorphous silica NP (Johnston et al., 2000; Kim et al., 2009; Napierska et al., 2010; Yang et al., 2010; Ye et al., 2010), and once more highlights the importance of using a testing battery approach in apoptosis research (Riss and Moravec, 2004). In our study, fine and nanosize TiO_2 were shown not to be cytotoxic and apoptotic in RAW 264.7 macrophages in any assay with the exception of the flow cytometric detection of hypodiploid DNA, where small but significant effects could be observed. Whether this is due to a particularly high sensitivity of this assay, or a yet-to-be identified assay artefact remains to be investigated. Similar to amorphous SiO_2, highly contrasting observations have been reported in the literature for TiO_2, likely resulting from sample-specific differences in physico-chemical properties (e.g. size, crystal structure, surface coating) as well as the selected cell type (Rahman et al., 2002; Vamanu et al., 2008; Johnston et al., 2009). Fine TiO_2 showed up positive for one assay despite being generally considered as non-toxic and inert, which suggests that MgO may serve as a more useful particulate negative control than the TiO_2 sample. The most potent NP analysed in our study appeared to be the ZnO for the majority of the assays. Apoptosis induction by ZnO in RAW 264.7 cells has been shown previously by Xia and colleagues (Xia et al., 2008). In our study, apoptosis was indicated by CDDE and flow cytometric investigation of hypodiploid DNA content concurrently with a clear necrotic response. However, apoptosis was not evidenced from the life/death staining data and caspase 3/7 activation. The contribution of caspases in ZnO-induced apoptosis as well as the involvement of other pathways of DNA-fragmentation are subjects of our ongoing investigations. Especially the strong necrotic effect observed in the present study has to be taken into account. At least to some extent this might be a result of secondary necrosis, an *in vitro* specific phenomenon, and requires further study focusing at earlier time points.

In summary, the toxicity testing of a panel of particles by various assays revealed ZnO NP as highly cytotoxic with strong indication for apoptotic effects on RAW 264.7 macrophages. In contrast, for MgO NP no adverse effects could be detected. The well-known ability of crystalline silica to induce apoptosis in macrophages could be confirmed and seems to apply for amorphous silica NP, too. For both TiO_2 samples, signs of necrosis/apoptosis induction in macrophages were merely absent. Taken together, our investigations highlight that valid statements on the potential induction of apoptosis by specific NP require measurement of multiple endpoints, and that specific further assay modifications are to be considered. Due to the individual physicochemical characteristics of each material as well as specific measurement algorithms of each technique common recommendations for certain assays are impossible to give at present. They also point out the need to control for assay interference and to include appropriate assay specific controls to avoid misinterpretation of specific *in vitro* test findings on a case-by case basis in the steadily expanding field of nanotoxicology.

Conflict of interest statement

None declared.

Acknowledgements

The authors wish to thank Christel Weishaupt for her technical assistance. The work was funded by the Research Commission of the Heinrich-Heine-University Düsseldorf as well as the Federal Ministry of Education and Research.

References

Albrecht, C., Borm, P.J., Adolf, B., Timblin, C.R., Mossman, B.T., 2002. *In vitro* and in vivo activation of extracellular signal-regulated kinases by coal dusts and quartz silica. Toxicol. Appl. Pharmacol. 184, 37–45.

Albrecht, C., Knaapen, A.M., Becker, A., Hohr, D., Haberzettl, P., van Schooten, F.J., Borm, P.J., Schins, R.P., 2005. The crucial role of particle surface reactivity in respirable quartz-induced reactive oxygen/nitrogen species formation and APE/Ref-1 induction in rat lung. Respir. Res. 6, 129.

Auffan, M., Rose, J., Wiesner, M.R., Bottero, J.Y., 2009. Chemical stability of metallic nanoparticles: a parameter controlling their potential cellular toxicity *in vitro*. Environ. Pollut. 157, 1127–1133.

Balbus, J.M., Maynard, A.D., Colvin, V.L., Castranova, V., Daston, G.P., Denison, R.A., Dreher, K.L., Goering, P.L., Goldberg, A.M., Kulinowski, K.M., Monteiro-Riviere, N.A., Oberdorster, G., Omenn, G.S., Pinkerton, K.E., Ramos, K.S., Rest, K.M., Sass, J.B., Silbergeld, E.K., Wong, B.A., 2007. Meeting report: hazard assessment for nanoparticles – Report from an interdisciplinary workshop. Environ. Health Perspect. 115, 1654–1659.

Borges, V.M., Falcao, H., Leite-Junior, J.H., Alvim, L., Teixeira, G.P., Russo, M., Nobrega, A.F., Lopes, M.F., Rocco, P.M., Davidson, W.F., Linden, R., Yagita, H., Zin, W.A., DosReis, G.A., 2001. Fas ligand triggers pulmonary silicosis. J. Exp. Med. 194, 155–164.

BSi_report, 2007. PAS 136 terminology for nanomaterials. <http://www.bsigroup.com/upload/standards%20&%20Publications/Nanotechnologies/PAS%20136.pdf>.

Chaudhry, Q., Scotter, M., Blackburn, J., Ross, B., Boxall, A., Castle, L., Aitken, R., Watkins, R., 2008. Applications and implications of nanotechnologies for the food sector. Food Addit Contam Part A Chem. Anal. Control Expo. Risk Assess. 25, 241–258.

Cho, W.S., Duffin, R., Poland, C.A., Duschl, A., Oostingh, G.J., Macnee, W., Bradley, M., Megson, I.L., Donaldson, K., 2011. Differential pro-inflammatory effects of metal oxide nanoparticles and their soluble ions *in vitro* and in vivo; zinc and copper nanoparticles, but not their ions, recruit eosinophils to the lungs. Nanotoxicology.

Donaldson, K., Stone, V., Tran, C.L., Kreyling, W., Borm, P.J., 2004. Nanotoxicology. Occup. Environ. Med. 61, 727–728.

Duffin, R., Mills, N.L., Donaldson, K., 2007. Nanoparticles – A thoracic toxicology perspective. Yonsei Med. J. 48, 561–572.

Fischer, U., Stroh, C., Schulze-Osthoff, K., 2006. Unique and overlapping substrate specificities of caspase-8 and caspase-10. Oncogene 25, 152–159.

Fubini, B., 1998. Surface chemistry and quartz hazard. Ann. Occup. Hyg. 42, 521–530.

Fubini, B., Hubbard, A., 2003. Reactive oxygen species (ROS) and reactive nitrogen species (RNS) generation by silica in inflammation and fibrosis. Free Radic. Biol. Med. 34, 1507–1516.

Hanley, C., Layne, J., Punnoose, A., Reddy, K.M., Coombs, I., Coombs, A., Feris, K., Wingett, D., 2008. Preferential killing of cancer cells and activated human T cells using ZnO nanoparticles. Nanotechnology 19, 295103.

Iyer, R., Hamilton, R.F., Li, L., Holian, A., 1996. Silica-induced apoptosis mediated via scavenger receptor in human alveolar macrophages. Toxicol. Appl. Pharmacol. 141, 84–92.

Johnston, C.J., Driscoll, K.E., Finkelstein, J.N., Baggs, R., O'Reilly, M.A., Carter, J., Gelein, R., Oberdorster, G., 2000. Pulmonary chemokine and mutagenic responses in rats after subchronic inhalation of amorphous and crystalline silica. Toxicol. Sci. 56, 405–413.

Johnston, H.J., Hutchison, G.R., Christensen, F.M., Peters, S., Hankin, S., Stone, V., 2009. Identification of the mechanisms that drive the toxicity of TiO(2)particulates: the contribution of physicochemical characteristics. Part Fibre Toxicol. 6, 33.

Kim, H., Ahn, E.-K., Jee, B., Yoon, H.-K., Lee, K., Lim, Y., 2009. Nanoparticulate-induced toxicity and related mechanism *in vitro* and in vivo. J.Nanoparticle Res. 11, 55–65.

Kroll, A., Pillukat, M.H., Hahn, D., Schnekenburger, J., 2009. Current *in vitro* methods in nanoparticle risk assessment: limitations and challenges. Eur. J. Pharm. Biopharm. 72, 370–377.

Krysko, D.V., Vanden Berghe, T., D'Herde, K., Vandenabeele, P., 2008. Apoptosis and necrosis: detection, discrimination and phagocytosis. Methods 44, 205–221.

Monteiro-Riviere, N.A., Inman, A.O., Zhang, L.W., 2009. Limitations and relative utility of screening assays to assess engineered nanoparticle toxicity in a human cell line. Toxicol. Appl. Pharmacol. 234, 222–235.

Napierska, D., Thomassen, L.C., Lison, D., Martens, J.A., Hoet, P.H., 2010. The nanosilica hazard: another variable entity. Part Fibre Toxicol. 7, 39.

Oberdorster, G., Maynard, A., Donaldson, K., Castranova, V., Fitzpatrick, J., Ausman, K., Carter, J., Karn, B., Kreyling, W., Lai, D., Olin, S., Monteiro-Riviere, N., Warheit, D., Yang, H., 2005a. Principles for characterizing the potential human health effects from exposure to nanomaterials: elements of a screening strategy. Part Fibre Toxicol. 2, 8.

Oberdorster, G., Oberdorster, E., Oberdorster, J., 2005b. Nanotoxicology: an emerging discipline evolving from studies of ultrafine particles. Environ. Health Perspect. 113, 823–839.

Ortiz, L.A., Moroz, K., Liu, J.Y., Hoyle, G.W., Hammond, T., Hamilton, R.F., Holian, A., Banks, W., Brody, A.R., Friedman, M., 1998. Alveolar macrophage apoptosis and TNF-alpha, but not p53, expression correlate with murine response to bleomycin. Am. J. Physiol. 275, L1208–1218.

Powell, J.J., Faria, N., Thomas-McKay, E., Pele, L.C., 2010. Origin and fate of dietary nanoparticles and microparticles in the gastrointestinal tract. J. Autoimmun. 34, J226–233.

Rahman, Q., Lohani, M., Dopp, E., Pemsel, H., Jonas, L., Weiss, D.G., Schiffmann, D., 2002. Evidence that ultrafine titanium dioxide induces micronuclei and apoptosis in Syrian hamster embryo fibroblasts. Environ. Health Perspect. 110, 797–800.

Riss, T.L., Moravec, R.A., 2004. Use of multiple assay endpoints to investigate the effects of incubation time, dose of toxin, and plating density in cell-based cytotoxicity assays. Assay Drug Dev. Technol. 2, 51–62.

Riviere, G., 2009. European and international standardisation progress in the field of engineered nanoparticles. Inhal. Toxicol. 21 (Suppl 1), 2–7.

Sarih, M., Souvannavong, V., Brown, S.C., Adam, A., 1993. Silica induces apoptosis in macrophages and the release of interleukin-1 alpha and interleukin-1 beta. J. Leukoc. Biol. 54, 407–413.

Silva, M.T., 2010. Secondary necrosis: the natural outcome of the complete apoptotic program. FEBS Lett. 584, 4491–4499.

Sohaebuddin, S.K., Thevenot, P.T., Baker, D., Eaton, J.W., Tang, L., 2010. Nanomaterial cytotoxicity is composition, size, and cell type dependent. Part Fibre Toxicol. 7, 22.

Stone, V., Johnston, H., Schins, R.P., 2009. Development of *in vitro* systems for nanotoxicology: methodological considerations. Crit. Rev. Toxicol. 39, 613–626.

Tamaoki, T., Nomoto, H., Takahashi, I., Kato, Y., Morimoto, M., Tomita, F., 1986. Staurosporine, a potent inhibitor of phospholipid/Ca^{2+} dependent protein kinase. Biochem. Biophys. Res. Commun. 135, 397–402.

Unfried, K., Albrecht, C., Klotz, L.-O., Von Mikecz, A., Grether-Beck, S., Schins, R., 2007. Cellular responses to nanoparticles: target structures and mechanisms. Nanotoxicology 1, 52–71.

Valko, M., Morris, H., Cronin, M.T., 2005. Metals, toxicity and oxidative stress. Curr. Med. Chem. 12, 1161–1208.

Vamanu, C.I., Cimpan, M.R., Hol, P.J., Sornes, S., Lie, S.A., Gjerdet, N.R., 2008. Induction of cell death by TiO_2 nanoparticles: studies on a human monoblastoid cell line. Toxicol. In Vitro 22, 1689–1696.

van Engeland, M., Nieland, L.J., Ramaekers, F.C., Schutte, B., Reutelingsperger, C.P., 1998. Annexin V-affinity assay: a review on an apoptosis detection system based on phosphatidylserine exposure. Cytometry 31, 1–9.

Xia, T., Kovochich, M., Liong, M., Madler, L., Gilbert, B., Shi, H., Yeh, J.I., Zink, J.I., Nel, A.E., 2008. Comparison of the mechanism of toxicity of zinc oxide and cerium oxide nanoparticles based on dissolution and oxidative stress properties. ACS nano. 2, 2121–2134.

Yang, X., Liu, J., He, H., Zhou, L., Gong, C., Wang, X., Yang, L., Yuan, J., Huang, H., He, L., Zhang, B., Zhuang, Z., 2010. SiO_2 nanoparticles induce cytotoxicity and protein expression alteration in HaCaT cells. Part Fibre Toxicol. 7, 1.

Ye, Y., Liu, J., Xu, J., Sun, L., Chen, M., Lan, M., 2010. Nano-SiO_2 induces apoptosis via activation of p53 and Bax mediated by oxidative stress in human hepatic cell line. Toxicol. In Vitro 24, 751–758.

Chapter III

Zinc oxide nanoparticles induce necrosis and apoptosis in macrophages in a p47phox- and Nrf2-independent manner

Verena Wilhelmi, Ute Fischer, Heike Weighardt, Klaus Schulze-Osthoff, Charlotte Esser, Roel P.F. Schins, Catrin Albrecht

PLOS ONE
Submitted for publication

Study 2: Zinc oxide nanoparticles induce necrosis and apoptosis in macrophages in a p47phox- and Nrf2-independent manner

Declaration

The manuscript is submitted to a peer-review journal.
All experimental work presented, except for TEM investigations, was performed by Verena Wilhelmi.
The impact on authoring this paper can be estimated in total with 80%.

3 Abstract

In view of the steadily increasing use of zinc oxide nanoparticles in various industrial and consumer applications, toxicological investigations to evaluate their safety are highly justified. We have investigated mechanisms of ZnO nanoparticle-induced apoptosis and necrosis in macrophages in relation to their important role in the clearance of inhaled particulates and the regulation of immune responses during inflammation. In the murine macrophage RAW 264.7 cell line, ZnO treatment caused a rapid induction of nuclear condensation, DNA fragmentation, and the formation of hypodiploid DNA nuclei and apoptotic bodies. The involvement of the essential effector caspase-3 in ZnO-mediated apoptosis could be demonstrated by immunocytochemical detection of activated caspase-3 in RAW 264.7 cells. ZnO specifically triggered the intrinsic apoptotic pathway, because Jurkat T lymphocytes deficient in the key mediator caspase-9 were protected against ZnO-mediated toxicity whereas reconstituted cells were not. ZnO also caused DNA strand breakage and oxidative DNA damage in the RAW 264.7 cells as well as $p47^{phox}$ NADPH oxidase-dependent superoxide generation in bone marrow-derived macrophages. However, ZnO-induced cell death was not affected in bone marrow-derived macrophages of mice deficient in $p47^{phox}$ or the oxidant responsive transcription factor Nrf2. Taken together, our data demonstrate that ZnO nanoparticles trigger $p47^{phox}$ NADPH oxidase-mediated ROS formation in macrophages, but that this is dispensable for caspase-9/3-mediated apoptosis. Execution of apoptotic cell death by ZnO nanoparticles appears to be NADPH oxidase and Nrf2-independent but rather triggered by alternative routes.

3.1 Introduction

Nanotechnology is one of the key technologies of the current and upcoming decades, creating an enormous number of novel marketing potentials. Especially metallic nanoparticles offer great industrial opportunities due to their unique properties. Among these are zinc oxide nanoparticles (ZnO NP), which are produced in high tonnage and utilized in many commercial products. Because of their excellent UV-adsorbing properties and concurrent transparency for visible light, ZnO NP have found their use as efficient UV-protectors in cosmetics like sunscreens as well as in paints or finishing materials of building storefronts [Schilling et al., 2010; Klupp Taylor et al., 2011]. Antibacterial properties of this material are used in household products like toothpaste or in food-packaging materials [Musee et al., 2011; Tankhiwale et al., 2012]. In the fields of biotechnology and nanomedicine ZnO-based biosensors and biomedical nanomaterials containing ZnO are being developed for cancer treatment applications and improved drug delivery [Rasmussen et al., 2010; Anish Kumar et al., 2011]. The broad applicability of ZnO nanoparticles implies human exposure via different body entrance routes, including inhalation and ingestion. Macrophages are strategically located throughout the body tissues and play a central role in the defense against foreign material, dead cells and debris; these processes are implicated in both protective and adverse functions of macrophages in the regulation of the immune response in various pathogenic processes including inflammation and fibrosis [Murray et al., 2012]. Regarding particulate matter, macrophages are the most important cell type for uptake and clearance processes [Unfried K 2007; Geiser 2010; Smith et al., 2011]. There is evidence that mononuclear cells, presumably the resident alveolar macrophages, mediate metal-related parenchymal disorders in occupational settings, such as metal fume fever which may result from inhalation of ZnO particles [Kelleher et al., 2000]. Investigations with crystalline silica dust have revealed a clear association between particle-induced apoptotic processes and the development of lung fibrosis [Iyer et al., 1996].

Several recent studies have shown considerable cytotoxicity of ZnO NP to specific cell types, microorganisms and *in vivo* models [Unfried K 2007; Xia et al., 2008; Cho et al., 2010; Sharma et al., 2011; Kermanizadeh et al., 2012; Sharma et al., 2012]. However, there are still a lot of controversies regarding the underlying pathways implicated in ZnO-induced cell death. This includes the impact of specific physico-chemical properties of this material, like particle size and dissolution as well as the formation of reactive oxygen species (ROS) and the associated oxidative stress involving induction of lipid peroxidation and oxidative DNA

damage [Xia et al. 2008; Huang et al., 2010; Ahamed et al., 2011; Sharma et al. 2011; Akhtar et al., 2012; Sharma et al. 2012]. In professional phagocytes, such as macrophages and neutrophils, the dominant source of ROS is the classic nicotinamide adenine dinucleotide phosphate (NADPH) oxidase enzyme complex NOX2. Activation of this complex involves the recruitment and assembly of multiple cytosolic subunits including $p47^{phox}$, $p67^{phox}$ and $p40^{phox}$ with its membrane-bound subcomplex consisting of $gp91^{phox}$, $p22^{phox}$ and Rac and results in the rapid generation of large amounts of superoxide anion (O_2^-) [Park 2003]. The NOX2-mediated oxidative burst represents a hallmark of the innate host defense to invading microorganisms. However, it is also strongly implicated in the adverse pulmonary effects of well-known particulate toxicants including asbestos and respirable crystalline silica dust [Castranova 2004; Dostert et al., 2008; van Berlo et al., 2010].

Cells typically accomplish oxidative stress with the induction of antioxidant and detoxification enzymes mediated by the transcription factor nuclear factor erythroid-derived 2 related factor 2 (Nrf2) and hence may counteract the effects of necrosis and apoptosis-inducing triggers [Dhakshinamoorthy et al., 2004; Li et al., 2005; Kang et al., 2012]. During oxidative stress, Nrf2 is released from its cytosolic repressor Keap1 and subsequently translocates into the nucleus where it binds to antioxidant response elements (ARE) residing within the promoter regions of many antioxidant and phase II genes [Lee et al., 2004]. The establishment of Nrf2 knockout mouse models has provided major support for the protective role of this pathway in ROS mediated cell death and diseases [Kobayashi et al., 2005; Cho et al., 2006]

The formation of ROS and associated induction of oxidative stress have been strongly linked to apoptosis in macrophages [Forman et al., 2002]. Apoptotic pathways induced by ROS-mediated DNA damage are fundamentally governed by mitochondria due to the release of apoptogenic factors out of the intermembrane space. The release of cytochrome c initiates the formation of the apoptosome, composed of Apaf-1 and the initiator caspase-9, resulting in caspase-9 activation. This complex in turn activates the executioner caspase-3, -6 and -7. Cleavage of their specific substrates leads to the typical apoptotic cellular changes and final cell death [Shi 2002].

The aim of our study was to explore the mechanisms of ZnO-induced cell death in macrophages, as these cells are of key importance in uptake and clearance of particulates and orchestration of inflammation. Therefore, we investigated the necrotic and apoptotic effects of ZnO in the murine macrophage cell line RAW 264.7 as well as in primary macrophages obtained from bone marrow of $p47^{phox}$ NADPH oxidase and Nrf2-deficient mice.

3.2 Materials and Methods

Cells

The murine macrophage-like cell line RAW 264.7 (ATCC# TIB-71; American Type Culture Collection, Manassas, VA, USA) was cultured at 37 °C in humidified 5% CO_2 atmosphere in Dulbecco's modified Eagle's medium (DMEM, Sigma-Aldrich, Deisenhofen, Germany) supplemented with 4 mM L-glutamine, 1.5 g/l sodium bicarbonate, 4.5 g/l glucose, penicillin (100 U/ml)/streptomycin (0.1 mg/ml) and 10% fetal calf serum (Sigma-Aldrich).

Generation of the caspase-9 restored cell clone JMR/C9 from the mutant T-cell line JMR deficient in caspase-9 was originally described by Samaraj and colleagues [Samraj et al., 2007]. Both cell lines were cultured in RPMI-1640 medium with 10% heat-inactivated fetal calf serum, 2 mM L-glutamine, 1.5 g/l sodium bicarbonate, 4.5 g/l glucose and penicillin/streptomycin. Culturing proceeded in a humidified 5% CO_2 atmosphere at 37°C. Subculturing of all cell lines was performed to maintain cells growing in the logarithmic phase.

Bone marrow cells were obtained from $p47^{phox\ -/-}$ and C57Bl/6J wild type (wt) mice (Taconic, Germantown, NY, USA), originally produced in the laboratory of S. M. Holland [Jackson et al., 1995]. Bone marrow cells were also obtained from $Nrf2^{-/-}$ mice and C57Bl/6J littermate controls (Riken BioResource, Tsukuba, Japan), originally produced in the laboratory of M. Yamamoto [Itoh et al., 1997]. Animals were maintained according to the guidelines of the Society for Laboratory Animals Science (GV-SOLAS). After sacrificing, both hind legs of mice were freed of soft tissue attachments. The tips of femur as well as the tibia were cut off and flushed with sterile PBS supplemented with penicillin/streptomycin. Cell suspensions were centrifuged (200 g, 10 min, 4 °C) and resuspended in culture medium RPMI-1640 (PAA, Cölbe, Germany) containing 10% FCS gold (PAA), 2 mM glutamine, penicillin/streptomycin and 0.1% MeSH. 10 ml of 5 x 10^6 cells in suspension containing 10% of L929 cell supernatant were seeded in bacterial culture plates (10 cm, Greiner bio-one, Solingen, Germany). After three days of incubation at 37°C in a humidified 5% CO_2 atmosphere, 10 ml of freshly prepared medium containing 10% M-CSF/GM-CSF containing L929 supernatant were adjusted. After six days, the adherent fraction of cells mainly contains macrophages and can be harvested by scraping the rinsed cell layer. Double staining of the macrophage markers CD11b-FITC (BD Biosciences, Heidelberg, Germany) and F4/80-PE (eBioscience, Frankfurt, Germany) identified 54 - 97% $CD11b^+/F4/80^+$ macrophages by FACS analysis using a FACSCalibur operating with CellQuestPro software (BD Biosciences).

Particle characteristics and treatment of the cells

The general cytotoxicity studies in RAW 264.7 cells were performed with four different samples of ZnO particles, indicated as ZnO I (from Nanostructured and Amorphous Materials Inc., with a declared primary particle diameter of 20 nm and a specific surface area (SSA) of 50 m^2/g), ZnO II (Nanoactive, from Nanoscale Materials Inc., with a declared crystallite size of < 10 nm and SSA of 70 m^2/g), ZnO III (from Sigma-Aldrich, with a declared SSA < 10 m^2/g), and ZnO IV (obtained through the European Commission Joint Research Centre (Ispra, Italy) as reference nanomaterial NM-110, with a diameter of 100 nm and SSA of 14 m^2/g). For all subsequent experiments, sample ZnO I was selected, and referred to as ZnO in this paper. This material has been analysed in detail within the EU 6th framework project NANOSH [http://www.ttl.fi/partner/nanosh/progress/Documents/nanosh_nanoatlas.pdf]. Further specific characteristics of the other three samples used in this project are described elsewhere [Gerloff et al., 2009; Cho et al. 2010; Gerloff et al., 2012b; Kermanizadeh et al. 2012]. All ZnO samples were baked at 220 °C for 16 h to destroy possible endotoxins.

Depending on the type of experiment, cells were seeded in a concentration of 1.1 x 10^5/cm² into 6-well plates, 24-well plates, 96-well plates or in 4-chamber-slides (BD Biosciences) and incubated for 24 h prior to treatment. Immediately before each experiment, the ZnO samples were freshly suspended at 0.7 g/L in complete cell culture medium by water bath sonication (60 W, 35 Hz, 10 min, Sonorex TK 52; Bandelin, Berlin, Germany), diluted to the final concentrations of 1, 5, 10, 40 or 80 µg/cm² and treated for 4 h or 24 h as indicated. As positive control, cells were treated with the apoptosis inducer staurosporine (STS, Sigma-Aldrich) at a concentration of 1 µM (4 h) or 0.1 µM (24 h). In a specific subset of experiments, the role of solubilization of ZnO nanoparticles in the cell treatment medium was also addressed. Therefore, RAW 264.7 cells were treated either with freshly prepared ZnO suspensions, or with suspensions that were first pre-incubated for 24 h at 37 °C. In addition, the effects of the respective particle-free supernatants and pellets of the 24 h pre-incubated suspensions were evaluated, as obtained following 10 min centrifugation at 16.000 g.

Cytotoxicity

Cell viability was determined using the WST-1 conversion assay (Roche, Mannheim, Germany). Care was taken to avoid artefacts in the measurement due to interference of the ZnO particles in this assay, as previously described in detail [Wilhelmi et al., 2012].

Analysis of DNA fragmentation

Determination of apoptosis was evaluated by chromosomal DNA fragmentation analysis after staining with the DNA-intercalating dye 7-aminoactinomycin D (7-AAD, Sigma-Aldrich). Details of the procedure, which included particle gating, was done as previously described [Wilhelmi et al. 2012]. Apoptotic DNA fragmentation was also detected by using a DNA Fragmentation Imaging Kit (Roche) following the manufacturer's instruction. Based on the TUNEL reaction using terminal deoxynucleotidyl transferase and fluorescein-labeled dUTP, fluorescence detection of cells with apoptotic DNA strand breaks was performed. To examine total cell numbers, nuclei were labeled simultaneously with Hoechst 33342. Merged images of both channels were shown using a fluorescence microscope (Zeiss AxioObserver.D1 with AxioCam MRm, controlled by AxioVision Rel. 4.8) at 100x magnification (Carl Zeiss, Oberkochen, Germany).

Oxidative DNA damage measurement by the fpg-modified comet assay

The alkaline comet assay was used to measure DNA strand breaks in RAW 264.7 macrophages, with inclusion of the enzyme formamidopyrimidine glycosylase (Fpg) to specifically determine oxidative DNA damage. This was done using the method as described by Speit et al. [Speit et al., 2004] with modifications as specified in Gerloff et al. [Gerloff et al. 2009]. Fpg-enzyme was kindly provided by Dr. Andrew Collins, Institute for Nutrition Research, University of Oslo, Norway. As a positive control, oxidative DNA damage was induced by treatment with the photosensitizer Ro 19-8022 ([R]-1-[(10-chloro-4-oxo-3-phenyl-4H-benzo[a]quinolizin-1-yl)carbonyl]-2-pyrrolidinemethanol) (Roche, Basel, Switzerland) after 2 min of light irradiation [Gerloff et al., 2012a]. DNA strand breakage data are presented as % comet tail values (in the absence of fpg). Oxidative DNA damage is calculated and shown as the differences in % tail DNA as measured in the presence or absence of the Fpg enzyme: delta (Δ)Fpg = [% tail DNA_{+Fpg}] – [% tail DNA_{-Fpg}].

Transmission electron microscopy (TEM)

TEM was used to evaluate ultrastructural hallmarks of cell death in RAW 264.7 macrophages. Therefore, cells were treated in 6-well plates, harvested by scraping and washed with PBS (200 g, 10 min). The pellet was fixed with 0.1 M phosphate-buffer (pH 7.4)/2.5% glutaraldehyde/4% paraformaldehyde, stained en bloc with uranyl acetate, and embedded in epoxy resin. Ultra-thin sections were cut and examined with a transmission electron microscope (Hitachi H-600, Hitachi High-Technologies Europe GmbH, Krefeld, Germany).

Fluorescence Analysis

Cells were grown and treated in four chamber culture slides (BD Biosciences). All following steps were performed at RT unless otherwise noted and kept separate by three washing steps each for 5 min in PBS. Cells were fixed in 4% paraformaldehyde/PBS (pH 7.4) for 20 min and permeabilised in 0.1% Triton X-100/PBS. Non-specific binding sites were saturated during 1 h incubation in 5% normal goat serum/PBS (Vector Laboratories, Burlingame, CA, USA). Primary antibody against cleaved caspase-3 was diluted 1:200 in PBS (rabbit monoclonal, Cell Signaling, Boston, MA, USA) and incubated at 4 °C overnight in a humid box. The secondary antibody (MFP488 goat anti-rabbit, MoBiTec, Göttingen, Germany) was applied for 1 h 1:200 in PBS. Nuclear staining was performed by using the dye Hoechst 33342 (Cell Signaling) in a final concentration of 1 µg/ml in PBS for 15 min at 37 °C in a humid box. In order to control for unspecific staining primary antibody was replaced by rabbit IgG in the same concentration (Vector Laboratories).

Analysis was performed using a fluorescence microscope (Olympus BX60, Germany) connected with a color camera (U-CMAD3, Olympus) controlled by an image analysis system (analySIS, Olympus, Hamburg, Germany) at 400x magnification.

Measurement of particle uptake

Cells containing particles may change their granularity, which is directly correlated to the sideward scatter (SSC) measured by FACS analysis. Particle uptake was measured in treated primary macrophages from $p47^{phox\ -/-}$ and wt mice upon discrimination of free ZnO particles from the cellular events as described previously [Wilhelmi et al. 2012]. After 3 h treatment, cells were washed and suspended in ice-cold $HBSS^{-/-}$ (Invitrogen, Karlsruhe, Germany) and analysed using FACS Calibur (BD Biosciences) Univariant histograms of SSC provided the median of cell granularity used as indicator for particle uptake.

Superoxide detection via lucigenin-amplified chemiluminescence (LucCL)

For chemiluminescence detection, cells were seeded at 3 x 10^5/50 µl in $HBSS^{+/+}$ (Invitrogen) in white 96-well microtiter-plates (BD Biosciences). After particle treatment (50 µl) followed by addition of 100 µl lucigenin (1 g/l in $HBSS^{+/+}$, Fluka, Seelze, Germany) measurement started immediately over 90 min with the luminometer (MicroLumat Plus Microplate Luminometer LB 96 V, EG&G Berthold, Bad Wildbach, Germany).

Statistical analysis

Data were expressed as mean ± standard deviation of the number of independent experiments as indicated in the figure legends. Statistical analysis was performed employing SPSS 20.0 for windows using ANOVA with Dunnett post-hoc comparison for all assays, except for the comet assay, for which LSD post-hoc testing was employed. Effects on statistical significance were marked by up to three asterisks (*, **, ***) representing significance at cut-off levels of $p \leq 0.05$, $p \leq 0.01$, and $p \leq 0.001$, respectively.

3.3 Results

ZnO induces necrosis and apoptotic DNA damage with marginal impact of their specific surface area or solubilization.

Four representative ZnO nanoparticle samples (ZnO I-IV) were used to evaluate their cytotoxic effects as well as their specific apoptosis-inducing capacities in the RAW 264.7 macrophages. The samples showed remarkably comparable mass dose-dependent decreases in cell viability as measured by the WST-1 assay (Fig. 3-1A), despite their contrasts in primary particle size and specific surface area (SSA) values. Analysis of the formation of hypodiploid cells, as a specific marker of apoptosis, revealed a dose-dependent increase reaching significance at the highest concentrations with all four ZnO samples (Fig. 3-1B). As all samples showed comparable results; therefore the sample ZnO I, labeled as ZnO in the following, was used exclusively for further investigations.

To address the potential influence of solubilization of ZnO and the contributions of ionic Zn to apoptosis induction in the RAW 264.7 cells, effects of freshly prepared ZnO suspensions were compared to those of 24 h pre-incubated suspensions. Furthermore, we compared the effects of the respective particulate-free supernatants and pellets of those pre-incubated samples. The latter allowed for the evaluation of the relative contributions of particulate versus non-particulate, i.e. solubilized fractions. As indicated in Fig. 3-1C, the supernatant fraction did not trigger any considerable hypodiploid cell formation after 24 h treatment, whereas all other treatments were equally effective. The effects were remarkably comparable to that of the positive control staurosporine (24 h treatment), a classical inducer of apoptotic cell death.

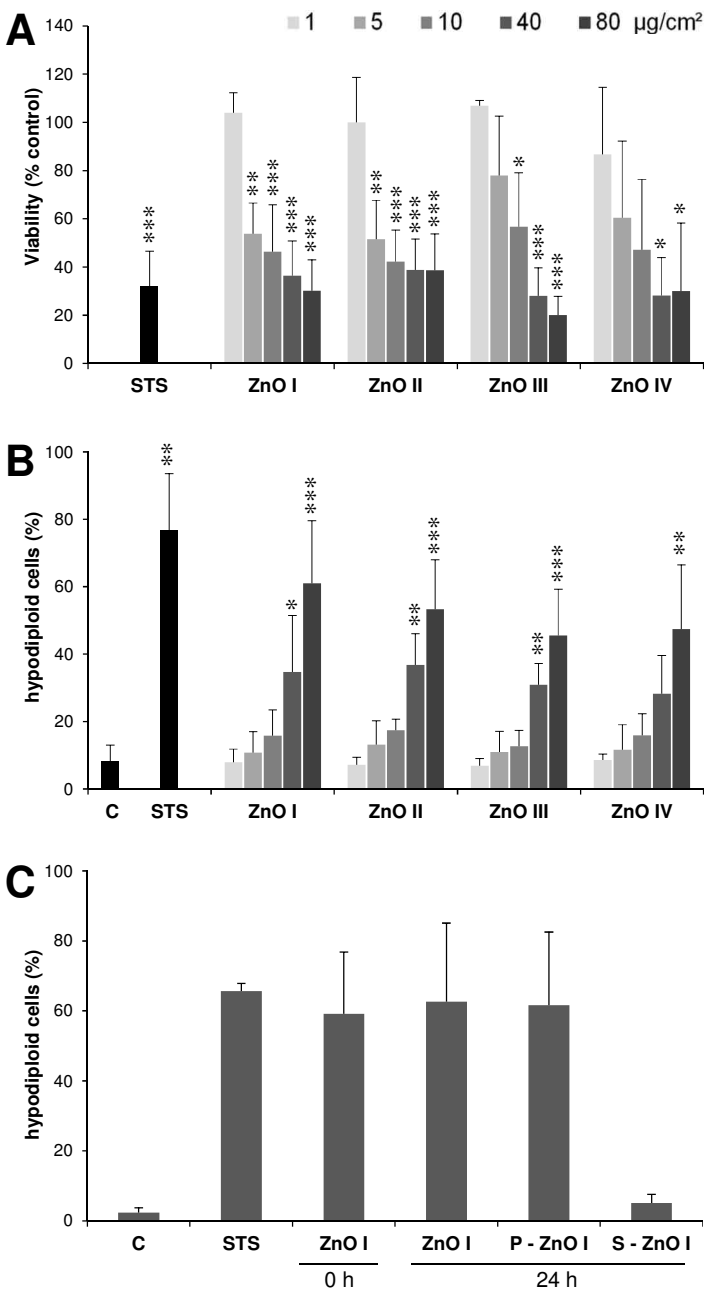

Fig. 3-1 Cytotoxic effects of a panel of ZnO particles in RAW 264.7 macrophages. (A) Cell viability determined by WST-1 assay after 4 h treatment with four different ZnO particles at the indicated concentrations. Data are expressed as a percentage of the non-treated control cells (n=3). As positive control, cells were treated for 4 h with 1 µM staurosporine (STS). (B) FACS analysis after 7-AAD staining revealing cells with hypodiploid DNA content after 4 h treatment with the panel of ZnO particles or staurosporine. Data are expressed as percentage of total cell events (n=3). (C) FACS analysis of RAW 264.7 following a 24 h treatment with freshly prepared ZnO nanoparticles (ZnO I, 0 h), with ZnO suspension that were pre-incubated for 24 h at 37 °C (ZnO I, 24 h), resuspended pellets of the 24 h pre-incubated suspension (P-ZnO I, 24 h) and the particle free supernatants collected after centrifugation of the pre-incubated suspension at 16.000 g (S-ZnO I, 24 h). All respective suspensions were prepared at 0.7 g/L, equaling the final treatment dose of 80 µg/cm². Staurosporine (STS, 24 h, 0.1 µM) was used as positive control. Data are expressed as percentage of total cell events (n=2).

ZnO nanoparticles trigger classical morphological signs of apoptotic cell death

In recent years, there has been increasing concern about the potential introduction of artefacts in specific *in vitro* tests for the hazard assessment of nanoparticles [Stone et al., 2009; Wilhelmi et al. 2012]. Accordingly, we also evaluated the ultrastructural changes in ZnO-treated RAW 264.7 macrophages by transmission electron microscopy to reveal characteristic morphological hallmarks of apoptotic cell death. In contrast to unaltered untreated control cells (Fig. 3-2A, B), staurosporine induced typical membrane blebbing, breakup of cells in apoptotic bodies and chromatin condensation (Fig. 3-2C, D). ZnO-treated RAW 264.7 macrophages revealed cells in different phases of cell death (Fig. 3-2E). In addition to brightly appearing "ghost" cells which were completely dismantled and without any clear shapes of cell compartments as clear signs of necrosis, less damaged cells showed embayed profiles and disaggregation due to apoptotic membrane blebbing. Higher magnification illustrates the deformation of the nucleus with condensed chromatin (Fig. 3-2F, G). Furthermore, phagocytotic processes in ZnO-treated cells were detected by the increased formation of pseudopodia which were closely connected to endocytotic vesicles.

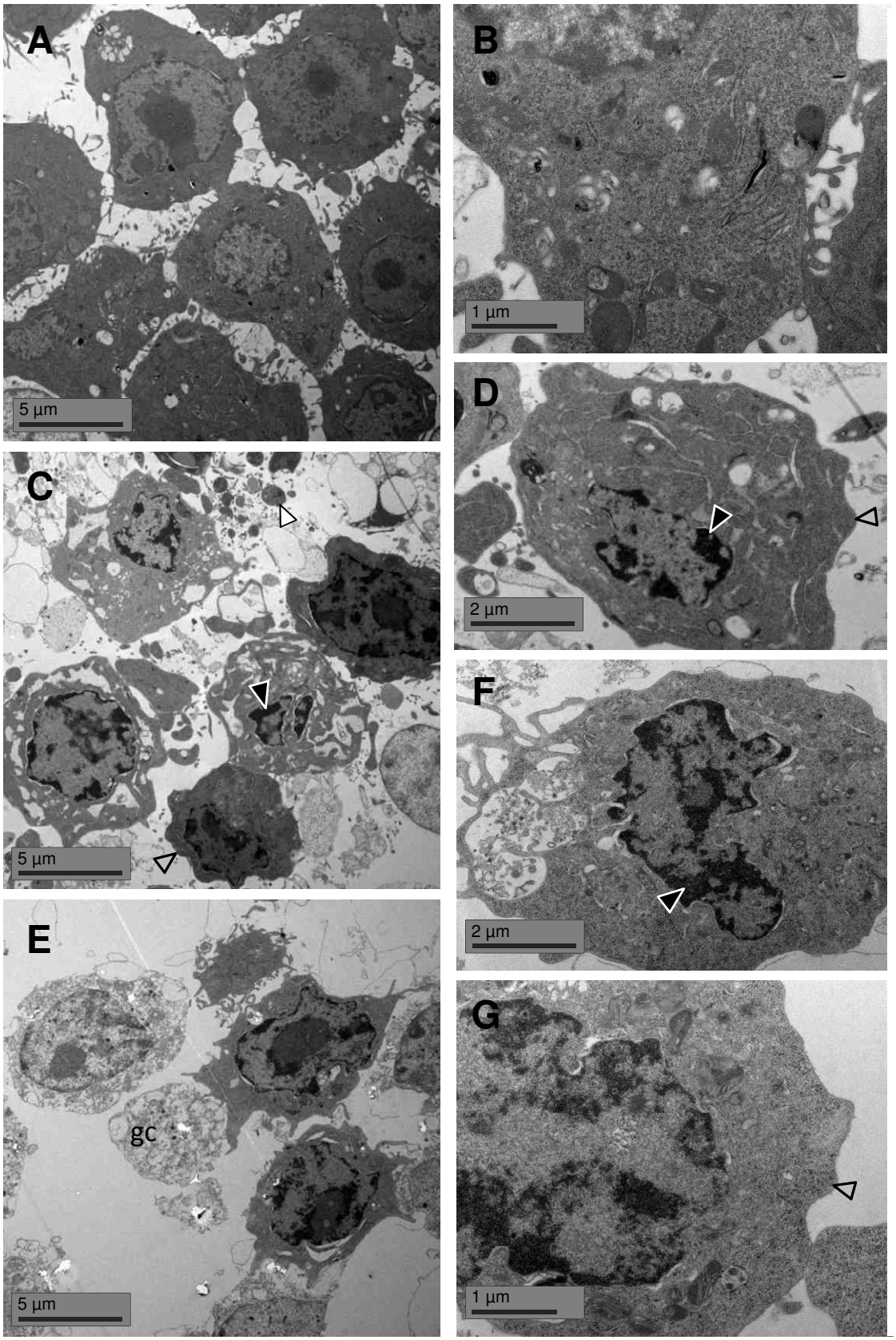

Fig. 3-2: Transmission electron microscopy images of RAW 264.7 cells. Ultra-structural changes are shown after 40 µg/cm² ZnO treatment for 4 h (E, F, G) compared to control cells (A, B) and staurosporine-treated cells (C, D). Nuclear condensation ◀, membrane blebbing ◁ , apoptotic bodies ▷, ghost cells (gc).

ZnO nanoparticles induce biochemical hallmarks of apoptosis in RAW 264.7 macrophages

For the identification of classical apoptosis, the detection of activated executioner caspases is of key importance. Immunohistochemical labeling of cleaved caspase-3 revealed a clear signal in RAW 264.7 macrophages treated with 5 µg/cm² ZnO, which in its intensity was comparable to the effect of the positive control staurosporine (Fig. 3-3). Concurrent DNA staining revealed nuclear chromatin condensation, which was seen neither in untreated cells nor in cells treated with lower ZnO concentrations. The staining procedure was also performed with unspecific IgG to allow for identification of potential false positive artefacts resulting from nonspecific antibody binding to ZnO particles and cellular structures or auto-fluorescence. This analysis revealed an increased dose-dependent non-specific signal for the two highest treatment concentrations (40 and 80 µg/cm²). Unlike caspase-3 activation which peaked at 5 µg/cm² treatment, DNA fragmentation and nuclear condensation proceeded in a clear dose-dependent manner.

Apoptotic DNA fragmentation was evaluated by fluorescence microscopy using the TUNEL assay (Fig. 3-4). Treatment of RAW 264.7 macrophages with staurosporine or with 1 and 5 µg/cm² ZnO revealed a significant appearance of positively labeled cells representing apoptotic DNA fragmentation.

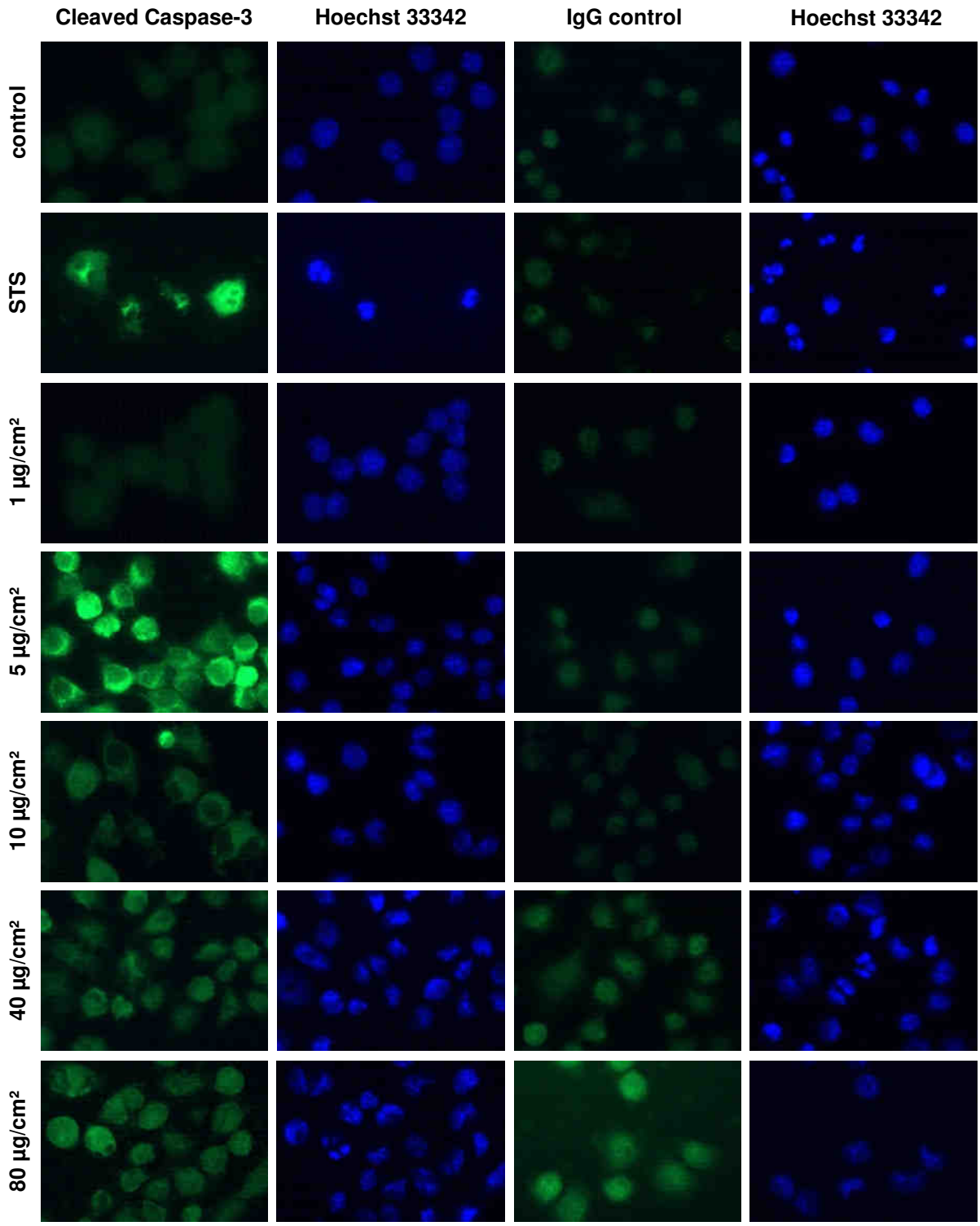

Fig. 3-3: Activated caspase-3 and DNA staining in RAW 264.7 macrophages after 4 h treatment with ZnO or staurosporine (STS). Representative images are shown for activated caspase-3 (first column) and corresponding DNA staining with Hoechst 33342 (second column). To control for unspecific staining, CC-3 antibody was substituted by IgG antibody (third column) and shown with the corresponding Hoechst 33342 staining (fourth column). Original magnification 400x.

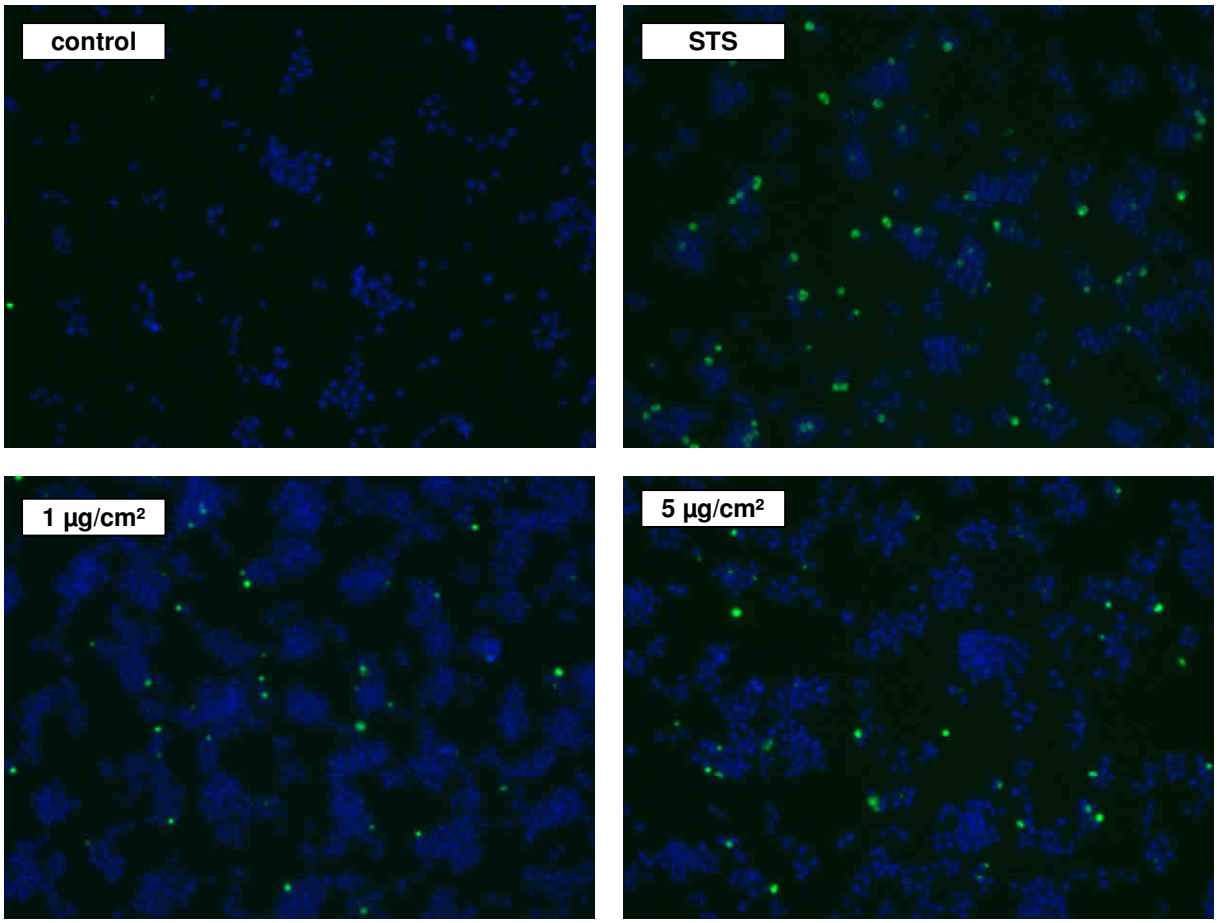

Fig. 3-4: Fluorescent staining of RAW 264.7 macrophages after 4 h treatment with ZnO or staurosporine (STS) using TUNEL assay. Representative multichannel images are shown for apoptotic DNA fragmentation (green staining) and corresponding nuclei (blue staining). Original magnification 100x.

ZnO nanoparticles induce apoptosis via the intrinsic mitochondria-mediated pathway

For the investigation of the role of the intrinsic apoptotic pathway in ZnO-induced effects, a caspase-9-deficient Jurkat T-cell line (JMR), resistant to apoptosis, was used in comparison with caspase-9-restored JMR/C9 cells. Indeed, staurosporine was capable of causing a significant reduction of viability in the JMR/C9 cells, but not in the caspase-9 deficient cell line (Fig. 3-5). Following treatment with 5 or 10 µg/cm^2 ZnO, the cell viability of JMR cells remained largely unaltered compared to the untreated control. In contrast, the viability of JMR/C9 cells dropped below 50% after the 4 h treatment with ZnO nanoparticles. At higher concentrations (40 to 80 µg/cm^2) a dose-dependent cytotoxicity was observed in both cell lines.

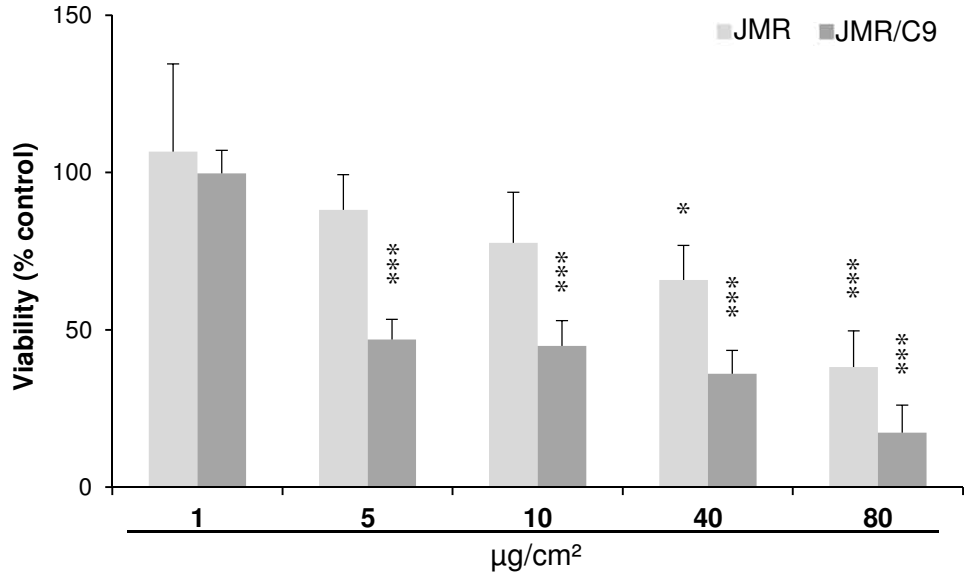

Fig. 3-5: Cell viability (WST-1 assay) after 4 h of ZnO exposure observed in a mutant Jurkat T-cell line deficient in caspase-9 (JMR) versus their caspase-9-restored counterpart (JMR/C9). Data of treated cells are related to corresponding control cells (100% activity, n=3).

ZnO induces DNA strand breakage and oxidative DNA damage induction

In order to investigate ZnO-induced oxidative stress and DNA damage, the formamidopyrimidine glycosylase (Fpg)-modified comet assay was used. DNA strand breakage by ZnO could be observed in a clear dose-dependent manner (Fig. 3-6A). Addition of Fpg, the murine homologue for the human DNA repair enzyme oxoguanine glycosylase, in the comet assay enables detection of oxidative DNA lesions, such as 8-hydroxydeoxyguanosine. Hence, this measurement can be considered as a sensitive marker of oxidative stress [Gerloff et al. 2012a]. The Fpg inclusion also demonstrated a specific induction of oxidative DNA damage after ZnO treatment at 10, 40 and 80 µg/cm² albeit in the absence of a clear dose dependency (Fig. 3-6B). Pre-treatment of the RAW 264.7 cells with the oxidative stress-inducing photosensitizer Ro 19-8022 followed by light exposure resulted in 15.8 ± 1.0 (% tail DNA Fpg-) and 30.2 ± 5.7 (Δ Fpg, data not shown).

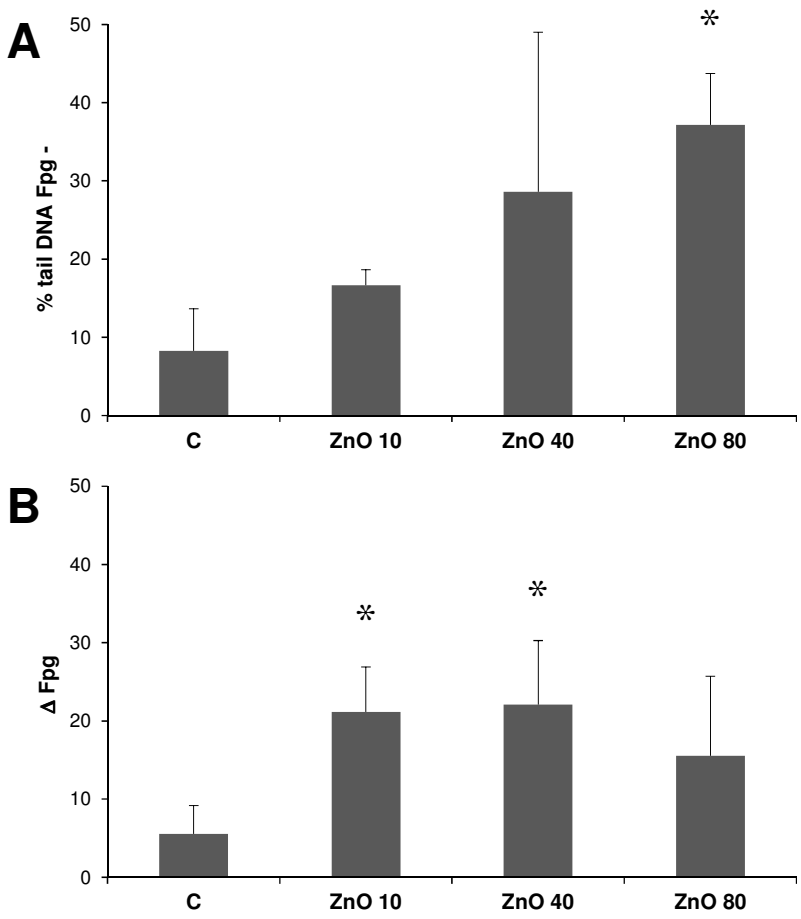

Fig. 3-6: DNA damage in RAW 264.7 macrophages after 4 h treatment with ZnO as evaluated by the fpg-modified comet assay. (A) Percentage of DNA strand breakage measured as % tail intensity in the absence of Fpg-enzyme (n=3). (B) Oxidative DNA damage induction as determined the presence of Fpg-enzyme (n=3). Oxidative DNA damage is shown as the differences in % tail DNA as measured in the presence or absence of the Fpg enzyme: delta (Δ)Fpg = [% tail DNA_{+Fpg}] – [% tail DNA_{-Fpg}].

ZnO toxicity in mouse macrophages is NADPH oxidase and Nrf2-independent

To address the role of the phagocyte-specific ROS production in ZnO-triggered cell death, experiments were performed with bone marrow macrophages derived from $p47^{phox-/-}$ mice along with the macrophages obtained from C57B6/J wild type (wt) mice. Using lucigenin-amplified chemiluminescence, enhanced ROS formation could be observed in ZnO-treated macrophages from wt mice, whereas this formation was impaired in the treated macrophages from the $p47^{phox-/-}$ animals (Fig. 3-7A). The uptake of ZnO particles by the respective macrophages was evaluated by FACS analysis. Analysis of the sideward scatter (SSC) evidenced no differences in ZnO particle uptake between wt and $p47^{phox-/-}$ macrophages (Fig. 3-7B). WST-1 assay and hypodiploid DNA content analyses revealed no differences in

the effects of ZnO in macrophages from p47$^{phox-/-}$ versus wt mice (Fig. 3-7C and D). In subsequent experiments we addressed the role of the redox-sensitive transcription factor Nrf2 using bone marrow-derived differentiated macrophages from Nrf2$^{-/-}$ mice and wt littermates. Clear dose-dependent effects of ZnO were observed, however, neither in the WST-1 assay nor in the hypodiploid DNA content measurement assay differences were observed in relation to the genetic background of the macrophages (Fig. 3-8A and B).

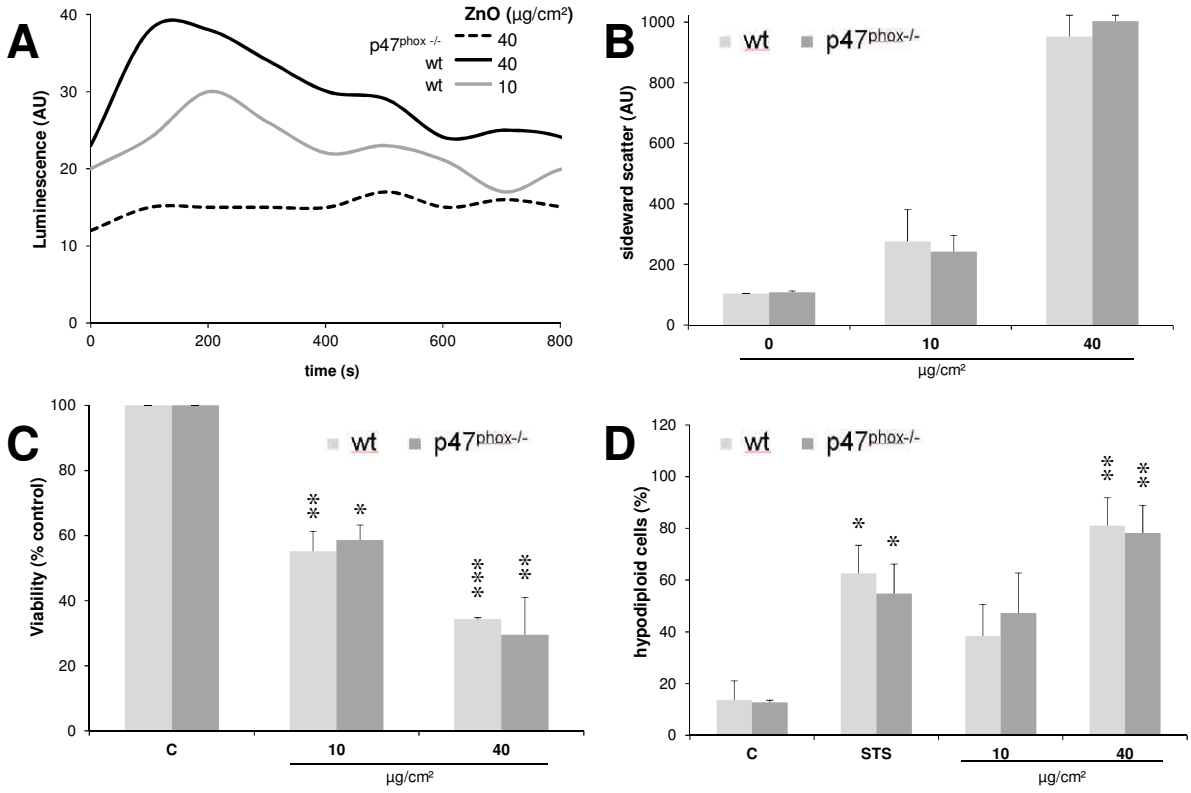

Fig. 3-7: Effects of ZnO exposure in murine bone marrow-derived macrophages of p47$^{phox-/-}$ versus wt animals. (A) Superoxide detection via lucigenin-amplified chemiluminescence depicted in arbitrary units (AU). (B) FACS analysis of sideward scatter related granularity to investigate particle uptake (n=2). (C) Cell viability determined by WST-1 assay (n=2). (D) Content of hypodiploid cells determined by FACS analysis after 7-AAD staining (n=2). STS: staurosporine.

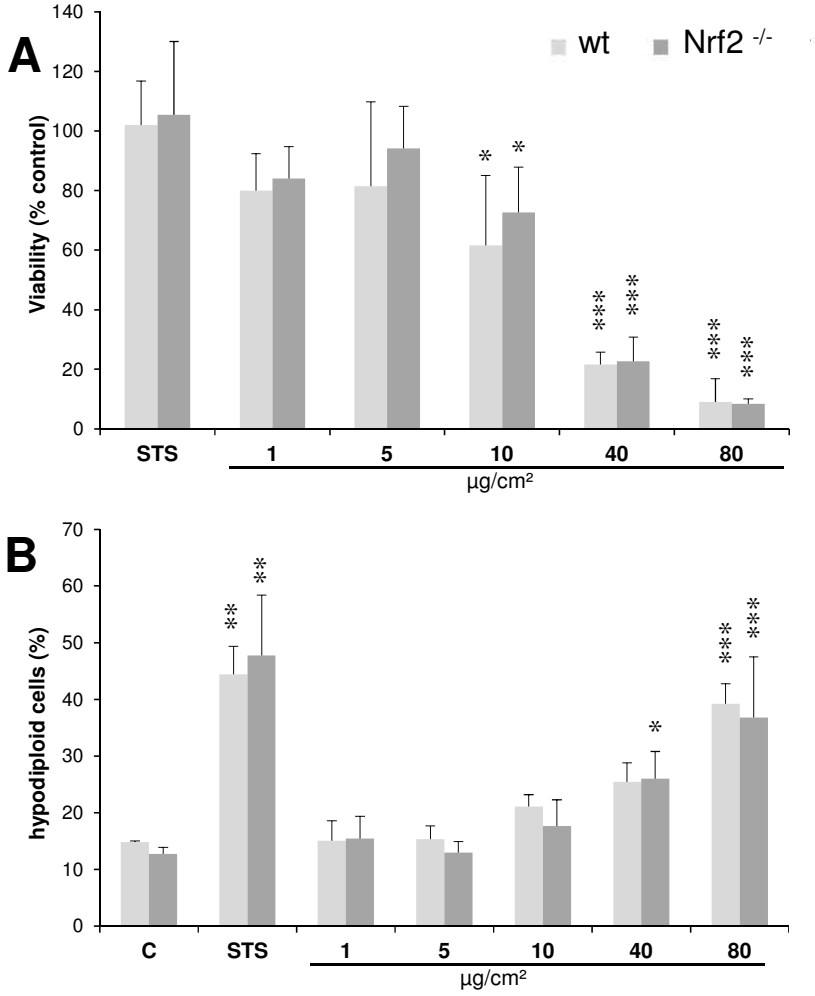

Fig. 3-8: Bone marrow-derived macrophages of Nrf2 $^{-/-}$ versus wt animals were investigated following 4 h ZnO treatment. (A) Cell viability (WST-1 assay) (n=3). (B) FACS analysis to detect the percentage of cells with hypodiploid DNA after 7-AAD staining.

3.4 Discussion

In the present study, zinc oxide nanoparticles caused NADPH-dependent oxidative burst and apoptotic responses, but both were not in a causal relation. Neither NADPH-dependent superoxide formation nor a master regulator of the antioxidant response, Nrf2, were involved in ZnO-induced apoptosis in RAW 264.7 macrophages. Apoptosis was apparent already within 4 h of treatment, in concordance with previous investigations in our laboratory [Wilhelmi et al. 2012]. A selection of four representative ZnO samples of varying primary particle size and specific surface area (SSA) revealed a remarkably similar impact on cytotoxicity and DNA fragmentation. As such, our present findings suggest that the toxic properties of ZnO towards macrophages occur merely independent of these physicochemical properties. The apoptosis-inducing effect of ZnO in the RAW 264.7 cells was also apparent by the occurrence of classical morphological and biochemical hallmarks of apoptotic death, such as nuclear condensation, apoptotic blebbing, and activation of caspase-3. Employing caspase-9-deficient and proficient Jurkat T cells, the involvement of the mitochondrial apoptotic pathway could be demonstrated. Our current observations are in line with recent studies showing activation of caspase-3 and -9 by ZnO nanorods in A549 human lung epithelial cells [Ahamed et al. 2011] and activation of caspase-3, DNA fragmentation and phosphatidylserine exposure by ZnO in dermal fibroblasts [Meyer et al., 2011]. ZnO induced DNA damage response were shown to involve increased activation of p53 and p38 mitogen-activated protein kinase, which mediate cell cycle arrest, DNA repair or apoptosis induction [Ahamed et al. 2011; Meyer et al. 2011]. In our current study great care was taken to avoid assay interferences that may have led to false outcomes. Previously, we identified ZnO-mediated quenching artefacts when employing a commercial chemiluminescence kit for the detection of caspase-3 activity [Wilhelmi et al. 2012]. In the present study, performing of an immunocytochemical staining of cleaved caspase-3 revealed to some extent particle-related artefacts in the form of non-specific staining. However, this problem only occurred at the highest treatment concentrations (i.e. 40 and 80 µg/cm²), while the strongest caspase-3 activity was observed at an artefact-free concentration of 5 µg/cm². The induction of apoptotic effects by ZnO at these lower treatment concentrations was confirmed by microscopical evaluation of DNA fragmentation. Noteworthy, also in this assay an impaired DNA fragmentation detection was found at the highest treatment concentrations, likely as a consequence of a quenching artefact. Taken together, this again emphasizes the necessity to

use multiple assays for apoptosis validation by nanoparticles, as demonstrated in our previous study [Wilhelmi et al. 2012].

The caspase-9 proficient Jurkat T lymphocytes and RAW 264.7 macrophages displayed a remarkably similar sensitivity towards the toxic effect of the ZnO nanoparticles in the WST-1 assay. This may reflect the requirement of the mitochondrial pathway for efficient apoptosis induction [Scaffidi et al., 1998]. In this progression, mitochondrial outer membrane permeabilisation causes cytochrome c release followed by the assembly of the caspase-9 containing apoptosome and subsequent activation of the executioner caspase-3, -6 and -7. Cleavage of their specific substrates leads to the typical changes associated with apoptosis within the cell [Shi 2002]. One of the first targets of active caspases are the permeabilised mitochondria themselves, leading to a decline in ATP levels, loss of mitochondrial transmembrane potential, and the production of ROS [Ricci et al., 2004]. However, the presently observed loss of viability at the higher ZnO concentrations in caspase-9-deficient Jurkat cells suggests an involvement of other non-apoptotic pathways. In concordance with this, our electron microscopical findings of neighbored ZnO-treated macrophages indicate heterogeneity of cell-damaging effects. Observations ranged from mildly affected cells to cells with more clear signs of apoptotic processes like nuclear condensation and membrane blebbing, as well as to completely disassembled remains of necrotic “ghost cells”.

The observed variations in the cellular response may depend on the individual differences in cellular dose, on various routes of uptake mechanisms under participation of different receptors, on the respective cell cycle phase and/or the rate of ZnO dissolution. In the literature, there is a controversy regarding the impact of ZnO solubility on its toxic effects. Xia and colleagues [Xia et al. 2008] discussed dissolution of ZnO in culture media and subsequent formation of ROS as a major mechanism of toxicity in both RAW 264.7 cells and BEAS-2B bronchial epithelial cells. In addition, for the macrophages, uptake and subsequent dissolution within phagocyte lysosomes was discussed. In contrast, we observed no difference in the induction of hypodiploid DNA by freshly prepared and pre-incubated ZnO suspensions as well as resuspended pellets of the pre-incubated suspensions while particle free supernatants were inactive in the macrophages.

In the present study we did not address the potential role of ionic Zn by means of macrophage treatments with zinc salts. Interestingly, in this regard, it was recently demonstrated that in culture media containing phosphate and carbon ions addition of soluble Zn2+ causes formation of potentially toxic nanoparticulate zinc consisting of Zn-phosphate-carbonate, and hence may not serve as an appropriate non-particulate control [Turney et al., 2012]. Our

present findings do not prove that dissolution may not be involved in ZnO toxicity. However, a contribution of a fraction of rapidly dissolved ZnO can be excluded for our experimental conditions. The observed differences between our and their data might relate to the different physico-chemical properties of the ZnO sample used in their experiments, which was synthesized by flame spray pyrolysis [Xia et al. 2008]. Our findings on the lacking role of non-particulate zinc are also in line with findings by various other investigators. Using a transwell membrane system, Moos and colleagues demonstrated that the toxicity of ZnO particles towards a colon cell line was independent of the amount of soluble Zn in the culture medium and required a direct particle-cell contact [Moos et al., 2012]. In A549 lung epithelial cells, ZnO-induced ROS production was also described as a particle-mediated effect [Lin et al., 2009]. Lastly, in a recent study with RAW 264.7 cells, particulate ZnO was shown to induce apoptosis and, at high concentrations also necrosis, while dissolved ions were found merely to induce metallothionein synthesis [Zhang et al.,].

Generation of ROS and induction of oxidative stress with subsequent perturbation of mitochondria and apoptosis was previously shown to be triggered by ZnO nanoparticles in RAW 264.7 macrophages [Xia et al. 2008] as well as in other cell types [Moos et al. 2012; Sharma et al. 2012]. In concordance with these findings, we found a concentration-dependent oxidative DNA damage induction in ZnO-treated RAW 264.7 cells using the Fpg-modified comet assay. Such oxidative DNA damage induction is closely related to the action of ROS and hence generally considered as a sensitive marker of oxidative stress [Gerloff et al. 2012a]. The oxidative DNA damage observed at higher doses of ZnO was nearly as strong as the effect that could be generated in the macrophages by the photosensitizer Ro 19-8022 (data not shown). Moreover, we could demonstrate that ZnO triggers a concentration-dependent formation of superoxide radicals in bone marrow-derived macrophages from C57Bl/6 wild type mice but not $p47^{phox}$ knockout animals. This demonstrated that the phagocytic NADPH oxidase enzyme complex NOX2 is a major source of ROS in ZnO-exposed macrophages. Receptor-dependent phagocytosis of pathogens by macrophages is a well described mechanism of rapid NADPH oxidase activation and superoxide formation known was respiratory burst [Park 2003]. Therefore, we also included ZnO uptake measurements in wt versus $p47^{phox}$-deficient macrophages. Neither an impairment of uptake of ZnO particles nor a reduction of hypodiploid DNA formation was found in the $p47^{phox-/-}$ model. As such, our findings indicate that $p47^{phox}$ NADPH oxidase-mediated ROS generation is not directly implicated ZnO-triggered apoptosis in macrophages.

To further explore the role of oxidative stress and a possible involvement of NADPH oxidase-independent sources of ROS like mitochondria, ZnO effects were also evaluated in primary macrophages from mice proficient or deficient in the oxidant-inducible transcription factor Nrf2, a master regulator of antioxidant response [Hybertson et al., 2011]. In a recent study, Nrf2 has been implicated in the DNA-damaging and apoptotic effect of silver nanoparticles in an ovarian carcinoma cell line via a mechanism involving cytoprotection by the Nrf2-regulated antioxidant heme oxygenase-1 [Kang et al. 2012]. However, Nrf2 may also be implicated in ROS-independent mechanisms of apoptosis induction. In T cells, Nrf2 deficiency was shown to be associated with increased sensitivity to anti-Fas mediated apoptosis [Morito et al., 2003]. Moreover, an Nrf2 binding antioxidant responsive element was recently identified within the gene promoter of the antiapoptotic protein Bcl-2 [Niture et al., 2012]. However, in our study we could not detect any significant difference in sensitivity of the wild type versus the Nrf2- deficient macrophages towards ZnO-triggered cell death. Interestingly, also the effects of our positive control staurosporine did not differ between both genetic backgrounds. This indicates that ZnO and staurosporine may act in macrophages via similar oxidative stress-independent pathways. This may also explain for the apparent discrepancies as observed in an earlier study on gene expression patterns of ZnO NP exposed BEAS-2B lung epithelial cells where genes involved in oxidative stress were upregulated in contrast to those coding for antioxidant enzymes [Huang et al. 2010].

In conclusion, ZnO nanoparticles can trigger a rapid $p47^{phox}$ NADPH oxidase-mediated superoxide radical generation, oxidative DNA damage induction, necrosis and caspase-9/3-dependent apoptosis in macrophages. However, the observed cell death effects appear to be independently of this major phagocytic oxidant generating pathway as well as of the oxidant responsive Nrf2 pathway. Further studies are needed to unravel the precise molecular mechanisms that drive ZnO-induced toxic responses.

Acknowledgments

The authors wish to thank Christel Weishaupt and Petra Gross from IUF for their technical support as well as Dr. Klaus Zanger and Brigitte Rohbeck for cell embedding and preparation of electronmicroscopical pictures. This study was financially supported by the Research Commission of the Medical Faculty of the Heinrich-Heine-University Düsseldorf as well as the DFG Graduate Schools GRK1033 and GRK1427.

3.5 References

Ahamed, M, Akhtar, MJ, Raja, M, Ahmad, I, Siddiqui, MK, AlSalhi, MS and Alrokayan, SA (2011). ZnO nanorod-induced apoptosis in human alveolar adenocarcinoma cells via p53, survivin and bax/bcl-2 pathways: role of oxidative stress. Nanomedicine 7(6): 904-913.

Akhtar, MJ, Ahamed, M, Kumar, S, Khan, MM, Ahmad, J and Alrokayan, SA (2012). Zinc oxide nanoparticles selectively induce apoptosis in human cancer cells through reactive oxygen species. Int J Nanomedicine 7: 845-857.

Anish Kumar, M, Jung, S and Ji, T (2011). Protein biosensors based on polymer nanowires, carbon nanotubes and zinc oxide nanorods. Sensors (Basel) 11(5): 5087-5111.

Castranova, V (2004). Signaling pathways controlling the production of inflammatory mediators in response to crystalline silica exposure: role of reactive oxygen/nitrogen species. Free Radic Biol Med 37(7): 916-925.

Cho, HY, Reddy, SP and Kleeberger, SR (2006). Nrf2 defends the lung from oxidative stress. Antioxid Redox Signal 8(1-2): 76-87.

Cho, WS, Duffin, R, Poland, CA, Howie, SE, MacNee, W, Bradley, M, Megson, IL and Donaldson, K (2010). Metal oxide nanoparticles induce unique inflammatory footprints in the lung: important implications for nanoparticle testing. Environ Health Perspect 118(12): 1699-1706.

Dhakshinamoorthy, S and Porter, AG (2004). Nitric oxide-induced transcriptional up-regulation of protective genes by Nrf2 via the antioxidant response element counteracts apoptosis of neuroblastoma cells. J Biol Chem 279(19): 20096-20107.

Dostert, C, Petrilli, V, Van Bruggen, R, Steele, C, Mossman, BT and Tschopp, J (2008). Innate immune activation through Nalp3 inflammasome sensing of asbestos and silica. Science 320(5876): 674-677.

Forman, HJ and Torres, M (2002). Reactive oxygen species and cell signaling: respiratory burst in macrophage signaling. Am J Respir Crit Care Med 166(12 Pt 2): S4-8.

Geiser, M (2010). Update on macrophage clearance of inhaled micro- and nanoparticles. J Aerosol Med Pulm Drug Deliv 23(4): 207-217.

Gerloff, K, Albrecht, C, Boots, AW, Förster, I and Schins, RP (2009). Cytotoxicity and oxidative DNA damage by nanoparticles in human intestinal Caco-2 cells. Nanotoxicology 3(4): 355-364.

Gerloff, K, Fenoglio, I, Carella, E, Kolling, J, Albrecht, C, Boots, AW, Forster, I and Schins, RP (2012a). Distinctive toxicity of TiO2 rutile/anatase mixed phase nanoparticles on Caco-2 cells. Chem Res Toxicol 25(3): 646-655.

Gerloff, K, Pereira, DI, Faria, N, Boots, AW, Kolling, J, Forster, I, Albrecht, C, Powell, JJ and Schins, RP (2012b). Influence of simulated gastrointestinal conditions on particle-

induced cytotoxicity and interleukin-8 regulation in differentiated and undifferentiated Caco-2 cells. Nanotoxicology.

http://www.ttl.fi/partner/nanosh/progress/Documents/nanosh_nanoatlas.pdf.

Huang, CC, Aronstam, RS, Chen, DR and Huang, YW (2010). Oxidative stress, calcium homeostasis, and altered gene expression in human lung epithelial cells exposed to ZnO nanoparticles. Toxicol In Vitro 24(1): 45-55.

Hybertson, BM, Gao, B, Bose, SK and McCord, JM (2011). Oxidative stress in health and disease: the therapeutic potential of Nrf2 activation. Mol Aspects Med 32(4-6): 234-246.

Itoh, K, Chiba, T, Takahashi, S, Ishii, T, Igarashi, K, Katoh, Y, Oyake, T, Hayashi, N, Satoh, K, Hatayama, I, Yamamoto, M and Nabeshima, Y (1997). An Nrf2/small Maf heterodimer mediates the induction of phase II detoxifying enzyme genes through antioxidant response elements. Biochem Biophys Res Commun 236(2): 313-322.

Iyer, R, Hamilton, RF, Li, L and Holian, A (1996). Silica-induced apoptosis mediated via scavenger receptor in human alveolar macrophages. Toxicol Appl Pharmacol 141(1): 84-92.

Jackson, SH, Gallin, JI and Holland, SM (1995). The p47phox mouse knock-out model of chronic granulomatous disease. J Exp Med 182(3): 751-758.

Kang, SJ, Ryoo, IG, Lee, YJ and Kwak, MK (2012). Role of the Nrf2-heme oxygenase-1 pathway in silver nanoparticle-mediated cytotoxicity. Toxicol Appl Pharmacol 258(1): 89-98.

Kelleher, P, Pacheco, K and Newman, LS (2000). Inorganic dust pneumonias: the metal-related parenchymal disorders. Environ Health Perspect 108 Suppl 4: 685-696.

Kermanizadeh, A, Pojana, G, Gaiser, BK, Birkedal, R, Bilanicova, D, Wallin, H, Jensen, KA, Sellergren, B, Hutchison, GR, Marcomini, A and Stone, V (2012). In vitro assessment of engineered nanomaterials using a hepatocyte cell line: cytotoxicity, pro-inflammatory cytokines and functional markers. Nanotoxicology.

Klupp Taylor, RN, Seifrt, F, Zhuromskyy, O, Peschel, U, Leugering, G and Peukert, W (2011). Painting by numbers: nanoparticle-based colorants in the post-empirical age. Adv Mater 23(22-23): 2554-2570.

Kobayashi, M and Yamamoto, M (2005). Molecular mechanisms activating the Nrf2-Keap1 pathway of antioxidant gene regulation. Antioxid Redox Signal 7(3-4): 385-394.

Lee, JM and Johnson, JA (2004). An important role of Nrf2-ARE pathway in the cellular defense mechanism. J Biochem Mol Biol 37(2): 139-143.

Li, J, Johnson, D, Calkins, M, Wright, L, Svendsen, C and Johnson, J (2005). Stabilization of Nrf2 by tBHQ confers protection against oxidative stress-induced cell death in human neural stem cells. Toxicol Sci 83(2): 313-328.

Lin, W, Xu, Y, Huang, C, Ma, Y, Shannon, K, Chen, D and Huang, Y (2009). Toxicity of nano- and micro-sized ZnO particles in human lung epithelial cells J Nanopart Res 11: 25-39.

Meyer, K, Rajanahalli, P, Ahamed, M, Rowe, JJ and Hong, Y (2011). ZnO nanoparticles induce apoptosis in human dermal fibroblasts via p53 and p38 pathways. Toxicol In Vitro 25(8): 1721-1726.

Moos, PJ, Chung, K, Woessner, D, Honeggar, M, Cutler, NS and Veranth, JM (2012). ZnO particulate matter requires cell contact for toxicity in human colon cancer cells. Chem Res Toxicol 23(4): 733-739.

Morito, N, Yoh, K, Itoh, K, Hirayama, A, Koyama, A, Yamamoto, M and Takahashi, S (2003). Nrf2 regulates the sensitivity of death receptor signals by affecting intracellular glutathione levels. Oncogene 22(58): 9275-9281.

Murray, PJ and Wynn, TA (2012). Protective and pathogenic functions of macrophage subsets. Nat Rev Immunol 11(11): 723-737.

Musee, N, Thwala, M and Nota, N (2011). The antibacterial effects of engineered nanomaterials: implications for wastewater treatment plants. J Environ Monit 13(5): 1164-1183.

Niture, SK and Jaiswal, AK (2012). Nrf2 protein up-regulates antiapoptotic protein Bcl-2 and prevents cellular apoptosis. J Biol Chem 287(13): 9873-9886.

Park, JB (2003). Phagocytosis induces superoxide formation and apoptosis in macrophages. Exp Mol Med 35(5): 325-335.

Rasmussen, JW, Martinez, E, Louka, P and Wingett, DG (2010). Zinc oxide nanoparticles for selective destruction of tumor cells and potential for drug delivery applications. Expert Opin Drug Deliv 7(9): 1063-1077.

Ricci, JE, Munoz-Pinedo, C, Fitzgerald, P, Bailly-Maitre, B, Perkins, GA, Yadava, N, Scheffler, IE, Ellisman, MH and Green, DR (2004). Disruption of mitochondrial function during apoptosis is mediated by caspase cleavage of the p75 subunit of complex I of the electron transport chain. Cell 117(6): 773-786.

Samraj, AK, Sohn, D, Schulze-Osthoff, K and Schmitz, I (2007). Loss of caspase-9 reveals its essential role for caspase-2 activation and mitochondrial membrane depolarization. Mol Biol Cell 18(1): 84-93.

Scaffidi, C, Fulda, S, Srinivasan, A, Friesen, C, Li, F, Tomaselli, KJ, Debatin, KM, Krammer, PH and Peter, ME (1998). Two CD95 (APO-1/Fas) signaling pathways. EMBO J 17(6): 1675-1687.

Schilling, K, Bradford, B, Castelli, D, Dufour, E, Nash, JF, Pape, W, Schulte, S, Tooley, I, van den Bosch, J and Schellauf, F (2010). Human safety review of "nano" titanium dioxide and zinc oxide. Photochem Photobiol Sci 9(4): 495-509.

Sharma, V, Anderson, D and Dhawan, A (2012). Zinc oxide nanoparticles induce oxidative DNA damage and ROS-triggered mitochondria mediated apoptosis in human liver cells (HepG2). Apoptosis 17(8): 852-870.

Sharma, V, Singh, P, Pandey, AK and Dhawan, A (2011). Induction of oxidative stress, DNA damage and apoptosis in mouse liver after sub-acute oral exposure to zinc oxide nanoparticles. Mutat Res 745(1-2): 84-91.

Shi, Y (2002). Apoptosome: the cellular engine for the activation of caspase-9. Structure 10(3): 285-288.

Smith, PD, Smythies, LE, Shen, R, Greenwell-Wild, T, Gliozzi, M and Wahl, SM (2011). Intestinal macrophages and response to microbial encroachment. Mucosal Immunol 4(1): 31-42.

Speit, G, Schutz, P, Bonzheim, I, Trenz, K and Hoffmann, H (2004). Sensitivity of the FPG protein towards alkylation damage in the comet assay. Toxicol Lett 146(2): 151-158.

Stone, V, Johnston, H and Schins, RP (2009). Development of in vitro systems for nanotoxicology: methodological considerations. Crit Rev Toxicol 39(7): 613-626.

Tankhiwale, R and Bajpai, SK (2012). Preparation, characterization and antibacterial applications of ZnO-nanoparticles coated polyethylene films for food packaging. Colloids Surf B Biointerfaces 90: 16-20.

Turney, TW, Duriska, MB, Jayaratne, V, Elbaz, A, O'Keefe, SJ, Hastings, AS, Piva, TJ, Wright, PF and Feltis, BN (2012). Formation of Zinc-Containing Nanoparticles from Zn(2+) Ions in Cell Culture Media: Implications for the Nanotoxicology of ZnO. Chem Res Toxicol.

Unfried K, AC, Klotz LO, von Mikecz A, Grether-Beck S, Schins RPF (2007). Cellular responses to nanoparticles: target structures and mechanisms. . Nanotoxicology 1: 52-71.

van Berlo, D, Wessels, A, Boots, AW, Wilhelmi, V, Scherbart, AM, Gerloff, K, van Schooten, FJ, Albrecht, C and Schins, RP (2010). Neutrophil-derived ROS contribute to oxidative DNA damage induction by quartz particles. Free Radic Biol Med 49(11): 1685-1693.

Wilhelmi, V, Fischer, U, van Berlo, D, Schulze-Osthoff, K, Schins, RP and Albrecht, C (2012). Evaluation of apoptosis induced by nanoparticles and fine particles in RAW 264.7 macrophages: facts and artefacts. Toxicol In Vitro 26(2): 323-334.

Xia, T, Kovochich, M, Liong, M, Madler, L, Gilbert, B, Shi, H, Yeh, JI, Zink, JI and Nel, AE (2008). Comparison of the mechanism of toxicity of zinc oxide and cerium oxide nanoparticles based on dissolution and oxidative stress properties. ACS Nano 2(10): 2121-2134.

Zhang, J, Song, W, Guo, J, Zhang, J, Sun, Z, Ding, F and Gao, M (2012). Toxic effect of different ZnO particles on mouse alveolar macrophages. J Hazard Mater 219-220: 148-155.

Chapter IV

Apoptotic, inflammatory, and fibrogenic effects of two different types of multi-walled carbon nanotubes in mouse lung

Damiën van Berlo*, Verena Wilhelmi*, Agnes W. Boots, Maja Hullmann, Thomas A. J. Kuhlbusch, Aalt Bast, Roel P.F. Schins, Catrin Albrecht

* with equal contributions

Study 3: Apoptotic, inflammatory, and fibrogenic effects of two different types of multi-walled carbon nanotubes in mouse lung

Declaration

The manuscript is submitted to a peer-review journal.
All experimental *in vitro* work presented was performed by Verena Wilhelmi.
The impact on authoring this paper can be estimated in total with 40%.

4 Abstract

There is increasing concern about the toxicity of inhaled multi walled carbon nanotubes (MW-CNT). Pulmonary macrophages represent the primary cell type involved in the clearance of inhaled particulate materials, and induction of apoptosis in these cells has been considered to contribute to the development of fibrosis. We have investigated the apoptotic, pro-inflammatory and fibrotic potential of two samples of MW-CNT, characterized by a contrasting average tube length and entanglement/agglomeration. Both nanotube types triggered H_2O_2 formation by RAW 264.7 macrophages, but *in vitro* toxicity was exclusively seen with the longer sample. Both types of nanotubes also caused granuloma in the mouse lungs. However, the long sample induced a more pronounced inflammogenic and pro-fibrotic response as indicated by Masson Trichrome staining, mRNA expression of matrix metalloproteinase-8 and tissue inhibitor of metalloproteinase-1, and increased serum level of Monocyte Chemotactic Protein-1. Enhanced apoptosis was detected by cleaved caspase 3 immunohistochemistry in the lungs of the mice treated with the long/rigid sample and, to a lesser extent, with the shorter more agglomerated sample. However, staining was merely localized to granulomatous foci, and neither of the samples induced apoptosis *in vitro*, evaluated by caspase 3/7 activity assay in the RAW 264.7 cells. Our study reveals that the inflammatory and fibrogenic effects of MW-CNT in mouse lung can vary considerably depending on their composition. The *in vitro* analysis of macrophage apoptosis appears to be a poor predictor of their pulmonary hazard.

4.1 Introduction

Carbon nanotubes (CNTs) are one of the novel promising nanomaterials which have been developed. They exist in two principal forms: single-walled (SW-CNT) or multi-walled (MW-CNT). Both of these forms feature specific physico-chemical, electrical, mechanical and thermal properties; they are highly conductive, thermally stable, resistant to many chemical agents and possess a remarkable tensile strength. However, the potential toxicity of CNTs to humans upon their inhalation, which can occur e.g. in specific industrial settings, is still not sufficiently known. Especially, potential parallels to asbestos fibres have been drawn [Donaldson et al., 2006; Poland et al., 2008], another material with remarkable and useful properties (e.g. strength, flame repellent) that was later revealed to be capable of inducing severe pathology including lung fibrosis and mesothelioma cancer. For asbestos it has been

revealed that specific physico-chemical characteristics are related to its pathogenicity. The "fibre paradigm" states that especially long and thin fibres of high rigidity and biopersistence are hazardous [Donaldson et al., 2011]. This relates to their ability to reach respiratory bronchioles and alveolar spaces as well as the problems they pose for subsequent clearance from the lung. Specifically, it has been shown that phagocytosis of long fibres by alveolar macrophages is less efficient, and the associated exaggerated release of inflammatory mediator release from these cells as well as retarded clearance functions due to macrophage motility impairment have been implicated in their pathogenicity [Oberdorster 1996; Miller et al., 1999]. The question whether these mechanisms also apply to inhaled CNT is avidly discussed within the nanotoxicology community [Donaldson et al. 2006; Jaurand et al., 2009; Kisin et al., 2011; Muhlfeld et al., 2011; Osmond-McLeod et al., 2011; van Berlo et al., 2012].

One of the most dangerous pathologies induced upon inhalation of asbestos and various other particulate materials, like crystalline silica, is lung fibrosis. So far, a number of studies have investigated the pro-fibrotic potential of MW-CNTs. Both positive (e.g. [Muller et al., 2005; Mercer et al., 2011; Wang et al., 2011]) and negative (e.g. [Li *et al.,* 2007a; Mitchell *et al.,* 2007; Kobayashi *et al.,* 2010; Roda *et al.,* 2011]) *in vivo* findings have been reported. Similar to these investigations, findings on granuloma formation are inconsistent as well [Muller *et al.* 2005; Li *et al.* 2007a; Mitchell *et al.* 2007; Poland *et al.* 2008; Kato *et al.,* 2012]. The differences in observations on the pathologies of CNTs have been hypothesized to be due to differences in the exposure method (i.e. intratracheal instillation/pharyngeal aspiration versus inhalation) but might also reflect species- or nanotube composition-specific differences.

Pulmonary macrophages are well recognized for their involvement in particle-induced adverse health effects [Doll et al., 1983; Hansen et al., 1987; Moolgavkar et al., 2001]. These cells represent the primary cell type involved in clearance of particulate material as well as a major source of pro-inflammatory and fibrogenic mediators, including cytokines, growth factors and reactive oxygen species (ROS). The induction of apoptosis in this cell type has been associated with the development of pulmonary fibrosis by silica particles [Beamer et al., 2007; Yao et al., 2011]. Moreover, in patients suffering from idiopathic pulmonary fibrosis, enhanced FasL mRNA, indicative of apoptosis, was found in bronchoalveolar lavage fluid cells [Kuwano et al., 1999]. However, whether apoptosis can be induced by MW-CNTs in pulmonary macrophages, and how this impacts on lung pathology, has not been fully addressed. Again, contrasting data are currently available for MW-CNT. Positive findings on apoptosis induction by MW-CNT have been reported *in vitro* in macrophage-like cells [Wang

et al., 2009; Di Giorgio et al., 2011; Gasser et al., 2012; Wang et al., 2012] and in macrophages *in vivo* [Elgrabli et al., 2008; Roda et al. 2011]. Negative *in vitro* findings in macrophages [Hirano et al., 2008; Sohaebuddin et al., 2010; Luo et al., 2012] have been published as well. The questions: (1) whether MW-CNTs elicit apoptosis in macrophages in relation to specific physico-chemical properties and, (2) if this correlates to the pulmonary hazard of this nanomaterial, are not resolved at present. In the current work, we have therefore assessed the necrosis and apoptosis inducing properties of two markedly different types of MW-CNT in RAW 264.7 mouse macrophages. In parallel, we investigated the ability of the same two materials to trigger inflammation, fibrosis and macrophage-associated apoptosis in the murine lung after pharyngeal aspiration.

4.2 Materials and Methods

Reagents

Hanks' balanced salt solution with calcium and magnesium ($HBSS^{+/+}$), Bovine Serum Albumine (BSA), phosphormolybdic acid hydrate, phosphotungstic acid hydrate, Biebrich scarlet-acid fuchsin solution and Fe(III)Cl were purchased from Sigma (Germany). Luminex cytokine assays were obtained from Biorad (the Netherlands). RNeasy mini kit and RNase-free DNase set were bought from Qiagen (Germany). The iScript cDNA Synthesis kit and SYBR© Green Supermix were ordered from Biorad (Germany). RT-PCR primers were designed using Primer Express software and supplied by Operon (Germany). Trizol and the Amplex Red assay were bought from Life Technologies (Germany). Isoflurane was purchased from Essex Pharma (Germany). All other chemicals were of the highest purity and were supplied by Merck (Germany).

Carbon nanotubes

Two MW-CNT powder samples were used in the current study. Sample 1 (MW-CNT1) was obtained as MWNT-7 from Mitsui & Co., Japan. This specific sample of CNT has been used in toxicological investigations by various research groups [Hirano et al. 2008; Poland et al. 2008; Mercer et al. 2011]. Sample 2 (MW-CNT2) was obtained through the nanomaterial depository at European Commission Joint Research Centre, Ispra, Italy (NM 400, from Nanocyl, Belgium) and has been used in several recent and ongoing European Framework nanotoxicology projects [Kermanizadeh et al., 2012]. Representative scanning electron microscopic (SEM) pictures of both samples are shown in Figure 4-1. For MW-CNT1 an average length of 13 µm and a diameter range from 40 – 100 nm is reported; MW-CNT2 is

much shorter with a declared average length of 5 µm and diameter of 30 nm [Poland et al. 2008; Kermanizadeh et al. 2012]. The contrasting morphologies of both samples are also apparent from the SEM evaluations; MW-CNT1 consisted of relatively dispersed bundles and singlets of long and intermediate-length tubes. In contrast, the MW-CNT2 contains shorter, less rigid highly entangled nanotubes, displaying a ball of wool-like appearance (see Figure 4-1).

Animals

Specific pathogen-free C57Bl6/J mice were obtained from Janvier (France). Mice were kept in an in-house facility (safety level 1) according to guidelines produced by the Society for Laboratory Animals Science (GV-SOLAS) and under strict SPF conditions. For housing of animals, plastic cages filled with hardwood bedding were placed within an air-conditioned (23 ± 2°C) animal room. A 12 h light/dark cycle was maintained throughout the study. Food and water were available ad libitum.

Cell culture and treatment

RAW 264.7 macrophage-like murine cells (ATCC Number TIB-71; American Type Culture Collection, US) were cultured at 37°C and 5% CO_2 in Dulbecco's modified Eagle's medium (Sigma, Germany) with the following supplements: 4 mM L-glutamine adjusted to contain 1.5 g/l sodium bicarbonate and 4.5 g/l glucose, penicillin (100 U/ml)/streptomycin (0.1 mg/ml) and 10% fetal calf serum (Sigma, Germany). Subculturing was performed to maintain cells growing in the logarithmic phase. A concentration of 2×10^5 cells/cm^2 was seeded in each well unless mentioned otherwise. Experiments were performed 24 h after seeding at a confluence of approximately 30%. Immediately before cell culture testing, the MW-CNT were suspended in 2% mouse serum in double distilled water, sonicated with a tip sonifier 450 (Branson, micro tip limit 3) and further diluted into complete culture medium.

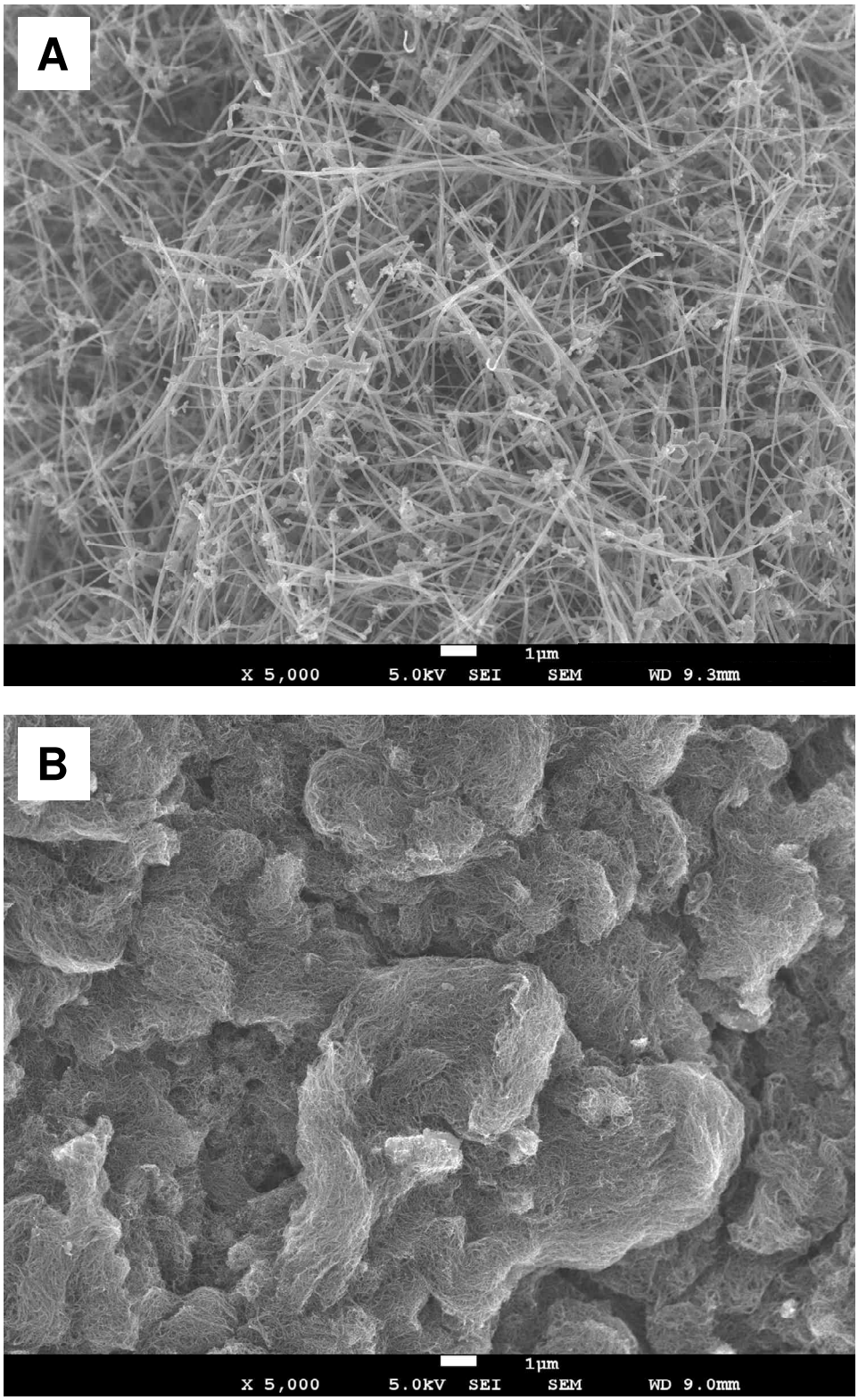

Fig. 4-1: Scanning electron microscopy images of MW-CNT1 (A) and MW-CNT2 (B). Images were made at 5,000x magnification with a JEOL 7500F SEM on pure silicon substrates. Samples were prepared by adding a drop of Ethanol onto the substrate and subsequent addition of MW-CNT powder to ensure adhesion of the CNT. The powders did not stick to the surface when directly applied.

Toxicity

Two independent assays were performed to assess MW-CNT-elicited toxicity in RAW 264.7 cells. The WST-1 conversion assay (Roche, Germany) quantifies the amount of tetrazolium salt WST-1 (4-[3-(4-iodophenyl)-2-(4-nitrophenyl)-2H-5-tetrazolio]-1,3-benzene disulfonate) converted to a soluble violet formazan product. This metabolisation takes place in the mitochondria, therefore a stronger colorimetric readout represents higher mitochondrial activity which is an indication for viable cells. The assay was performed as previously described in detail [Wilhelmi et al., 2012]. Briefly, cells were treated in octoplicate. After 24 h, for each treatment WST-1 solution was added to 5 wells. The other 3 wells without substrate were used as particle background control. Color development was measured after 10 min at 450 nm using a Multiscan ELISA reader (Thermo Fisher Scientific, Germany). Viability was calculated by subtraction of the mean values without WST-1 from those with WST-1 substrate and was expressed as percentage of control.

The lactate dehydrogenase (LDH) assay (Roche, Germany) was used to detect membrane permeability as an indicator of necrosis. Cells were treated in triplicate incubations per experiment. Additional cell-free triplicates with particles were prepared for subtraction of absorption effects. The lysis buffer included in the kit was used as positive control. The amount of LDH released in the supernatant was expressed as fold increase of untreated cells.

Apoptosis assay

The Caspase-Glo® 3/7 Assay (Promega, Germany) was used to detect caspase 3/7-activity according to manufacturer's instruction with some modifications to avoid particle-associated signal quenching. After treatment for 24 h cells were centrifuged (5 min, 300 g, 4°C) and supernatant was replaced by 400 µl of lysis buffer (1% NP-40, 50 mM Tris, 150 µM NaCl, 0.5 mM EDTA, 2 mM DTT). Cellular lysates were centrifuged again for 10 min at 20.000 g and supernatant was mixed 1:1 with the kit's reaction mixture. Cleavage of kit-included caspase substrate leads to a luminescent signal produced by luciferase proportional to the amount of caspase activity which could be measured by MicroLumat Plus Microplate Luminometer LB 96 V (EG&G Berthold, Germany). Data were expressed as percentage of untreated control.

Measurement of reactive oxygen species

The ability of the two MW-CNT samples to elicit reactive oxygen species (ROS) generation in RAW 264.7 mouse macrophages was measured using an Amplex Red assay (Life

Technologies, Germany). The assay detects extracellular H_2O_2 be measurement of the oxidation of the nonfluorescent molecule 10-acetyl-3, 7-dihydroxyphenoxazine (Amplex Red) to the highly fluorescent resorufin, which is catalyzed by horseradish peroxidase. Cells were seeded at a concentration of 1 x 10^6 cells/cm^2 and cultured over night. Immediately before treatment medium supernatants were replaced by reaction buffer (129 mM NaCl, 4.86 mM KCl, 1.22 mM $CaCl_2$ x $2H_2O$, 15.8 mM NaH_2PO_4 x H_2O). Particle treatment occurred at 0.625, 2.5 and 10 µg/cm^2. Zymosan (Sigma, Germany) was used as a positive control. Directly after addition of particle suspension or positive control, the same amount of Amplex Red working solution (120 µl Amplex Red stock solution, 11.82 ml reaction buffer, 24 µl NaN_3, 40 ml HPO, 600 U/ml) was added and incubated for 90 min until measurement using a Multiscan ELISA reader at 570 nm (Thermo Fisher Scientific, Germany).

Pharyngeal aspiration

Mice aged 9 - 10 weeks were exposed to MW-CNTs by pharyngeal aspiration of 40 µl of a 1 mg/ml suspension per 20 g body weight. The samples were suspended in PBS / 0.6 mg/ml bovine serum albumin / 0.01 mg/ml Dipalmitoyl-phosphatidylcholine (DPPC), and sonicated for 10 min in a Sonorex sonication bath (60 W, 35 kHz) before their application. Nanotube aspiration took place under isoflurane anesthesia. Control animals received the same volume of vehicle only (PBS/BSA/DPPC). After 8 weeks, animals were brought under deep anesthesia by injection of pentobarbital (50 mg/kg body weight) and were euthanized via exsanguination through the aorta abdominalis. Blood was obtained by cardiac puncture and the lungs were removed for histopathological and immunohistochemical evaluation.

Bio-Plex cytokine assay

Systemic inflammation was assessed by measurement of the concentrations of the cytokines IL-1β, IL-10, IL-13, G-CSF, MCP-1, TNF-α en MIP-2 in mouse serum. To this end, a Bio-Plex murine cytokine 10-plex panel (Biorad, using Luminex xMAP technology) was used. In this assay, a mixture of beads coated with antibodies is used to detect an array of cytokines simultaneously in one sample. Upon binding of beads to their target molecule, a fluorescently labeled antibody is in its turn able to conjugate with the bead-biomolecule complex and can be detected using a flow cytometer. The Bio-Plex assay was performed according to the manufacturer's instructions. Data were analysed with a Luminex 100 IS 2.3 system coupled to Bio-Plex Manager 4.1.1 software.

Quantitative RT-PCR

Eight weeks after MW-CNT aspiration, the left lung of five mice per treatment group was excised and homogenized in Trizol. RNA was isolated and purified using an RNeasy kit (Qiagen) including an additional DNase incubation to remove residual DNA. RNA quality was determined using spectrophotometry; a ratio of values obtained at wave lengths of 280 and 260 nm of at least 1.8 was acceptable for subsequent analysis. cDNA was synthesized using an iScript DNA Synthesis kit (BioRad) and was diluted 15× in RNase-free water. Primers were designed for heme oxygenase-1 (HO-1), γ-glutamyl cysteine synthetase (γ-GCS), nuclear factor (erythroid-derived 2)-like 2 (Nrf2), the matrix metalloproteinases (MMPs) 2, 8 and 9, tissue inhibitor of metalloproteinase-1 (TIMP-1) and the housekeeping gene glyceraldehyde 3-phosphate dehydrogenase (GAPDH) using Primer Express software (Applied Biosystems). The PCR efficiency was determined for each primer set using cDNA dilution curves and was deemed sufficient at 90% or more. Sequences of the used primer sets are listed in table 4-1.

Table 4-1: Primer sequences used in this study

	forward	reverse
GAPDH	5'-AACCTGCCAAGTATGATGACATCA-3'	5'-GGTCCTCAGTGTTAGCCCAAGAT-3'
HO-1	5'-CCTCACTGGCAGGAAATCATC-3'	5'-CCTCGTGGAGACGCTTTACATA-3'
γ-GCS	5'-CGACCAATGGAGGTGCAGTTA-3'	5'-ACCCTAGTGAGCAGTACCACGAA-3'
Nrf2		5'-CTAGTTTTTCTTTGTATCTGG-3'
MMP-2	5'-TGTCCCGAGACCGCTATGTC-3'	5'-TTGTTGCCCAGGAAAGTGAAG-3'
MMP-8	5'-AATTCCGGTCTTCGAGGAATG-3'	5'-TTCCCAGTCTCTGCTAAGCTGAA-3'
MMP-9	5'-GGACGACGTGGGCTACGT-3'	5'-CACGGTTGAAGCAAAGAAGGA-3'
TIMP-1	5'-GGCCCCCTTTGCATCTCT-3'	5'-ACAGGCCTTACTGGAAGCTATCA-3'

For PCR, 2.5 µl of forward and reverse primer (both 0.3 µM) was mixed with 2.5 µl RNase-free water, 5 µl diluted cDNA and 12.5 µl SYBR© Green Supermix (Biorad), generating 25 µl reaction mixture that was transferred to each well of a 96 well plate. Top perform quantitative real time PCR, a Single Color real time PCR detection system (BioRad) was used; the protocol consisted of a denaturation step (95ºC, 3 min) followed by 40 cycles (per cycle: 95ºC for 15 sec and then 60ºC for 45 sec). Dissociation curves were made to ascertain that PCR data represent the amplification of the correct product. Data were analyzed using a MyiQ Software system (BioRad) and were expressed as the relative gene expression (fold increase)

compared to the average value for control animals according to the 2-ΔΔCt method [Livak et al., 2001]. Results were normalized for the housekeeping gene GAPDH.

Immunohistochemistry of cleaved caspase 3

For three mice per treatment group, lungs were instilled with 4% paraformaldehyde in PBS (pH 7.4) in situ using a 1 ml syringe. Subsequently they were excised, fixated in 4% paraformaldehyde, dehydrated and embedded in a paraffin block. Lung tissue was cut in thin slices that were fixed on microscopic slides and were stained for cleaved caspase 3 after rehydration. For counterstaining, hematoxylin was used. The binding of the primary antibody anti-cleaved caspase 3 (1:100, Cell Signaling, USA) was detected by a secondary biotinylated goat anti-rabbit antibody and a streptavidin-biotin complex according to the protocol of the manufacturer (Vector Laboratories, USA). As substrate, diaminobenzidine (Sigma) was used. Nonspecific binding was assessed by incubation with the appropriate IgG control instead of primary antibody, at the same IgG concentration. Microphotographs were made after oil immersion using a light microscope (BX60) and analysis software (Olympus, Germany) at a 1000× original magnification.

Masson's Trichrome staining

Tissue sections were cut from paraffin-embedded lungs at a thickness of 3 µm. Slides were stained with Masson Trichrome, which stains cell nuclei, cytoplasm and collagen in three different colors. Subsequently, slides were evaluated visually at an original magnification of 1000×.

Statistical evaluation

Data are expressed as mean ± SEM. For all in vitro methods, three independent experiments were performed for an n=3, unless specified otherwise. For the *in vivo* Bio-plex and real time PCR techniques, material was obtained from five mice per treatment group (n=5). Immunohistochemical evaluation was performed in lung tissue from three mice per group (n=3). Data were analyzed using SPSS version 15 for Windows. Treatment-related differences were evaluated by one way analysis of variance (ANOVA) or the non-parametric Mann-Whitney U test (Luminex cytokine assay only). Multiple comparisons were assessed by ANOVA post-hoc analysis according to Tukey's method or LSD method (for LDH and WST-1 assays). A difference was considered to be statistically significant when $p<0.05$.

4.3 Results

Toxicity in RAW 264.7 cells.

Two independent assays, i.e. the WST-1 assay as well the LDH assay, were used for evaluation of the toxicity of the CNT samples (Fig. 4-2). No significant effects were found for MW-CNT2. However, MW-CNT1 elicited a significant toxicity in both assays in a dose-dependent manner. Mitochondrial activity was reduced up to 60% of the activity in control cells (Fig. 4-2A), while membrane integrity loss was increased by up to 20% (Fig. 4-2B).

Inflammation and fibrosis

Systemic inflammation was assessed by the measurement of seven different cytokines in the blood collected from the mice after pharyngeal aspirations. Several trends in expression changes of these inflammatory markers were observed after 8 weeks of exposure to both types of MW-CNT (Fig. 4-3A). For MCP-1, significantly higher levels ($p<0.001$) were measured in the blood of animals exposed to MW-CNT1, while a non-significant trend was observed for MW-CNT2.

In the lungs of MW-CNT exposed mice the pro-fibrotic response was measured by whole lung tissue mRNA expression analysis of MMP2, MMP8, MMP9 and TIMP-1 (Figure 4-3B) as well as by histopathological investigation (Figure 4-3C-E). A significant 1.8-fold induction of MMP-8 and a significant 2.2-fold induction of TIMP-1 were found in lung tissue from mice exposed to MW-CNT1. Masson Trichrome staining of lung tissue sections for collagen visualization confirmed the real time PCR data; higher pulmonary collagen deposition was found in MW-CNT1-exposed mice. Granulomatous lesions, nodular structural alterations with very high cellular density, were observed in animals instilled with both MW-CNT lesions. These areas likely reflect the accumulation of CNTs and inflammatory cells such as macrophages, providing an encapsulation of the fibrous materials as has been observed for other materials such as quartz and asbestos.

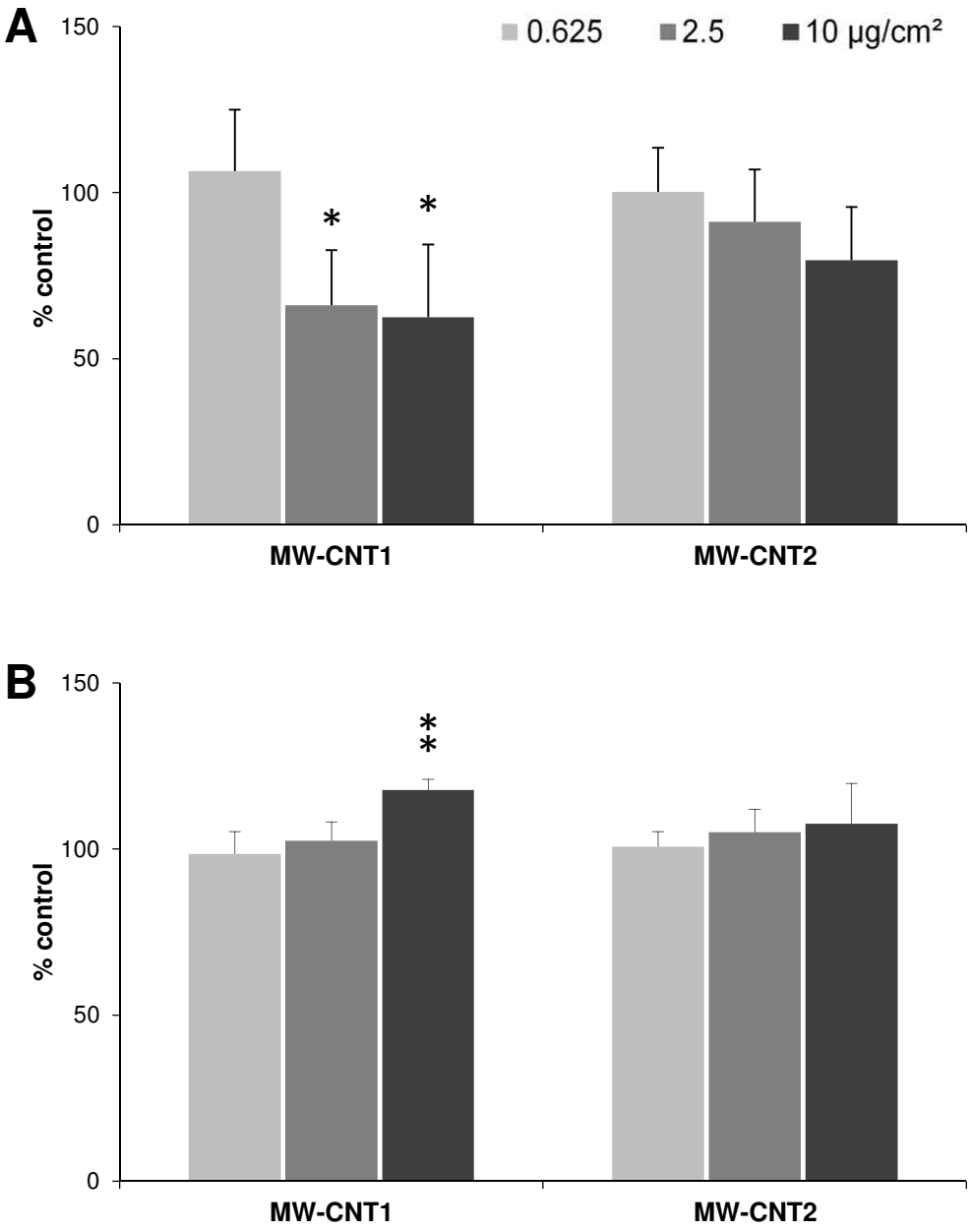

Fig. 4-2: Investigation of MW-CNT toxicity in RAW 264.7 macrophages. Cells were treated with MW-CNT as before (0.625-10 µg/cm^2). Viability was assessed by the WST-1 assay (A), which measures mitochondrial activity, and release of the enzyme LDH (B) which represents membrane leakage. Data are related to non-treated control cells and represent an n=3.

Oxidative stress marker expression in mouse lungs and reactive oxygen species formation from RAW 264.7 macrophages

Pulmonary oxidative stress responses were investigated by measurement of the mRNA expression of the antioxidant genes HO-1 and γ-GCS [van Berlo et al., 2010], as well as of Nrf2, the pivotal transcription factor involved in the up-regulation of these and other antioxidant genes [Cho et al., 2006]. A clear induction of HO-1 and γ-GCS was measured in whole lung tissue from mice instilled with MW-CNT1 although this did not reach statistical significance (Fig. 4-4A). The mRNA expression of Nrf2 was not affected by the CNT treatments.

The ability of MW-CNT to trigger ROS production in macrophages was evaluated by Amplex red assay in the RAW 264.7 cells. After treatment with either MW-CNT sample, augmented production of H_2O_2 was detected (Fig. 4-4B).

Fig. 4-3: Inflammatory and fibrotic effects of MW-CNT in mice after pharyngeal aspiration [on page 93]. (A) Systemic levels of inflammatory cytokines. Blood was taken from 5 mice per treatment group and was analysed for a number of inflammatory cytokines using a Bio-Plex cytokine assay. Cytokine levels are displayed as mean ± SEM in pg/ml. *** $p<0.001$ vs. control animals (instilled with PBS/BSA/DPPC). (B-E) Investigation of CNT-induced pro-fibrotic effects in whole lung homogenate by qRT-PCR (MMP2, 8, 9; TIMP 1, B) and after Massons's Trichrome staining in lung sections of control (C), MW-CNT1 (D) or MW-CNT2 (E). Whole lung homogenates from 5 mice per treatment group were analysed by real time PCR. Data are expressed as mean ± SEM compared to the mean expression in animals exposed to the suspension medium PBS/BSA/DPPC and normalized for GAPDH. * $p<0.05$, *** $p<0.001$ vs. control animals. Representative images from lung sections stained with Masson Trichrome are shown for mice exposed to vehicle control (3C), MW-CNT1 (3D) and MW-CNT2 (3E). Cellular nuclei are stained dark purple while the cytoplasm is stained purple and collagen can be identified by blue staining. Original magnification: 1000×

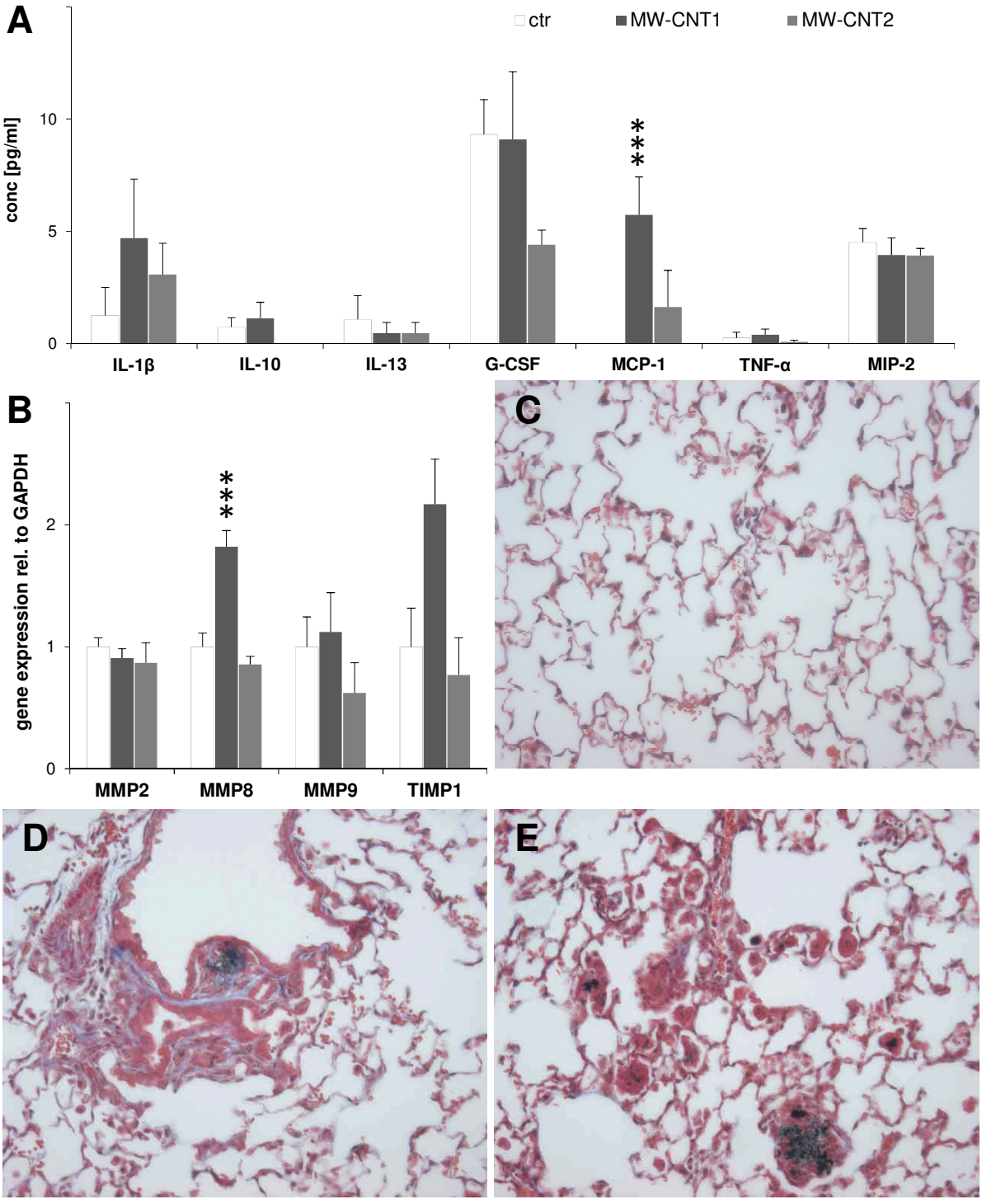
A
ctr
MW-CNT1
MW-CNT2
conc [pg/ml]
10
5
0
***
IL-1β
IL-10
IL-13
G-CSF
MCP-1
TNF-α
MIP-2
B
gene expression rel. to GAPDH
2
1
0
***
MMP2
MMP8
MMP9
TIMP1
C
D
E

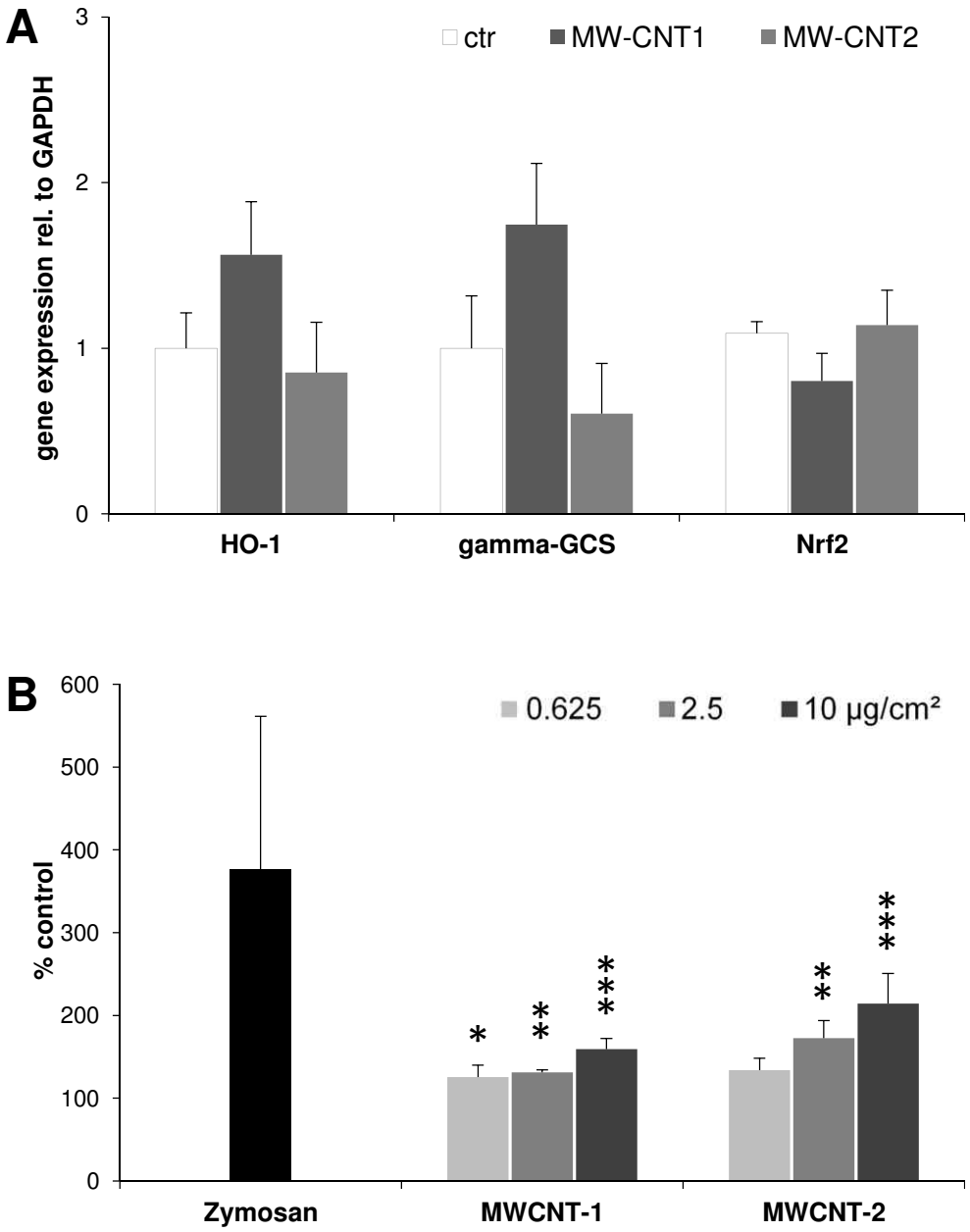

Fig. 4-4: Expression of oxidative stress markers in lungs of MW-CNT-exposed mice (A) as well as ROS production by MW-CNT-treated RAW 264.7 murine macrophages (B). (A) The expression of heme oxygenase-1 (HO-1), γ-glutamyl cysteine synthetase (γ-GCS) and nuclear factor (erythroid-derived 2)-like 2 (Nrf2) was measured in whole lung tissue by real time PCR. Lungs were obtained from 5 mice per treatment group. Data are expressed as GAPDH-adjusted mean ± SEM relative to mRNA expression in control mice. (B) An Amplex Red assay was used to investigate ROS generation in response to a 90 minute treatment with 0.625, 2.5 or 10 µg/cm^2 MW-CNTs. Zymosan treatment was included as positive control. Data are related to ROS generation in untreated control cells and are thus expressed as % control. Data represent three independent experiments.

Investigation of apoptosis induction by MW-CNTs in vivo and in vitro.

The induction of apoptosis in MW-CNT exposed mouse lungs was investigated by cleaved caspase 3 immunohistochemistry (Fig. 4-5A, C, E). Whereas apoptosis was nearly absent in lung tissue from control animals (Fig. 4-5A), enhanced cleaved caspase 3 staining was clearly observed in tissue sections from CNT-exposed animals (Figure 4-5C, E). In particular the MW-CNT1 sample elicits enhanced staining, which was primarily localized within granulomatous foci (Fig. 4-5C). For MW-CNT2, similar observations were made; although the intensity of staining was clearly lower (Fig. 4-5E). In all sections stained with the primary antibody the intensity was clearly higher than the staining for the IgG control (Fig. 4-5B, D, F) of serial sections. Taken together, the data show that MW-CNT treatment elicits enhanced apoptosis although it is strongly localized within granuloma for the most part. Assessment of the activity of the effector caspases 3 and 7 in MW-CNT-treated RAW 264.7 cells using a Caspase-Glo assay revealed that neither sample caused apoptosis at any of the three treatment concentrations (Fig. 4-5G). In contrast, the positive control staurosporine caused a clear caspase 3/7 activation in the RAW 264.7 cells.

Fig. 4-5: Investigation of apoptosis induction by MW-CNT *in vivo* and *in vitro* [on page 96]. (A-F) Representative images of cleaved caspase 3 staining in mouse lung. The presence of cleaved caspase 3, an apoptotic marker, was assessed in lung tissue sections by immunohistochemical analysis. Animals were sacrificed 8 weeks after pharyngeal aspiration of vehicle control (PBS/BSA/DPPC; A, B), MW-CNT1 (C, D) or MW-CNT2 (E, F). Slides were incubated with an antibody against cleaved caspase 3 (A, C, E) or the appriopriate IgG control (B, D, F) and were counterstained with hematoxylin. Light purple staining reflects cellular cytoplasm, dark purple staining the nuclei and brown staining indicates activated caspase 3. Original magnification: 1000×. (G) The activity of the caspases 3 and 7 in response to MW-CNT at concentrations of 0.625 to 10 μg/cm^2 was measured in RAW 264.7 cells using a Caspase-Glo 3/7 assay. Data are expressed as % of caspase 3 and 7 activity in non-treated control cells and represent three independent experiments.

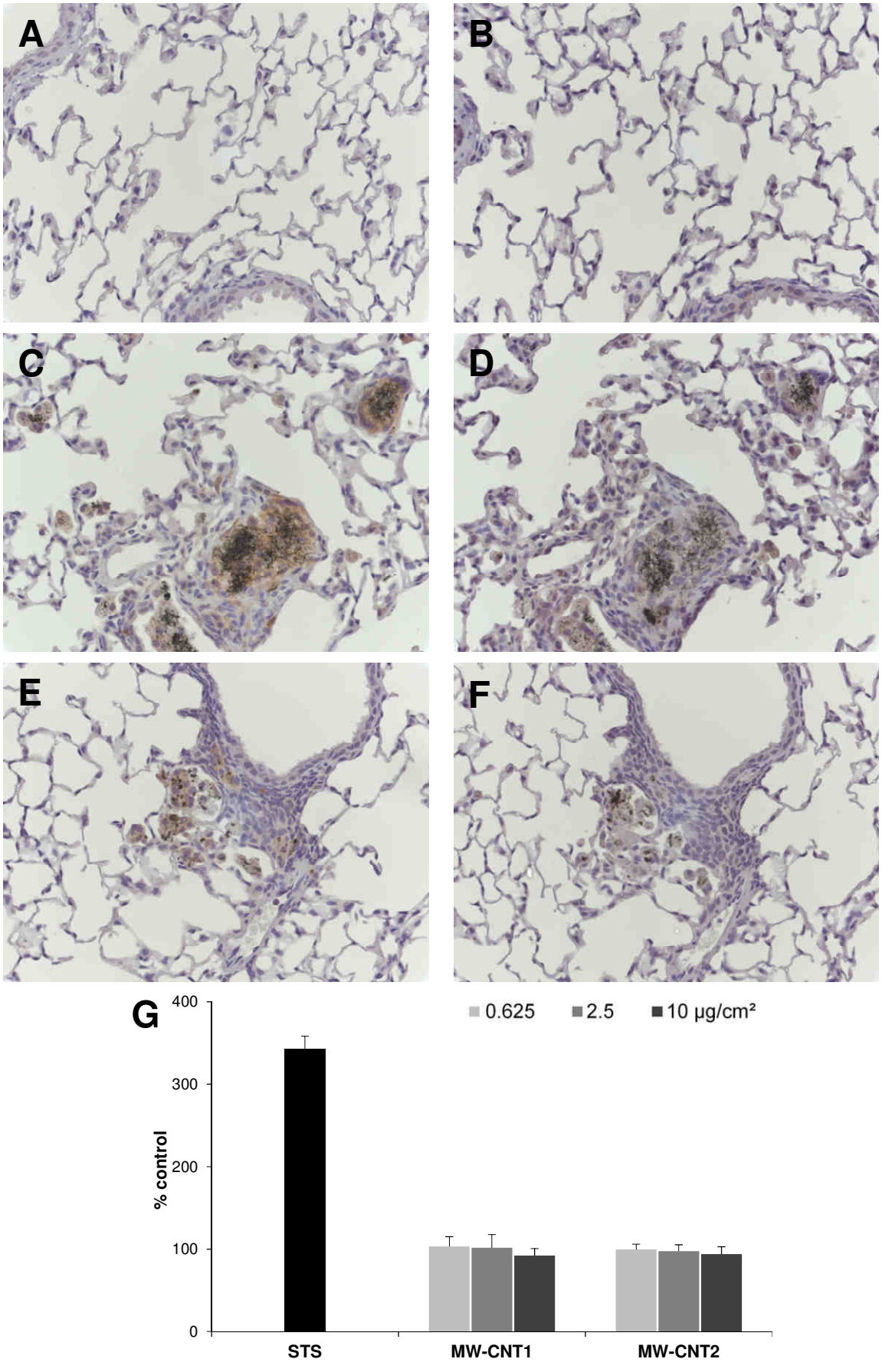
A
B
C
D
E
F
G
0.625
2.5
10 µg/cm²
% control
400
300
200
100
0
STS
MW-CNT1
MW-CNT2

4.4 Discussion

When considering the novelty of carbon nanotubes and their foreseen widespread application, it is clear that there is a pressing need to investigate potential adverse health effects associated with CNTs at an early stage of their development. Also, it is essential to identify physico-chemical properties that are responsible for any CNT-associated toxicity by focusing on the identification of the key responsible mechanisms to allow avoidance of possible health hazards. The results of the current work clearly demonstrate various contrasting effects for the two different MW-CNT samples after pharyngeal aspiration. Most importantly, the long MW-CNT caused a more pronounced pulmonary toxicity than the short MW-CNT, characterized by increased inflammogenic and pro-fibrotic responses. Our current observations are in concordance with the "fibre paradigm" as established for asbest and asbestiform man made fibres and as recently expanded for fibre-shaped nanomaterials like nanotubes and nanofibres [Osmond-McLeod et al. 2011; Schinwald et al., 2012] although specific investigations have also revealed that shorter CNTs may show stronger pulmonary toxicity under specific experimental conditions [Muhlfeld et al. 2011]. Importantly, in this regard, apart from having a different average length, both MW-CNT samples also differed in their agglomeration behavior. Whereas the one sample typically appears to consist of rigid needle-shaped CNTs existing as bundles as well as singlets, the other sample contained highly entangled nanotubes, thereby resembling a ball of wool. Of course, the materials have been characterized by electron microscopy in a cell free environment and might behave rather differently under physiological conditions. However, also conventional light microscopy observations of the CNT-treated RAW 264.7 cells indicated that, at least *in vitro*, the MW-CNT2 were typically present as dense agglomerates, whereas the MW-CNT1 sample appeared more dispersed and not as much coiled up (data not shown).

Our *in vitro* investigations also revealed stronger cytotoxicity effects with the longer MW-CNT sample in the macrophages, both for the WST-1 assay and the LDH assay. Surprisingly, however, the formation of H_2O_2 by the RAW 264.7 cells did not differ for both types of MW-CNT. This would suggest that the contrasting physico-chemical properties of the materials do not affect the ability to trigger oxidative burst from the phagocytes. However, the absence of an enhanced ROS formation by the longer nanotubes may also relate to the concurrently observed increased cytotoxic effects of this sample. A role of ROS formation and the associated induction of oxidative stress in the pulmonary toxicity of MW-CNT may also be forwarded by the observed, albeit non-significant, mRNA expression increases of

HO-1 and γ-GCS in MW-CNT1 exposed mice. Enhanced pulmonary expression of the oxidative stress responsive gene HO-1 has been shown previously for various inhaled particulates including asbestos, silica as well as for single walled carbon nanotubes [Nagatomo et al., 2005; Sato et al., 2006; Li et al., 2007b]. Changes in the mRNA expression of γ-GCS may be considered as a further sensitive marker of ROS generation and oxidative stress by particles, as it encodes the rate limiting enzyme of the major pulmonary antioxidant glutathione. In a recent study, we observed silica induced mRNA expression increases of both HO-1 and γ-GCS in the lungs of wildtype mice, but not in the lungs of $p47^{phox}$ NADPH oxidase knockout mice [van Berlo *et al.* 2010]. This knockout model is characterized by an entirely lacking function of the NADPH oxidase enzyme complex in macrophages and neutrophils, and therefore suggests that the presently observed differences in pathogenicity of the two MW-CNT samples are driven, at least in part, by phagocyte burst independent processes.

The long MW-CNT sample was found to induce clear pro-fibrotic pulmonary responses as assessed by the expression of the fibrotic genes MMP-8 and TIMP-1 as well as the augmented deposition of collagen, the hallmark of lung fibrosis. In marked contrast to these findings, no modulation of these endpoints was found in response to the short/entangled sample, with the exception of a mildly enhanced collagen deposition. However, both samples induced the formation of nodular granulomatous lesions in the lung, as has been reported by others (e.g. [Poland et al. 2008; Kim et al., 2010; Kato et al. 2012]). The lesions are characterized by the concentration of CNT material, greater cellular density and an accumulation of immune cells, especially macrophages. Within the granulomas, enhanced pro-apoptotic responses were observed, as demonstrated by an enhanced staining for the cleaved form of the executioner caspase 3.

The observation of apoptotic cells specifically within granulomas, has been made by others in silica-exposed rats [Leigh et al., 1997]). The granulomas observed in response to MW-CNT might represent the attempt to encapsulate foreign biopersistent materials to shield them from healthy tissue, as also occurs upon exposure to silica or asbestos [Kane et al., 1986; Driscoll et al., 1990; Koerten et al., 1990; Mariani et al., 1996]. Alternatively, they could be caused by infection of the lung with pathogenic bacteria, which might occur more readily in CNT-exposed mice due to a compromised pulmonary immune system. Apoptosis has been for instance been observed in tuberculosis-induced granulomas [Davis et al., 2009] and is known to play an important role in the development of immunity against tuberculosis [Fairbairn 2004]. The importance of the respiratory burst to the microbicidal effects of macrophages and

neutrophils is underpinned by the clinical features in chronic granulomatous disease (CGD) patients, caused by a rare, inherited mutations in specific subunits of the phagocytic NADPH oxidase enzyme complex, including the aforementioned $p47^{phox}$ subunit [Fox et al., 2010]. As a result, CGD patients suffer from recurrent bacterial and fungal infections and develop characteristic granulomas, typical of unresolved antimicrobial response, in their organs. The increased caspase 3 staining observed in the granuloma of the MW-CNT treated mice may thus reflect at least to some extent apoptosis in neutrophils, rather than in macrophages. Whether this reflects a feedback attempt of the host against an MW-CNT driven development or progression of fibrotic nodules needs further investigation. In this regard, promotion of neutrophil apoptosis has been proposed as a therapeutic strategy in pulmonary inflammatory diseases [Fox et al. 2010]. Interestingly, in our current study significantly increased serum MCP-1 levels were observed after treatment with the long MW-CNT sample. This may reflect a pathway of recruitment of macrophages by the potent chemokine in an attempt to orchestrate the resolution of inflammation and/or tissue repair, as was demonstrated recently in experimental models of pulmonary inflammation [Tanaka et al., 2010; Liang et al., 2012].
Whether apoptosis localized exclusively to granulomas has any relevance for human exposure situations involving particulate material is yet unknown. Except for positive staining within granulomas, no enhanced staining for caspase 3 could be observed in the lung tissue, in any cell type. Within the currently available literature, few in vivo studies are included so far reporting findings on apoptosis induced by MW-CNT. In rats intratracheally instilled with 0.01 or 0.1 mg MW-CNTs, enhanced apoptosis was found in alveolar macrophages obtained by bronchoalveolar lavage [Elgrabli et al. 2008]. In another study, enhanced apoptosis has been observed in lungs of MW-CNT exposed rats including various cell types such as macrophages [Roda et al. 2011]. Interestingly, neither fibrosis nor granuloma was present in both these studies, in contrast to our current findings in mice. It is unlikely, that the differential responses in the two rat studies and our study reflect species specific differences, as mice generally feature less severe pulmonary pathogenicity than rats in response to similar levels particle exposure [Donaldson 2000; Mossman 2000]. More likely, the observed contrasts relate to differences in treatment dose, the physicochemical properties of the used MW-CNT samples as well as the way they are applied to the respective animal models. Herein, it should also be emphasized that apart from length, rigidity and agglomeration, also targeted functionalization of CNT, which is increasingly applied in the nanotechnology sector, can affect its toxic properties [Roda et al. 2011; van Berlo et al. 2012]. The effect of CNT functionalization on pro-inflammatory and fibrotic pulmonary responses was not

specifically addressed in our current study, but obviously represents an important aspect for future investigations.

For the evaluation of the specific relevance of apoptosis induction in macrophages, our *in vitro* studies in RAW 264.7 macrophages were performed with the same two MW-CNT samples that were investigated in our mouse model. Remarkably, no apoptosis was observed in response to MW-CNT, as indicated by a complete lack of activation of the effector caspases 3 and 7. In contrast, we recently observed in the same cell line that silica particles elicited a clear caspase 3 activation [Wilhelmi et al. 2012]. False negative results due to interference with specific assay components could be excluded on the basis of control experiments employing MW-CNT spiking into the lysates of staurosporine-pretreated macrophages (data not shown). Contrasting results have been published concerning the induction of apoptosis in RAW 264.7 cells by MW-CNT. In some studies, a positive apoptotic response has been observed [Di Giorgio et al. 2011; Wang et al. 2012], whereas in other studies apoptosis was not induced in the same cell line [Sohaebuddin et al. 2010; Luo et al. 2012]. Remarkably, in the Di Giorgio et al. study, apoptosis was observed in the absence of marked toxicity. In our study apoptosis was absent both at cytotoxic and non-cytotoxic concentrations, as evidenced by two independent assays that can detect necrosis (i.e. LDH and WST-1). Within the nanotoxicology community, a strong focus has been directed on the exclusion of artefacts, which can readily occur when nanoparticles interfere with assay components or read-outs [Stone et al., 2009]. In our study, we took great care to exclude any interference for the evaluation of apoptosis, according to additional measures as recently published [Wilhelmi et al. 2012]. It is therefore possible that some of the reported findings on apoptosis, especially when toxicity is not observed, were due to artefacts. An alternative explanation is that different MW-CNT samples might possess markedly different pro-apoptotic potential in macrophages.

In conclusion, our study reveals that the hazard of inhaled MW-CNT depends on specific physico-chemical properties of this morphologically heterogeneous group of nanomaterials: Nanotube length, rigidity and the likely associated agglomeration properties of MW-CNT appeared to have major impact on their ability to induce inflammation and pro-fibrotic responses in mouse lung. Herein, however, apoptosis of pulmonary macrophages does not does seem to be a causal initiating trigger. The observed apoptosis in the lungs of MW-CNT exposed mice may reflect merely a secondary response to focal inflammatory effects and/or a feedback process to trigger resolution of inflammation and limit granuloma formation. As such, our study also demonstrates that *in vitro* testing of macrophage apoptosis by MW-CNT is a poor predictor of their pulmonary hazard.

Acknowledgements

The authors thank Dr. Burkhard Stahlmecke (IUTA) for the electron microscopical characterization of the nanotubes, and Mrs. Christel Weishaupt and Mrs. Petra Gross (IUF) for their technical support in the biological assays. This study was financially supported by the Federal Ministry of Education and Research (BMBF) and an ERS/Marie Curie Fellowship (awarded to AWB).

4.5 References

Beamer, CA and Holian, A (2007). Antigen-presenting cell population dynamics during murine silicosis. Am J Respir Cell Mol Biol 37(6): 729-738.

Cho, HY, Reddy, SP and Kleeberger, SR (2006). Nrf2 defends the lung from oxidative stress. Antioxid Redox Signal 8(1-2): 76-87.

Davis, JM and Ramakrishnan, L (2009). The role of the granuloma in expansion and dissemination of early tuberculous infection. Cell 136(1): 37-49.

Di Giorgio, ML, Di Bucchianico, S, Ragnelli, AM, Aimola, P, Santucci, S and Poma, A (2011). Effects of single and multi walled carbon nanotubes on macrophages: cyto and genotoxicity and electron microscopy. Mutat Res 722(1): 20-31.

Doll, NJ, Stankus, RP and Barkman, HW (1983). Immunopathogenesis of asbestosis, silicosis, and coal workers' pneumoconiosis. Clin Chest Med 4(1): 3-14.

Donaldson, K (2000). Nonneoplastic lung responses induced in experimental animals by exposure to poorly soluble nonfibrous particles. Inhal Toxicol 12(1-2): 121-139.

Donaldson, K, Aitken, R, Tran, L, Stone, V, Duffin, R, Forrest, G and Alexander, A (2006). Carbon nanotubes: a review of their properties in relation to pulmonary toxicology and workplace safety. Toxicol Sci 92(1): 5-22.

Donaldson, K, Murphy, F, Schinwald, A, Duffin, R and Poland, CA (2011). Identifying the pulmonary hazard of high aspect ratio nanoparticles to enable their safety-by-design. Nanomedicine (Lond) 6(1): 143-156.

Driscoll, KE, Lindenschmidt, RC, Maurer, JK, Higgins, JM and Ridder, G (1990). Pulmonary response to silica or titanium dioxide: inflammatory cells, alveolar macrophage-derived cytokines, and histopathology. Am J Respir Cell Mol Biol 2(4): 381-390.

Elgrabli, D, Abella-Gallart, S, Robidel, F, Rogerieux, F, Boczkowski, J and Lacroix, G (2008). Induction of apoptosis and absence of inflammation in rat lung after intratracheal instillation of multiwalled carbon nanotubes. Toxicology 253(1-3): 131-136.

Fairbairn, IP (2004). Macrophage apoptosis in host immunity to mycobacterial infections. Biochem Soc Trans 32(Pt3): 496-498.

Fox, S, Leitch, AE, Duffin, R, Haslett, C and Rossi, AG (2010). Neutrophil apoptosis: relevance to the innate immune response and inflammatory disease. J Innate Immun 2(3): 216-227.

Gasser, M, Wick, P, Clift, MJ, Blank, F, Diener, L, Yan, B, Gehr, P, Krug, HF and Rothen-Rutishauser, B (2012). Pulmonary surfactant coating of multi-walled carbon nanotubes (MWCNTs) influences their oxidative and pro-inflammatory potential in vitro. Part Fibre Toxicol 9(1): 17.

Hansen, K and Mossman, BT (1987). Generation of superoxide (O2-.) from alveolar macrophages exposed to asbestiform and nonfibrous particles. Cancer Res 47(6): 1681-1686.

Hirano, S, Kanno, S and Furuyama, A (2008). Multi-walled carbon nanotubes injure the plasma membrane of macrophages. Toxicol Appl Pharmacol 232(2): 244-251.

Jaurand, MC, Renier, A and Daubriac, J (2009). Mesothelioma: Do asbestos and carbon nanotubes pose the same health risk? Part Fibre Toxicol 6: 16.

Kane, AB, MacDonald, JL and Moalli, PA (1986). Acute injury and regeneration of mesothelial cells produced by crocidolite asbestos fibers. Am Rev Respir Dis 133: A198.

Kato, T, Totsuka, Y, Ishino, K, Matsumoto, Y, Tada, Y, Nakae, D, Goto, S, Masuda, S, Ogo, S, Kawanishi, M, Yagi, T, Matsuda, T, Watanabe, M and Wakabayashi, K (2012). Genotoxicity of multi-walled carbon nanotubes in both in vitro and in vivo assay systems. Nanotoxicology.

Kermanizadeh, A, Pojana, G, Gaiser, BK, Birkedal, R, Bilanicova, D, Wallin, H, Jensen, KA, Sellergren, B, Hutchison, GR, Marcomini, A and Stone, V (2012). In vitro assessment of engineered nanomaterials using a hepatocyte cell line: cytotoxicity, pro-inflammatory cytokines and functional markers. Nanotoxicology.

Kim, JE, Lim, HT, Minai-Tehrani, A, Kwon, JT, Shin, JY, Woo, CG, Choi, M, Baek, J, Jeong, DH, Ha, YC, Chae, CH, Song, KS, Ahn, KH, Lee, JH, Sung, HJ, Yu, IJ, Beck, GR, Jr. and Cho, MH (2010). Toxicity and clearance of intratracheally administered multiwalled carbon nanotubes from murine lung. J Toxicol Environ Health A 73(21-22): 1530-1543.

Kisin, ER, Murray, AR, Sargent, L, Lowry, D, Chirila, M, Siegrist, KJ, Schwegler-Berry, D, Leonard, S, Castranova, V, Fadeel, B, Kagan, VE and Shvedova, AA (2011). Genotoxicity of carbon nanofibers: are they potentially more or less dangerous than carbon nanotubes or asbestos? Toxicol Appl Pharmacol 252(1): 1-10.

Kobayashi, N, Naya, M, Ema, M, Endoh, S, Maru, J, Mizuno, K and Nakanishi, J (2010). Biological response and morphological assessment of individually dispersed multi-wall carbon nanotubes in the lung after intratracheal instillation in rats. Toxicology 276(3): 143-153.

Koerten, HK, Hazekamp, J, Kroon, M and Daems, WT (1990). Asbestos body formation and iron accumulation in mouse peritoneal granulomas after the introduction of crocidolite asbestos fibers. Am J Pathol 136(1): 141-157.

Kuwano, K, Miyazaki, H, Hagimoto, N, Kawasaki, M, Fujita, M, Kunitake, R, Kaneko, Y and Hara, N (1999). The involvement of Fas-Fas ligand pathway in fibrosing lung diseases. Am J Respir Cell Mol Biol 20(1): 53-60.

Leigh, J, Wang, H, Bonin, A, Peters, M and Ruan, X (1997). Silica-induced apoptosis in alveolar and granulomatous cells in vivo. Environ Health Perspect 105 Suppl 5: 1241-1245.

Li, JG, Li, WX, Xu, JY, Cai, XQ, Liu, RL, Li, YJ, Zhao, QF and Li, QN (2007a). Comparative study of pathological lesions induced by multiwalled carbon nanotubes in lungs of mice by intratracheal instillation and inhalation. Environ Toxicol 22(4): 415-421.

Li, Z, Hulderman, T, Salmen, R, Chapman, R, Leonard, SS, Young, SH, Shvedova, A, Luster, MI and Simeonova, PP (2007b). Cardiovascular effects of pulmonary exposure to single-wall carbon nanotubes. Environ Health Perspect 115(3): 377-382.

Liang, J, Jung, Y, Tighe, RM, Xie, T, Liu, N, Leonard, M, Gunn, MD, Jiang, D and Noble, PW (2012). A macrophage subpopulation recruited by CC chemokine ligand-2 clears apoptotic cells in noninfectious lung injury. Am J Physiol Lung Cell Mol Physiol 302(9): L933-940.

Livak, KJ and Schmittgen, TD (2001). Analysis of relative gene expression data using real-time quantitative PCR and the 2(-Delta Delta C(T)) Method. Methods 25(4): 402-408.

Luo, M, Deng, X, Shen, X, Dong, L and Liu, Y (2012). Comparison of cytotoxicity of pristine and covalently functionalized multi-walled carbon nanotubes in RAW 264.7 macrophages. J Nanosci Nanotechnol 12(1): 274-283.

Mariani, TJ, Roby, JD, Mecham, RP, Parks, WC, Crouch, E and Pierce, RA (1996). Localization of type I procollagen gene expression in silica-induced granulomatous lung disease and implication of transforming growth factor-beta as a mediator of fibrosis. Am J Pathol 148(1): 151-164.

Mercer, RR, Hubbs, AF, Scabilloni, JF, Wang, L, Battelli, LA, Friend, S, Castranova, V and Porter, DW (2011). Pulmonary fibrotic response to aspiration of multi-walled carbon nanotubes. Part Fibre Toxicol 8: 21.

Miller, BG, Searl, A, Davis, JM, Donaldson, K, Cullen, RT, Bolton, RE, Buchanan, D and Soutar, CA (1999). Influence of fibre length, dissolution and biopersistence on the production of mesothelioma in the rat peritoneal cavity. Ann Occup Hyg 43(3): 155-166.

Mitchell, LA, Gao, J, Wal, RV, Gigliotti, A, Burchiel, SW and McDonald, JD (2007). Pulmonary and systemic immune response to inhaled multiwalled carbon nanotubes. Toxicol Sci 100(1): 203-214.

Moolgavkar, SH, Brown, RC and Turim, J (2001). Biopersistence, fiber length, and cancer risk assessment for inhaled fibers. Inhal Toxicol 13(9): 755-772.

Mossman, BT (2000). Mechanisms of action of poorly soluble particulates in overload-related lung pathology. Inhal Toxicol 12(1-2): 141-148.

Muhlfeld, C, Poland, CA, Duffin, R, Brandenberger, C, Murphy, FA, Rothen-Rutishauser, B, Gehr, P and Donaldson, K (2011). Differential effects of long and short carbon nanotubes on the gas-exchange region of the mouse lung. Nanotoxicology.

Muller, J, Huaux, F, Moreau, N, Misson, P, Heilier, JF, Delos, M, Arras, M, Fonseca, A, Nagy, JB and Lison, D (2005). Respiratory toxicity of multi-wall carbon nanotubes. Toxicol Appl Pharmacol 207(3): 221-231.

Nagatomo, H, Morimoto, Y, Oyabu, T, Hirohashi, M, Ogami, A, Yamato, H, Kuroda, K, Higashi, T and Tanaka, I (2005). Expression of heme oxygenase-1 in the lungs of rats exposed to crocidolite asbestos. Inhal Toxicol 17(6): 293-296.

Oberdorster, G (1996). Evaluation and use of animal models to assess mechanisms of fibre carcinogenicity. IARC Sci Publ(140): 107-125.

Osmond-McLeod, MJ, Poland, CA, Murphy, F, Waddington, L, Morris, H, Hawkins, SC, Clark, S, Aitken, R, McCall, MJ and Donaldson, K (2011). Durability and inflammogenic impact of carbon nanotubes compared with asbestos fibres. Part Fibre Toxicol 8: 15.

Poland, CA, Duffin, R, Kinloch, I, Maynard, A, Wallace, WA, Seaton, A, Stone, V, Brown, S, Macnee, W and Donaldson, K (2008). Carbon nanotubes introduced into the abdominal cavity of mice show asbestos-like pathogenicity in a pilot study. Nat Nanotechnol 3(7): 423-428.

Roda, E, Coccini, T, Acerbi, D, Barni, S, Vaccarone, R and Manzo, L (2011). Comparative pulmonary toxicity assessment of pristine and functionalized multi-walled carbon nanotubes intratracheally instilled in rats: morphohistochemical evaluations. Histol Histopathol 26(3): 357-367.

Sato, T, Takeno, M, Honma, K, Yamauchi, H, Saito, Y, Sasaki, T, Morikubo, H, Nagashima, Y, Takagi, S, Yamanaka, K, Kaneko, T and Ishigatsubo, Y (2006). Heme oxygenase-1, a potential biomarker of chronic silicosis, attenuates silica-induced lung injury. Am J Respir Crit Care Med 174(8): 906-914.

Schinwald, A, Murphy, FA, Prina-Mello, A, Poland, CA, Byrne, F, Movia, D, Glass, JR, Dickerson, JC, Schultz, DA, Jeffree, CE, Macnee, W and Donaldson, K (2012). The threshold length for fiber-induced acute pleural inflammation: shedding light on the early events in asbestos-induced mesothelioma. Toxicol Sci 128(2): 461-470.

Sohaebuddin, SK, Thevenot, PT, Baker, D, Eaton, JW and Tang, L (2010). Nanomaterial cytotoxicity is composition, size, and cell type dependent. Part Fibre Toxicol 7: 22.

Stone, V, Johnston, H and Schins, RP (2009). Development of in vitro systems for nanotoxicology: methodological considerations. Crit Rev Toxicol 39(7): 613-626.

Tanaka, T, Terada, M, Ariyoshi, K and Morimoto, K (2010). Monocyte chemoattractant protein-1/CC chemokine ligand 2 enhances apoptotic cell removal by macrophages through Rac1 activation. Biochem Biophys Res Commun 399(4): 677-682.

van Berlo, D, Boots, AW, Albrecht, C, Schins, RP and Clift, M (2012). Carbon nanotubes: An insight into the mechanisms of their potential genotoxicity. Swiss Med Wkly in press.

van Berlo, D, Wessels, A, Boots, AW, Wilhelmi, V, Scherbart, AM, Gerloff, K, van Schooten, FJ, Albrecht, C and Schins, RP (2010). Neutrophil-derived ROS contribute to oxidative DNA damage induction by quartz particles. Free Radic Biol Med 49(11): 1685-1693.

Wang, X, Guo, J, Chen, T, Nie, H, Wang, H, Zang, J, Cui, X and Jia, G (2012). Multi-walled carbon nanotubes induce apoptosis via mitochondrial pathway and scavenger receptor. Toxicol In Vitro 26(6): 799-806.

Wang, X, Jia, G, Wang, H, Nie, H, Yan, L, Deng, XY and Wang, S (2009). Diameter effects on cytotoxicity of multi-walled carbon nanotubes. J Nanosci Nanotechnol 9(5): 3025-3033.

Wang, X, Katwa, P, Podila, R, Chen, P, Ke, PC, Rao, AM, Walters, DM, Wingard, CJ and Brown, JM (2011). Multi-walled carbon nanotube instillation impairs pulmonary function in C57BL/6 mice. Part Fibre Toxicol 8: 24.

Wilhelmi, V, Fischer, U, van Berlo, D, Schulze-Osthoff, K, Schins, RP and Albrecht, C (2012). Evaluation of apoptosis induced by nanoparticles and fine particles in RAW 264.7 macrophages: facts and artefacts. Toxicol In Vitro 26(2): 323-334.

Yao, SQ, Rojanasakul, LW, Chen, ZY, Xu, YJ, Bai, YP, Chen, G, Zhang, XY, Zhang, CM, Yu, YQ, Shen, FH, Yuan, JX, Chen, J and He, QC (2011). Fas/FasL pathway-mediated alveolar macrophage apoptosis involved in human silicosis. Apoptosis 16(12): 1195-1204.

Chapter V

General Summary

5 General discussion and conclusions

The ongoing industrial development and commercialisation of innovative nanomaterials has gained enormous importance. This fact inevitably results in an increased particle exposure of the population. Despite this, current knowledge of their possible adverse effects is limited. From a toxicological point of view, the lung represents the main entry portal for particles into the human body. Silicosis, a fibrotic lung disease caused by inhalation of crystalline silicon dioxide dust (e.g. quartz), is one of the best studied particle-induced lung diseases with great impact all over the world [Rushton 2007]. The development of fibrotic scar tissue in the lung is closely linked to the release of inflammatory mediators by macrophages under chronic inflammatory conditions [Todd *et al.,* 2012]. Investigations on apoptotic mechanisms induced by quartz dust have revealed important novel insights in the pathogenesis of silicosis [Iyer *et al.,* 1996; Borges *et al.,* 2001]. However, a final cause-and-effect relationship can not yet be drawn. Generally, macrophages are the key actors of the innate immune system and of central relevance both in the development and progression of fibrosis as well as other serious diseases [Murray *et al.,* 2011]. Building the first line of defence against particulate materials as well as biological pathogens, their inherent role in phagocytosis may be affected by particles that trigger their cell death mechanisms. Defective macrophage engulfment can contribute to exaggerated inflammatory responses and dysregulation of tissue homeostasis [Fadeel *et al.,* 2005]. Since severe lung damage due to pulmonary fibrosis is still incurable and life-threatening, there is a call to assess potential fibrotic hazards of other particulate matter along with silica. Several studies have demonstrated a clear association between lung fibrosis and apoptosis in alveolar macrophages [Hamilton *et al.,* 2008; Yao *et al.,* 2011]. In silicosis, the concomitant particle-induced apoptotic cell death can be activated by different caspase-mediated pathways, both the intrinsic mitochondrial and extrinsic receptor mediated pathway [Tumane *et al.,* 2010].

The nano-safety research community as well as specific nanotechnology sectors (e.g. nanomedicine) would benefit greatly from an improved understanding of the mechanisms of particle-induced apoptosis. The achievements of biotechnology have offered a broad spectrum of highly specific tools for the detection of cell death modalities in clinical and experimental research. However, nanotoxicology research is lagging behind in these aspects [Andon *et al.,* 2012]. Currently, nano-safety researchers are forced to run laborious case-by-case studies. Regarding the tremendous industrial progressions in development of novel nanomaterials and their increased applications in our daily life products, there is an urgent need for standardised

high-throughput-studies to uncover potentially harmful materials [Lewinski *et al.,* 2008]. As outlined in this thesis, even the application of basic cytotoxicity and viability assays is often afflicted with methodical artefacts that may result in false positive or negative results. There is an urgent need to focus on present research efforts in nanotoxicology as reliable and reproducible study designs are often lacking [Schrurs *et al.,* 2012]. Elucidation of the physicochemical properties of nanomaterials in relation to their pharmacological and toxicological activity is the projecting idea of Quantitative Structure-Activity Relationship (QSAR) strategies, which is a far-reaching demand of this thesis. In the field of particle toxicology some candidate markers that predict lung inflammation have already been emerged recently and suggested to be useful for future QSAR approaches [Duffin *et al.*, 2007].

Nowadays, the manufacturing of nanoparticles in a controlled way to design their specific structure or functionality (e.g. by covalent binding or coating) is relatively easy to perform. However, currently there is no well-directed strategy, in terms of desired biological mode of action, to create low toxicity analogues of nanomaterials, in other words, materials that are safe-by-design. The present studies are focused on *in vitro* investigations to contribute to the "3R concept" of reduction, refinement and replacement of animal experimentations [Richmond 2002]. This is especially relevant in view of the increasing demands for ongoing chemical safety assessments in the "Registration, Evaluation, Authorisation and Restriction of Chemicals" (REACH) system [Schoeters 2010].

In study 1 (**Chapter II**) a set of merely six particulate samples, differing in their physico-chemical properties (size, crystal structure, chemical composition), revealed highly specific modalities and kinetics of cell death as well as unpredictable interferences with the conventional cytotoxicity and apoptosis assays in macrophages. These elaborative investigations of pointed out the complexity of factors that has to be considered in apoptosis detection studies. The data in the chapter showed 1.) how to appreciate possible particle interferences with assay systems, 2.) how to evolve particular modifications in practical as well as calculational elimination, and 3.) how to include appropriate controls to identify and estimate possible interferences. In case of a positive apoptosis finding, detected by multiple assays, the appropriate subsequent step would be the elucidation of the underlying mechanisms in follow-up research. Indeed, there is an increasing consensus in the toxicology community, that mechanistic insights are very important for improved risk assessment strategies and decisions.

With this intention, study 2 (**Chapter III**) was performed, to evaluate nanosized ZnO, which in study 1 was identified as a highly potent particle sample inducing necrosis and especially

apoptosis in macrophages. A recent concept in the understanding of apoptosis induction is the involvement of oxidative stress due to excessive ROS formation [Forman *et al.,* 2002]. Mild oxidative stress is known to induce apoptosis by damage of intracellular molecules and organelles, especially DNA strand breaks [Mates *et al.,* 2012]. Moreover, cysteine-dependent and therefore redox-sensitive caspases themselves may be activated in an oxidative stress dependent manner [Orrenius *et al.,* 2006]. The role of ROS in ZnO-exposed macrophages has been discussed controversially regarding its impact on cytotoxic and apoptotic mechanisms. As outlined in study 2, with the use of primary macrophages obtained from knockout mouse models we could show that ZnO nanoparticles trigger 1.) an oxidative burst mediated by the phagocytic NADPH oxidase enzyme complex and 2.) an apoptotic response in macrophages. However, both processes were demonstrated to be not causally related. Moreover, ZnO induced cell death was also found to be unaffected by the master regulator of the antioxidant response, Nrf2. The controversies drawn on ZnO mediated toxicity may indicate for subtle but extensive interactions with multiple cellular functions, strongly associated with dose metrics. Even neighboured cells revealed distinct modes of cell death, as was demonstrated by electron microscopic investigations. This effect can be explained by activation of different death pathways depending on the individual doses of particles in the *in vitro* system, as previously shown for other toxic agents [Dypbukt *et al.,* 1994]. This aspect is also relevant for the *in vivo* situation, since it is known that particles have location specific differences in deposition patterns in the body, for instance after inhalation. In this regard, ZnO seems to be capable to interact with several essential signalling cascades. To elucidate the underlying mechanisms, further studies should also attend the emerging concept of pyroptosis, another form of programmed cell death apart from apoptosis [Bergsbaken *et al.,* 2009]. In distinct conditions, the inflammatory capacity of ZnO particles might be a result of inflammasome activation as recently shown for crystalline silica [Dostert *et al.,* 2008]. The controversies in currently published data for this type of nanoparticle emphasises the need to design well-adjusted experiments in particle toxicology research.

Generally, *in vitro* test systems are useful to elaborate defined endpoints for the development of paradigms in nanoparticle toxicity and screening assays. Certainly, *in vitro* approaches have to be critically scrutinised on their physiological relevance. To validate these *in vitro* assays and to investigate implications of potential systemic effects for particle-related diseases, there is still a need of adequate *in vivo* models. Therefore the aim of study 3 (**Chapter IV**) was to investigate the pro-fibrotic response of two morphological types of MW-CNTs *in vivo*, and to evaluate whether their fibrotic potential can be predicted from in

in vitro experiments using the macrophage cell line Raw 264.7. Two types of MW-CNT samples were used, a long and a short type nanotubes sample. Both materials were found capable to induce granuloma lesions in mouse lung tissue. However, only the long MW-CNT caused a significant systemic inflammatory response and this sample also caused a more pronounced pro-fibrotic response. Cells with active caspase-3 could be detected in the granulomatous lesions in response to both materials, but this seemed to be a secondary effect, since both MW-CNT samples did not primary initiate apoptotic effects in macrophages *in vitro*. The data from this study therefore indicate that there is no causal relation between apoptosis in macrophages and fibrotic processes by carbon nanotubes, in contrast to the observations with crystalline silica particles [Iyer *et al.,* 1996; Hamilton *et al.,* 2008]. Especially for this specific type of nanomaterial attention should be paid to the macrophage-specific phenomenon of frustrated phagocytosis depending on the length of the respective nanotube, as known from the asbestos toxicity [Donaldson *et al.,* 2010]. The observations with the two contrasting MW-CNT types also suggest that a nanotube-hazard classification based on necrosis rather than apoptosis may be sufficient.

In conclusion, the current thesis highlights that several major practical pitfalls can be encountered when using commercial as well as other well-established detection systems and methods to elucidate particle-triggered cell death mechanisms. The methods presented in the thesis were designed and subsequently adapted to allow for controlled and valid *in vitro* toxicity testing. Present work contributes to the rather young discipline of nanotoxicology by providing methodological backgrounds for improved safety-assessment and further developments of animal replacement testing strategies. In addition, the different studies described in this thesis have revealed a very individual behaviour of specific particulate samples within biological systems in relation to their diverse physico-chemical properties. This emphasises that for novel particulate materials that enter the market it will still be necessary to determine their toxic potential hazard on a case-by-case approach.

5.1 References

Andon, FT and Fadeel, B (2012). Programmed Cell Death: Molecular Mechanisms and Implications for Safety Assessment of Nanomaterials. Acc Chem Res.

Bergsbaken, T, Fink, SL and Cookson, BT (2009). Pyroptosis: host cell death and inflammation. Nat Rev Microbiol 7(2): 99-109.

Borges, VM, Falcao, H, Leite-Junior, JH, Alvim, L, Teixeira, GP, Russo, M, Nobrega, AF, Lopes, MF, Rocco, PM, Davidson, WF, Linden, R, Yagita, H, Zin, WA and DosReis, GA (2001). Fas ligand triggers pulmonary silicosis. J Exp Med 194(2): 155-164.

Donaldson, K, Murphy, FA, Duffin, R and Poland, CA (2010). Asbestos, carbon nanotubes and the pleural mesothelium: a review of the hypothesis regarding the role of long fibre retention in the parietal pleura, inflammation and mesothelioma. Part Fibre Toxicol 7: 5.

Dostert, C, Petrilli, V, Van Bruggen, R, Steele, C, Mossman, BT and Tschopp, J (2008). Innate immune activation through Nalp3 inflammasome sensing of asbestos and silica. Science 320(5876): 674-677.

Duffin, R, Mills, NL and Donaldson, K (2007). Nanoparticles-a thoracic toxicology perspective. Yonsei Med J 48(4): 561-572.

Dypbukt, JM, Ankarcrona, M, Burkitt, M, Sjoholm, A, Strom, K, Orrenius, S and Nicotera, P (1994). Different prooxidant levels stimulate growth, trigger apoptosis, or produce necrosis of insulin-secreting RINm5F cells. The role of intracellular polyamines. J Biol Chem 269(48): 30553-30560.

Fadeel, B and Orrenius, S (2005). Apoptosis: a basic biological phenomenon with wide-ranging implications in human disease. J Intern Med 258(6): 479-517.

Forman, HJ and Torres, M (2002). Reactive oxygen species and cell signaling: respiratory burst in macrophage signaling. Am J Respir Crit Care Med 166(12 Pt 2): S4-8.

Hamilton, RF, Jr., Thakur, SA and Holian, A (2008). Silica binding and toxicity in alveolar macrophages. Free Radic Biol Med 44(7): 1246-1258.

Iyer, R, Hamilton, RF, Li, L and Holian, A (1996). Silica-induced apoptosis mediated via scavenger receptor in human alveolar macrophages. Toxicol Appl Pharmacol 141(1): 84-92.

Lewinski, N, Colvin, V and Drezek, R (2008). Cytotoxicity of nanoparticles. Small 4(1): 26-49.

Mates, JM, Segura, JA, Alonso, FJ and Marquez, J (2012). Oxidative stress in apoptosis and cancer: an update. Arch Toxicol 86(11): 1649-1665.

Murray, PJ and Wynn, TA (2011). Protective and pathogenic functions of macrophage subsets. Nat Rev Immunol 11(11): 723-737.

Orrenius, S and Zhivotovsky, B (2006). The future of toxicology--does it matter how cells die? Chem Res Toxicol 19(6): 729-733.

Richmond, J (2002). Refinement, reduction, and replacement of animal use for regulatory testing: future improvements and implementation within the regulatory framework. ILAR J 43 Suppl: S63-68.

Rushton, L (2007). Chronic obstructive pulmonary disease and occupational exposure to silica. Rev Environ Health 22(4): 255-272.

Schoeters, G (2010). The REACH perspective: toward a new concept of toxicity testing. J Toxicol Environ Health B Crit Rev 13(2-4): 232-241.

Schrurs, F and Lison, D (2012). Focusing the research efforts. Nat Nanotechnol 7(9): 546-548.

Todd, NW, Luzina, IG and Atamas, SP (2012). Molecular and cellular mechanisms of pulmonary fibrosis. Fibrogenesis Tissue Repair 5(1): 11.

Tumane, RG, Pingle, SK, Jawade, AA and Nath, NN (2010). An overview of caspase: Apoptotic protein for silicosis. Indian J Occup Environ Med 14(2): 31-38.

Yao, SQ, Rojanasakul, LW, Chen, ZY, Xu, YJ, Bai, YP, Chen, G, Zhang, XY, Zhang, CM, Yu, YQ, Shen, FH, Yuan, JX, Chen, J and He, QC (2011). Fas/FasL pathway-mediated alveolar macrophage apoptosis involved in human silicosis. Apoptosis 16(12): 1195-1204.

5.2 Abstract

The ongoing industrial development and commercialisation of innovative nanomaterials is associated with an increased exposure of the population. However, the assessment of potential human health risks can barely keep up with the progressive achievements in nanotechnology.
From the toxicological point of view, the lung is seen as main entry portal for particles. Several studies using respirable crystalline silica demonstrated a relation between particle-induced fibrosis and apoptotic processes in alveolar macrophages. Besides that, apoptotic macrophages are impaired in their clearance function. Therefore, knowledge about particle-induced apoptosis is considered to be a crucial readout to predict the pathogenic hazard of particles. In this regard, appropriate detection systems are a prerequisite to perform systematic screening studies. With this intention, in the first study a set of well-established methods and commercial cell death assays was applied to RAW 264.7 macrophages after treatment with six types of particulate materials, i.e. crystalline and amorphous SiO_2, fine and ultrafine (nano-)TiO_2, and two further nanomaterials (ZnO, MgO). Through detailed inclusion of positive and negative controls, several particle-specific artefacts could be identified in specific cell death detection assays. These tests were subsequently optimised by experimental or mathematical adaptations in order to eliminate these artefacts.
Since this study revealed that the nanomaterial ZnO was the most potent inducer of cytotoxicity, in particular apoptosis, a follow-up study focused specifically on the identification of underlying pro-apoptotic mechanisms. To investigate the role of oxidative stress in ZnO toxicity, primary bone marrow derived macrophages from murine knockout models were used. These investigations revealed that neither the phagocytic $p47^{phox}$ NADPH oxidase nor the redox-sensitive transcription factor Nrf2 are involved in the induction of apoptosis by ZnO. Further results obtained from experiments with caspase-9 deficient Jurkat T-lymphocytes demonstrated the involvement of the intrinsic mitochondrial apoptosis pathway.
In a third study, the pulmonary toxicity of two types of carbon nanotubes, mainly differing in length and agglomeration behaviour, were investigated after pharyngeal aspiration in mice. Besides inflammatory effects in blood plasma and pro-fibrotic lesions in lung sections, granolumas were observed containing cells with activated caspase-3. However, accompanying *in vitro*-investigations on RAW 264.7 cells did not show direct caspase-3 activation by carbon nanotubes. Therefore, a screening for apoptotic effects in macrophages does not appear to be an appropriate tool to predict the fibrogenic hazard of carbon nanotubes.
The studies described in this thesis provide a major contribution to the urgently required standardisation and validation of test systems, especially for the detection of particle-induced apoptosis. Furthermore, it demonstrates the impact of different physico-chemical properties on toxic effects of particles. This emphasises, that evaluation of the toxic hazard of these materials still requires testing on a case-by-case basis.

5.3 Zusammenfassung

Die fortschreitende industrielle Entwicklung und Kommerzialisierung innovativer Nanomaterialien geht mit einer zunehmenden Partikelbelastung der Bevölkerung einher. Die Abschätzung möglicher Risiken für die menschliche Gesundheit kann mit dem nanotechnologischen Fortschritt jedoch kaum Schritt halten. Aus toxikologischer Sicht stellt die Lunge eine Haupteintrittspforte für Partikel dar. Aus früheren Forschungen mit respirablen Quarzpartikeln ist bekannt, dass partikelinduzierte Fibrose im Zusammenhang mit apoptotischen Prozessen in Alveolarmakrophagen steht. Außerdem können apoptotische Makrophagen nicht mehr ihrer Clearance-Funktion nachkommen. Deshalb gilt die Induktion von Apoptose als wichtiger Hinweis auf die Pathogenität von Partikeln, für deren Nachweis geeignete Screening-Testsysteme erforderlich sind. In der ersten Studie dieser Arbeit wurden daraufhin gängige gut etablierte wie auch kommerziell erhältliche Detektionssysteme zur Quantifizierung von Zelltod anhand einer systematischen Auswahl von sechs Partikelmaterialien (kristallines und amorphes SiO_2, feines und ultrafeines (nano-) TiO_2, zwei weitere Nanomaterialien ZnO und MgO) in RAW 264.7 Zellen eingesetzt. Durch den Einsatz gezielter Positiv- wie Negativkontrollen wurden spezifische Störfaktoren, sowie Möglichkeiten zur Eliminierung dieser auf experimentellem oder rechnerischem Wege aufgezeigt. Das in dieser Studie als Auslöser von Zytotoxizität, speziell von Apoptose, prominenteste Nanomaterial ZnO wurde in einer Folgestudie hinsichtlich der apoptotischen Mechanismen untersucht. Die Fragestellung, ob oxidativer Stress als Auslöser für ZnO-induzierte toxische Effekte fungiert, wurde durch den Einsatz defizienter primärer Knochenmarksmakrophagen untersucht. Weder die phagozytische $p47^{phox}$ NADPH-Oxidase noch der redoxsensitive Transkriptionsfaktor Nrf2 zeigten einen Einfluss auf die Apoptoseinduktion durch ZnO-Partikel. Ergebnisse mit Caspase-9 defizienten Jurkat T-Lymphozyten konnten eine Beteiligung des intrinsischen mitochondrialen Apoptoseweges belegen. In einer dritten Studie wurde die pulmonale Toxizität zweier Kohlenstoffnanoröhrchen, die sich vor allem in Länge und Agglomerationsverhalten unterscheiden, nach pharyngealer Aspiration am Mausmodell untersucht. Neben entzündlichen Effekten im Blutplasma und profibrotischen Läsionen in Lungenschnitten wurden Zellen mit aktivierter Caspase-3 in Granulomen nachgewiesen. Parallele *in vitro*-Untersuchungen an RAW 264.7 Zellen belegten jedoch keine direkte Caspase-3-Aktivierung durch Kohlenstoffnanoröhrchen. Ein Apoptose-Screening faserförmiger Partikel in Makrophagen ermöglicht somit keine Vorhersage hinsichtlich potentieller Fibrogenität *in vivo*. Die Ergebnisse dieser Dissertation leisten einen Beitrag zur dringend geforderten Standardisierung und Validierung von Testsystemen insbesondere zum Nachweis partikelinduzierter Apoptose. Darüber hinaus stellen sie die Bedeutung unterschiedlicher physicochemischer Eigenschaften für die toxischen Effekte von Partikeln heraus und verdeutlichen, dass nach wie vor eine Fall-zu-Fall-Testung spezifischer Materialien hinsichtlich ihrer Toxizität erfolgen muss.

5.4 Abbreviations

8-OHdG	8-hydroxydeoxyguanosine
Apaf-1	apoptotic protease activating factor
ARE	Antioxidant response element
BH3	Bcl-2 homology domain 3
BSA	Bovine serum albumin
BSI	British Standards Institute
Caspase	Cysteinyl aspartate–specific protease
CNT	Carbon nanotube
CSF	Colony-stimulating factor
DISC	Death-inducing signalling complex
DMEM	Dulbecco's modified Eagle's medium
DMSO	Dimethyl sulfoxide
DNA	Deoxyribonucleic acid
DPPC	Dipalmitoyl-phosphatidylcholine
DQ 12	Dörentrup Quartz „ground product no.12"
DTT	Dithiothreitol
ECH	Epichlorohydrin
EDTA	Ethylendiaminetetraacetic acid
FCS	Foetal calf serum
GAPDH	Glyceraldehyde 3-phosphate dehydrogenase
GSH	Glutathione
HBSS	Hank's Buffered Salt Solution
$HO^{\bullet}$	Hydroxyl radical
HO-1	Heme Oxygenase-1
HOCl	Hypochlorous acid
IL	Interleukin
Keap1	Kelch-like ECH-associated protein 1
LDH	Lactate dehydrogenase
MAP	Mitogen activated protein
MCP	Monocyte chemotactic protein
MIP	Macrophage inflammatory protein
MMP	Metalloproteinase

MW-CNT	Multi walled CNT
MΦ	Macrophage
NADPH	Nicotinamide adenine dinucleotide phosphate
NFκB	Nuclear factor kappa B
$NO^{\bullet}$	Nitric oxide radical
NOX	NADPH oxidase
Nrf2	Nuclear factor erythroid-derived 2 related factor 2
$O_2^{-\bullet}$	Superoxide radical
$ONOO^-$	Peroxynitrite
PBS	Phosphate buffered saline
PCR	Polymerase chain reaction
RNS	Reactive Nitrogen Species
$RO_2^{\bullet}$	Peroxyl radical
ROS	Reactive Oxygen Species
SOD	Superoxide dismutase
SW-CNT	Single walled CNT
TNF	Tumour necrosis factor
UV	Ultra violet
γ-GCS	Gamma-glutamylcysteine synthetase

Publications

Haberzettl, P, Schins, RP, Hohr, D, Wilhelmi, V, Borm, PJ and Albrecht, C (2008). Impact of the FcgammaII-receptor on quartz uptake and inflammatory response by alveolar macrophages. Am J Physiol Lung Cell Mol Physiol 294(6): L1137-1148.

van Berlo, D*, Wessels, A*, Boots, AW, Wilhelmi, V, Scherbart, AM, Gerloff, K, van Schooten, FJ, Albrecht, C and Schins, RP (2010). Neutrophil-derived ROS contribute to oxidative DNA damage induction by quartz particles. Free Radic Biol Med 49(11): 1685-1693. *equal contributions

Wilhelmi, V, Fischer, U, van Berlo, D, Schulze-Osthoff, K, Schins, RP and Albrecht, C (2012a). Evaluation of apoptosis induced by nanoparticles and fine particles in RAW 264.7 macrophages: facts and artefacts. Toxicol In Vitro 26(2): 323-334.

Wilhelmi, V, Fischer, U, Weighardt, H, Schulze-Osthoff, K, Esser, C, Schins, RP and Albrecht, C (2012b). Zinc oxide nanoparticles induce necrosis and apoptosis in macrophages in a p47phox- and Nrf2-independent manner. article submitted for publication.

Wilhelmi, V*, van Berlo, D*, Boots, AW, Hullmann, M, Stahlmecke, B, Kuhlbusch, TA, Bast, A, Schins, RP and Albrecht, C (2012c). Apoptotic, inflammatory, and fibrogenic effects of two different types of multi-walled carbon nanotubes in mouse lung. article submitted for publication. *equal contributions

Dankwort

Frau Prof. Dr. Charlotte Esser danke ich für die Übernahme des Erstgutachtens und die wertvollen Impulse für die Fertigstellung des Manuskripts. Die Kooperation mit Ihrer Arbeitsgruppe war zudem ein wesentlicher Teil meiner Arbeit, vielen Dank!

Frau Prof. Dr. Christine R. Rose danke ich für die Übernahme des Zweitgutachtens.

Mein besonderer Dank gilt Dr. Catrin Albrecht für die Bereitstellung des interessanten Themas und der intensiven Betreuung in freundschaftlicher Atmosphäre. Zusammen mit Dr. Roel Schins, Arbeitsgruppenleiter der Partikelforschung am IUF, durfte ich teilhaben an einem wirklich unschlagbaren Team, in dem Kreativität, Begeisterung und Motivation sprudeln! Ich habe unglaublich viel gelernt – Danke!

Zur netten Arbeitsatmosphäre gehörte ein bunter Haufen lustiger „party(cle) people“, wie Dr. Damiën van Berlo uns nannte. Dir Damiën noch ein Extra-Dankschön für das flotte Korrekturlesen so kurz vor deinem Urlaub! Weiterhin gehörten Dr. Anton Wessels und Dr. Bryan Hellack zum „Jungszimmer“ der Etage 3. Nicht weniger kreativ-chaotisch war unser „Mädelszimmer“ mit meinen Kolleginnen Dr. Agnes Scherbart, Dr. Kirsten Gerloff, Dr. Agnes Boots, Maja Hullmann, Walluree Thongkam und Julia Kolling. Danke, es war wirklich toll mit Euch!

Für die technische Assistenz im Laboralltag danke ich Frau Kirstin Ledermann, Frau Christel Weishaupt und Frau Gabriele Wick.

Vielen Dank an Dr. Ute Fischer, die mir von Anfang an mit ihrer außergewöhnlichen Hilfsbereitschaft, profundem Expertenwissen aus der Apoptoseforschung und Testmaterial zur Seite stand! Außerdem habe ich ihr Felltier Balu ins Herz geschlossen, eine Freundin von Catrins Java, unserem lieben Laborhundi ☺

Eine große Hilfe für meine Arbeiten am Durchflusszytometer war mir Dr. Heike Weighard. Vielen lieben Dank für das ausgeklügelte Insiderwissen und dem Aushelfen mit Material für die Knochenmarkspräparationen!

Außerdem konnte ich immer auf die mit Abstand allerbeste Familie der ganzen Welt zählen, dafür kann ich gar nicht genug danken!

Eidesstattliche Erklärung

Hiermit versichere ich, dass ich die vorliegende Arbeit eigenständig verfasst und keine anderen als die angegebenen Quellen und Hilfsmittel verwendet habe.

Ferner versichere ich, dass ich weder an der Heinrich-Heine-Universität noch an einer anderen Universität versucht habe, diese Doktorarbeit einzureichen.

Ebenso habe ich bisher keine erfolglosen Promotionsversuche unternommen.

Düsseldorf, den

_____

Verena Wilhelmi